

The Role of Secreted Frizzled Related Protein 3 (SFRP3) and the Wnt Signaling Pathway
in PAX3-FOXO1-Positive Alveolar Rhabdomyosarcoma

by

Julie Jeanne Grondin Kephart

Department of Pharmacology and Cancer Biology
Duke University

Date: _____

Approved:

Corinne M. Linardic, Supervisor

Gerard C. Blobe

Christopher M. Counter

David G. Kirsch

Xiao-Fan Wang

Dissertation submitted in partial fulfillment of
the requirements for the degree of Doctor
of Philosophy in the Department of
Pharmacology and Cancer Biology in the Graduate School
of Duke University

2015

ABSTRACT

The Role of Secreted Frizzled Related Protein 3 (SFRP3) and the Wnt Signaling Pathway
in PAX3-FOXO1-Positive Alveolar Rhabdomyosarcoma

by

Julie Jeanne Grondin Kephart

Department of Pharmacology and Cancer Biology
Duke University

Date: _____

Approved:

Corinne M. Linardic, Supervisor

Gerard C. Blobe

Christopher M. Counter

David G. Kirsch

Xiao-Fan Wang

An abstract of a dissertation submitted in partial
fulfillment of the requirements for the degree
of Doctor of Philosophy in the Department of
Pharmacology and Cancer Biology in the Graduate School of
Duke University

2015

Copyright by
Julie Jeanne Grondin Kephart
2015

Abstract

Rhabdomyosarcoma is the most common pediatric soft tissue sarcoma and demonstrates features of skeletal muscle. Of the two predominant (pediatric) subtypes, embryonal (eRMS) and alveolar (aRMS), aRMS has the poorer prognosis, with a 5-year survival rate of <50%. The majority of aRMS tumors express the fusion protein PAX3/7-FOXO1. As PAX3/7-FOXO1 is not currently druggable, we aimed to identify proteins that are downstream from or cooperate with PAX3-FOXO1 (PF) to enable tumorigenesis with the hope that these proteins may be more amenable to pharmacological inhibition.

First, in a microarray analysis of the transcriptomes of human skeletal muscle myoblasts expressing PF, we observed alterations of several Wnt pathway genes, including the Wnt inhibitor Secreted Frizzled Related Protein 3 (SFRP3). Loss-of-function studies interrogated the role of SFRP3 in human aRMS cell lines using shRNAs. Suppression of SFRP3 inhibited aRMS cell growth, reduced proliferation accompanied by a G₁ arrest and induction of p21, and induced apoptosis. SFRP3 suppression modestly increased Wnt signaling; however, activation of the Wnt pathway in human aRMS cells *in vitro* and in a xenograft murine model of aRMS *in vivo* only partially recapitulated the phenotype observed with SFRP3 suppression. To identify other signaling pathways downstream of SFRP3 signaling, we conducted an oncogenic signaling pathways screen and a microarray. In the former, we identified Notch

signaling as conferring resistance to SFRP3 suppression-mediated decreased cell growth and confirmed Notch crosstalk with Wnt signaling and SFRP3 in aRMS cells. In the latter, SFRP3 suppression increased genes associated with skeletal muscle differentiation and decreased those associated with cell cycle progression.

Second, we established a role for SFRP3 in a conditional xenograft murine model of aRMS. Doxycycline-inducible suppression of SFRP3 reduced aRMS tumor growth and weight by more than three-fold. Analysis of the tumors by qPCR and IHC revealed an increase in myogenic differentiation and β -catenin signaling. The combination of SFRP3 suppression and vincristine was more effective at reducing aRMS cell growth *in vitro* than either treatment alone, and ablated tumorigenesis *in vivo*. In conclusion, SFRP3 is necessary for the growth of human aRMS cells both *in vitro* and *in vivo* and is a promising new target for investigation in aRMS.

Dedication

To my husband, Travis, for without his support and love this project would not have been possible.

Contents

Abstract	iv
List of Tables.....	xi
List of Figures	xii
List of Abbreviations	xiv
Acknowledgements	xviii
1. Introduction	1
1.1 Rhabdomyosarcoma	1
1.1.1 PAX3-FOXO1	2
1.1.2 RMS cell of origin	3
1.2 Wnt pathway.....	5
1.2.1 Secreted frizzled related proteins.....	8
1.3 The Wnt pathway's role in skeletal myogenesis.....	10
1.3.1 Skeletal myogenesis	10
1.3.2 The Wnt pathway's function in skeletal myogenesis.....	13
1.4 The Wnt pathway's role in cancer.....	17
1.4.1 SFRPs' role in cancer	19
1.5 The Wnt pathway's role in RMS	20
1.6 Targeting the Wnt pathway in cancer	23
1.7 Collaborative work.....	25
2. Material and methods	27

2.1 Microarray	27
2.2 Cell Lines	29
2.3 Expression of shRNAs and cDNAs in cells	30
2.3.1 Expression of SFRP3 shRNAs and HA*-SFRP3	30
2.3.2 Expression of oncogenic pathway activating cDNAs, including Notch 1 ICD	32
2.4 PCR	33
2.4.1 RT-PCR	33
2.4.2 qPCR.....	34
2.5 Immunoblotting.....	37
2.6 MTT, BrdU, cell cycle analysis, and cell growth assays.....	38
2.7 Differentiation and senescence assays.....	41
2.8 Wnt3a conditioned media	42
2.9 Mouse xenograft studies.....	43
2.9.1 Genetic suppression of SFRP3 in aRMS xenograft tumors.....	43
2.9.2 Activation of Wnt signaling using oral LiCl in aRMS xenograft tumors	44
2.10 Immunohistochemistry.....	44
2.11 Drug treatments.....	45
2.12 Statistics	46
3. SFRP3 is required for aRMS tumorigenesis <i>in vitro</i>	47
3.1 Introduction.....	47
3.2 Secreted Wnt inhibitors, including SFRP3, are upregulated in PAX3-FOXO1- expressing primary human myoblasts and in human aRMS cell lines.	48

3.3 Genetic suppression of SFRP3 inhibits aRMS cell growth.	51
3.4 Suppression of SFRP3 in aRMS inhibits cell proliferation and causes a G ₁ arrest.	56
3.5 Suppression of SFRP3 in aRMS cells also induces apoptosis.....	61
3.6 Discussion.....	62
4. SFRP3 suppression alters the Wnt, Notch, and TGF β embryonic signaling pathways	64
4.1 Introduction.....	64
4.2 Crosstalk between SFRP3 and the Wnt signaling pathway	64
4.2.1 Activation of the Wnt pathway partially phenocopies SFRP3 suppression	67
4.3 Screen to uncover oncogenic signaling pathways capable of rescuing SFRP3 suppression-mediated decreased cell growth.....	71
4.4 The role of Notch in RMS	81
4.5 Crosstalk between the Wnt and Notch signaling pathways	81
4.6 Crosstalk between SFRP3 and the Notch signaling pathway	83
4.7 Crosstalk between SFRP3 and the TGF β signaling pathway	85
4.8 Activated Notch confers resistance to vincristine.....	87
4.9 Conclusions	89
5. SFRP3 is required for aRMS tumorigenesis <i>in vivo</i>	91
5.1 Introduction.....	91
5.2 Suppression of SFRP3 inhibits aRMS tumorigenesis <i>in vivo</i>	94
5.3 Suppression of SFRP3 <i>in vivo</i> induces markers of differentiation and Wnt pathway activation.....	95
5.4 SFRP3 suppression in combination with vincristine abrogates aRMS tumorigenesis.....	107

5.5 Discussion.....	111
6. Conclusions.....	113
6.1 The connection between PF and SFRP3	113
6.2 SFRP3 suppression decreases cell and tumor growth.....	114
6.3 The connection between SFRP3 and the Wnt pathway	117
6.4 SFRP3 suppression sensitizes aRMS cells to vincristine and potential for use in aRMS patients	119
6.5 Conclusions and future directions	121
References	122
Biography	137

List of Tables

Table 1: SFRP3 shRNAs sequences.....	30
Table 2: Primers for semi-quantitative PCR.....	34
Table 3: Primers for qPCR.....	36
Table 4: Conditions for MTT assays with genetic interventions	39
Table 5: Conditions for MTT assays with drug interventions	40
Table 6: GO enriched and repressed probesets	100
Table 7: Wnt pathway genes identified in SFRP3 suppression microarray.....	102

List of Figures

Figure 1: The canonical Wnt pathway	7
Figure 2: Model of skeletal myogenesis, with possible cellular origins of rhabdomyosarcoma as suggested experimentally.	11
Figure 3: Diagram of SFRP3 and HA*-SFRP3	31
Figure 4: Secreted Wnt inhibitors, including SFRP3, are upregulated in PAX3-FOXO1-expressing primary human myoblasts and in human aRMS cell lines.	49
Figure 5: SFRP3 suppression inhibits aRMS cell growth.	52
Figure 6: Doxycycline-inducible SFRP3 shRNA inhibit cell growth.	53
Figure 7: SFRP3 suppression reduces cell growth in eRMS and fibrosarcoma cells	54
Figure 8: SFRP3 suppression inhibits cell proliferation, causes a G ₁ arrest, and increases apoptosis.	57
Figure 9: SFRP3 suppression does not alter myogenic differentiation or senescence.....	59
Figure 10: SFRP3 suppression modestly elevates AXIN2 levels	66
Figure 11: Activation of the Wnt pathway decreases cell growth and cause a cell cycle arrest.	68
Figure 12: LiCl does not affect growth of Rh28 cells murine xenograft as measured by tumor volume, but trends towards a decrease in tumor weight.....	70
Figure 13: Strategy for manipulating oncogenic signaling pathways	72
Figure 14: Screen of oncogenic pathways in SFRP3 suppressed cells	73
Figure 15: Attempts to confirm results from screen of oncogenic pathways in SFRP3 suppressed cells.....	75
Figure 16: Validation of the oncogenic pathway screen results using GI50 curves	79
Figure 17: The Wnt and Notch pathways interact in aRMS cells.....	82

Figure 18: SFRP3 suppression, particularly SFRP3 sh3, activates the Notch pathway.....	84
Figure 19: Notch confers resistance to vincristine	88
Figure 20: SFRP3 suppression inhibits tumor growth <i>in vivo</i>	92
Figure 21: Shorter duration of SFRP3 suppression inhibits tumor growth <i>in vivo</i>	96
Figure 22: SFRP3 suppression increases β -catenin expression.....	98
Figure 23: Pathway signature analysis.....	104
Figure 24: Validation Wnt pathway members identified in the microarray.	105
Figure 25: SFRP3 suppression in combination with vincristine inhibits aRMS cell and tumor growth and causes tumor regression.	108

List of Abbreviations

APC	Adenomatous polyposis coli gene product
aRMS	Alveolar rhabdomyosarcoma
BrdU	5-bromo-2'-deoxyuridine
CCND1	Cyclin D1
CDK4	Cyclin-dependent kinase 4
cDNA	Complementary deoxyribonucleic acid
CK1	Casein kinase 1
CRD	Cysteine-rich domain
CRISPR	Clustered regularly interspaced short palindromic repeats
CTBP2	C-terminal binding protein 2
CXCR4	Chemokine (C-X-C motif) receptor 4
DKK	Dickkopf-related protein
DMSO	Dimethyl sulfoxide
DVL	Dishevelled
E2F1	E2F transcription factor 1
EGF	Epidermal growth factor
ER	Estrogen receptor
eRMS	Embryonal rhabdomyosarcoma
FGFR4	Fibroblast growth factor receptor 4
FOXO1	Forkhead box O1
FZD	Frizzled class receptor
GEMM	Genetically engineered mouse model
GO	Gene ontology
GSK3 β	Glycogen synthase kinase β

H&E	Hematoxylin and eosin stain
HA*-SFRP3	HA-tagged secreted frizzled related protein 3
HDAC	Histone deacetylase
HES1	Hes family bHLH transcription factor 1
HEY1	Hes-related family bHLH transcription factor with YRPW motif 1
HSMM	Human skeletal muscle myoblast
hTERT	Telomerase reverse transcriptase
IHC	Immunohistochemistry
IACUC	Institutional Animal Care & Use Committee
ICD	Intracellular domain
IGF1R	Insulin-like growth factor 1 receptor
IGFBP-4	Insulin-like growth factor binding protein 4
LEF	Lymphoid enhancer factor
LiCl	Lithium chloride
LRP5/6	Low density lipoprotein receptor-related protein 5/6
MAPK	Mitogen-activated protein kinase
MEK-1	Mitogen-activated protein kinase kinase 1
MET	Met proto-oncogene
MMTV	Mouse mammary tumor virus
MSC	Mesenchymal stem cells
mTOR	Mechanistic target of rapamycin
MTT	3-(4,5-Dimethyl-2-thiazolyl)-2,5-diphenyl-2H-tetrazolium bromide methylthiazolyldiphenyl-tetrazolium bromide
MYCN	v-myc avian myelocytomatosis viral oncogene neuroblastoma derived homolog
MYF5	Myogenic factor 5

MYF6	Myogenic factor 6 (herculin)
MYOD	Myogenic differentiation 1
NAV2	Neuron navigator 2
NTR	Netrin-related motif
PCR	Polymerase chain reaction
PF	PAX3-FOXO1
PI	Propidium iodide
PI3K	Phosphoinositide 3-kinase
qPCR	Quantitative polymerase chain reaction
PAX3	Paired box 3
PAX7	Paired box 7
PCP	Planar cell polarity
PKC	Protein kinase C
RAS	Rat sarcoma viral oncogene
RMA	Robust multi-array average
RMS	Rhabdomyosarcoma
RT-PCR	Reverse transcription polymerase chain reaction
SAM	Significance analysis of microarrays
SFRP	Secreted frizzled related protein
SFRP3	Secreted frizzled related protein 3
SNAI2	Snail family zinc finger 2
SOST	Sclerostin
sRMS	Sclerosing rhabdomyosarcoma
TCF	T cell factor
TGF β	Transforming growth factor, beta
TGFBR1	Transforming growth factor, beta receptor 1

TUNEL	Terminal deoxynucleotidyl transferase dUTP nick end labeling
UPS	Undifferentiated pleomorphic sarcoma
VPA	Valproic acid
WNT	Wingless-type MMTV integration site family

Acknowledgements

Science is far too difficult to attempt alone. It is only when we work on the problem as a team, each contributing our own expertise, knowledge, and points of view, that we can have any hope of uncovering new knowledge and create solutions with the potential of improving human lives. As such, I am incredibly grateful for all of the mentors and collaborators that have supported this project.

First, thank you to my advisor, Corinne Linardic for all of her support and advice throughout my graduate career. I could not have asked for a better mentor, and I am honored to have been her first graduate student. I would also like to acknowledge my thesis committee, Gerry Blobe, Chris Counter, David Kirsch, and Xiao-Fan Wang.

I am grateful to the entire Linardic laboratory, past and present, particularly Rosanne Tiller, Lisa Crose, and Katrina Slemmons who have contributed significantly to this project. For the students I have had the honor of mentoring, I am thankful to them for allowing me that opportunity and for their work towards this project.

The microarrays in this project would not have been possible without Jen-Tsen Ashley Chi and Po Han Chen who provided valuable help with experimental design and analysis. Likewise, the oncogenic pathway screen would not have been possible without help from Kris Wood and the Wood laboratory. I am grateful for our pathologist, Rex Bentley, for reviewing the histology of tumors and Benjamin Alman

and Heather Whetstone for assistance with the β -catenin IHC protocol. In addition, I would like to acknowledge the Kirsch, Wechsler, Becher, and Armstrong laboratories for their insightful comments and advice.

Finally, I would like to thank my husband, Travis Kephart, for his incredible encouragement and patience throughout my graduate career.

1. Introduction

1.1 *Rhabdomyosarcoma*

Cancer in pediatric and adolescent populations, while relatively rare, still accounts for 12% and 5%, respectively, of deaths in those age groups (Pizzo and Poplack 2011). Overall pediatric cancer 5-year survival rates have improved dramatically since the 1960s, increasing from 28% to almost 80%. This increase in overall 5-year survival rates is due to greatly improved new therapies for some malignancies, such as acute lymphoblastic leukemia; however, other malignancies continue to have stagnant survival rates, including alveolar rhabdomyosarcoma.

Soft tissue sarcomas compromise 7% of all pediatric malignancies (Ognjanovic et al. 2009). Of these rhabdomyosarcoma (RMS) is the most common soft tissue sarcoma of childhood and adolescence (Huh and Skapek 2010), compromising 40% of all childhood soft tissue sarcomas (Ognjanovic et al. 2009). Biologically diverse, RMS is further subdivided based on histology into embryonal (eRMS; ~60% of all cases), alveolar (aRMS; ~20% of all cases), botryoid, and pleomorphic (Huh and Skapek 2010). Current therapy is multi-modal, combining chemotherapy, surgery, and radiation (Saab et al. 2011). While eRMS 5-year survival rates have continued to improve, aRMS 5-year survival rates continue to remain less than 50% (Ognjanovic et al. 2009). Location in the body also differs by subtype with eRMS occurring most frequently in the head and neck

and genitourinary areas and aRMS most frequently in the trunk and extremities (Huh and Skapek 2010).

1.1.1 PAX3-FOXO1

Approximately 80% of aRMS cases are driven by a fusion of the proteins PAX3 or PAX7 and FOXO1 (previously known as FKHR) (Huh and Skapek 2010). The rearrangements, t(2:13)(q35;q14) for PAX3-FOXO1(PF) and t(1:13)(p36;q34) for PAX7-FOXO1 fuse the DNA-binding domain of PAX3/7 to the transactivation domain of FOXO1 (Galili et al. 1993; Davis et al. 1994).

Recently, an unbiased genome-wide screen to identify PF binding sites and associated target genes revealed that PF binds to sites that are mostly distal to transcription start sites, suggesting that it alters transcription by binding to enhancers, rather than the promoters of genes (Cao et al. 2010). Many, but not all, of the sites were also enriched for PAX3-motifs, indicating overlap between PAX3 and PF binding. Indeed, PF bound to the MyoD and Myf5 enhancers also bound by PAX3. Finally, PF was found to bind to regions associated with genes known to be overexpressed in aRMS including FGFR4, MET, MycN, and IGFR1 (Cao et al. 2010).

PF-positive aRMS tumors demonstrate few mutations in addition to the translocation, especially when compared with PF-negative eRMS (Shukla et al. 2012; Chen et al. 2013; Shern et al. 2014). Two notable exceptions are copy-number alterations in MYCN and CDK4 (Shern et al. 2014).

1.1.2 RMS cell of origin

The RMS cell of origin remains controversial; however, RMS is often considered to be of skeletal muscle in origin as it expresses markers of myogenic differentiation, including MyoD, myogenin, desmin, and actin (Hettmer and Wagers 2010; Saab et al. 2011). Evidence also suggests that there may be more than one cell of origin of RMS and may differ by subtype (Hettmer and Wagers 2010). Understanding the cell of origin of RMS is valuable as it may provide information to create better *in vitro* and mouse models. It may also contribute to an understanding of the biology underlying these malignancies, leading to new therapeutic targets.

Evidence for a cell of origin of aRMS ranges from mesenchymal stem cells to fully differentiated muscle cells. aRMS-like mouse xenograft tumors arise from human skeletal muscle myoblasts expressing PF, hTert, and MycN (Naini et al. 2008). Similarly, aRMS-like mouse xenograft tumors can also form from mouse mesenchymal stem cells expressing PF and the SV-40 early region, which inactivates Rb and p53 (Ren et al. 2008). However, in a genetically engineered mouse model (GEMM) of aRMS, Myf6-expressing differentiated skeletal muscle cells serve as the cell of origin for tumors when expressing PF and inactivated Ink4a/ARF or p53 (Keller et al. 2004). While Keller et al. (2004) used a Myf6-CRE as a marker of differentiated skeletal muscle cells, other studies have suggested that Myf6 may have a role in embryonic myogenesis, suggesting a Myf6-CRE may not limit expression of PF and inactivation of Ink4a/ARF or p53 only to fully

differentiated muscle cells (Kassar-Duchossoy et al. 2004; Bryson-Richardson and Currie 2008). In order to clarify the cell of origin of the aRMS GEMM, a subsequent study demonstrated that the expression of PF under the control of a Pax3-CRE (expressed in hypaxial cells), Myf5-CRE, or Myf6-CRE and inactivation of p53 produced tumors resembling aRMS. However, all of the CRE drivers used were constitutively expressed. If differentiated skeletal muscle is indeed the cell of origin, one would predict that expression of PF and inactivation of p53 or Ink4a/ARF could occur after birth using a tamoxifen-induced CRE (CRE-ER) expressed in skeletal muscle. When a CRE-ER was used in Pax7-, Myf5-, or Myf6-expressing cells, tumors arose only in the Pax7 condition. Interestingly, the tumors did not resemble aRMS or express myogenic markers, but rather resembled pleomorphic sarcomas. The CRE was induced 30 days after birth and based on previous data suggesting a fully differentiated muscle cell as the cell of origin, tumors would have been expected in the Myf6 CRE-ER conditions; however, none were observed (Abraham et al. 2014). Further studies and new models are needed to clarify these findings. One approach may be a promising new model using CRISPR-Cas9 nuclease technology to generate PF fusions in myoblasts found in the limbs of mice (Lagutina et al. 2015). However, it remains to be seen if this model will result in tumors resembling aRMS.

In eRMS, muscle satellite cells have been proposed as a cell of origin; however in a mouse model of sarcomas, loss of p53 in satellite cells resulted in sarcomas that were

predominantly spindle cell sarcomas (also called undifferentiated pleomorphic sarcomas or UPS), while p53 loss in maturing myoblasts generated tumors resembling eRMS (Rubin et al. 2011). However, as with aRMS, the evidence is not clear as a study found that satellite cells could serve as the cell of origin for both eRMS and UPS (Blum et al. 2013), while a separate study found that satellite cells generated tumors resembling pleomorphic rhabdomyosarcoma and pleomorphic sarcomas lacking myogenic features (Hettmer et al. 2011). This suggests that eRMS and UPS may be related tumors, but demonstrate different phenotypes based on their cell of origin.

Finally some eRMS or aRMS cells of origin may not be myogenic, as not all RMS tumors arise in locations where skeletal muscle is present. Indeed some RMS presents with bone marrow involvement, suggesting the possibility of another cell of origin, such as a mesenchymal stem cell capable of entering the skeletal muscle lineage (Charytonowicz et al. 2009).

1.2 Wnt pathway

Wnt was first identified in the early 1980s in mammals in a search for oncogenes. It was known that the mouse mammary tumor virus (MMTV) integrated in the genome causing mammary tumors by activation of an oncogene, and Int-1 (later renamed Wnt1) was identified as one of those sites of integration (Nusse and Varmus 1982). Over the next 30 years, the other members of the pathway were identified, and their role in development and disease, particularly cancer, were characterized (Nusse and Varmus

2012). While the pathway is conserved in all metazoan animals, the pathway is particularly complex in mammals consisting of 19 Wnt ligands and 10 receptor (McDonald and Silver 2009). While the number of Wnt members is large, redundancy exists within the pathway particularly among Wnts and LRP5/6 (McDonald and Silver 2009).

The Wnt pathway, like other embryonic pathways such as Hippo, Hedgehog, and Notch, plays an important role in development through directing cell proliferation, polarity, and fate (McDonald and Silver 2009). It can further be subdivided into the non-canonical planar cell polarity (PCP) and Wnt/Ca²⁺ pathways, and the canonical Wnt/ β -catenin pathway (Clevers 2006; Niehrs 2012). The canonical pathway is inactive in the absence of Wnt or the presence of inhibitors including the secreted frizzled related proteins (SFRPs) and Dickkopf-related proteins (DKKs) (**Fig. 1**). In this state, the Axin complex consisting of Axin, adenomatous polyposis coli gene product (APC), casein kinase 1 (CK1), and glycogen synthase kinase 3 β (GSK3 β) facilitates phosphorylation of β -catenin by CK1 and GSK3 β . Phosphorylated β -catenin is targeted for degradation in the proteasome. Activation of the canonical pathway initiates when Wnt binds to the receptor Frizzled (FZD) and the co-receptor, low density lipoprotein receptor-related protein 5 (LRP5) or LRP6. This binding recruits Dishevelled (DVL) to the Wnt-Fzd-LRP5/6 complex and inhibits the Axin complex and phosphorylation of β -catenin. No longer phosphorylated, β -catenin accumulates in cytoplasm, allowing it to translocate to

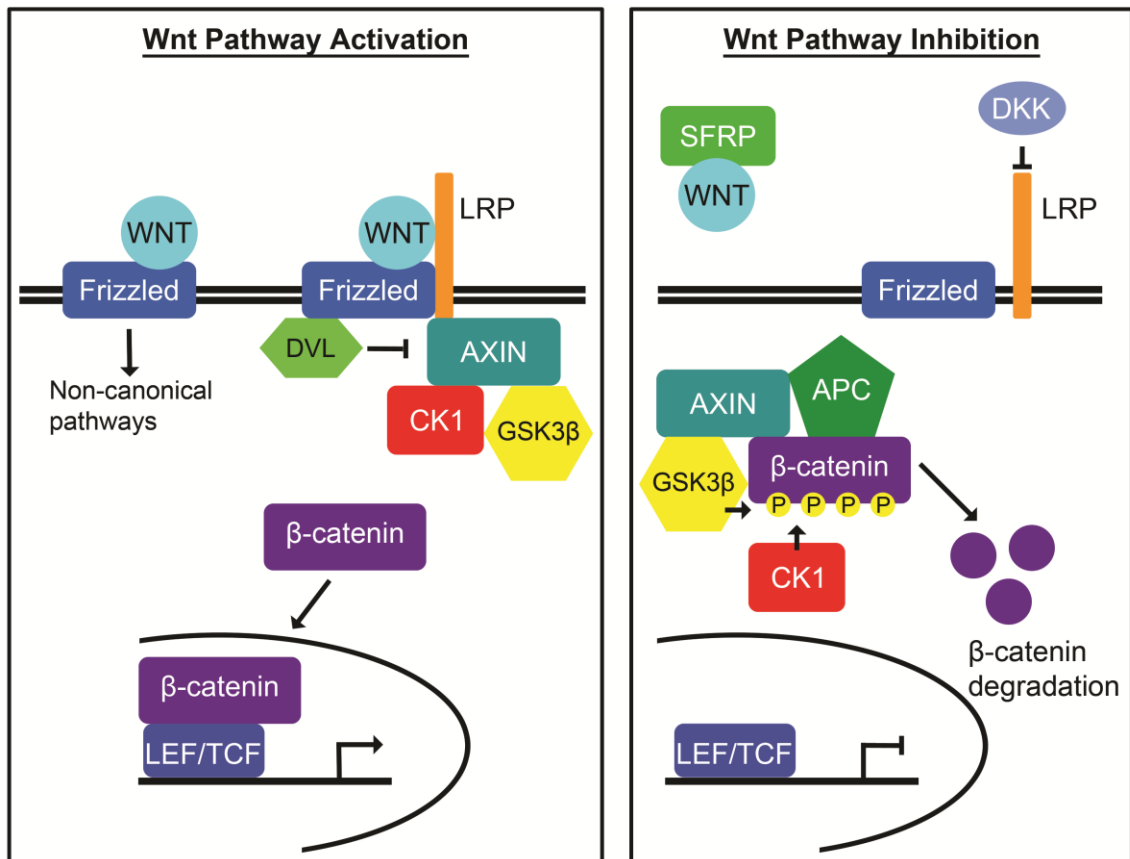


Figure 1: The canonical Wnt pathway

Overview of the canonical Wnt pathway. In the active state, Wnt binds Frizzled (FZD) and LRP. Dishevelled (DVL) and Axin are recruited to the Wnt-Fzd-LRP complex, which inhibits the Axin complex. β -catenin is no longer phosphorylated and can translocate to the nucleus to activate transcription of target genes. In the inhibited or inactive state, Wnt is no longer bound to Frizzled and β -catenin is phosphorylated by the Axin complex, leading to its degradation. (Adapted from Kephart et al. 2015)

the nucleus, form a complex with T cell factor/lymphoid enhancer factor (TCF/LEF), and activate transcription of Wnt target genes (McDonald and Silver 2009).

Interestingly, the planar cell polarity pathway inhibits the canonical Wnt signaling pathway, suggesting that while the different Wnt signaling pathways are often thought of as distinct entities, crosstalk does occur (Kikuchi et al. 2011).

1.2.1 Secreted frizzled related proteins

Inhibition of the Wnt pathway also occurs through several families of secreted Wnt inhibitors, including Wnt-inhibitory factor 1 (WIF), Dickkopf proteins (DKK), Sclerostin (SOST), insulin-like growth factor binding protein 4 (IGFBP-4), and secreted frizzled related proteins (SFRPs). WIFs inhibit WNT; DKKs, SOST, and IGFBP-4 inhibit LRP5/6; however, the largest family of Wnt inhibitors are the SFRPs which exert their effect through binding with Wnt, Fzd, and other SFRPs (Bovolenta et al. 2008; Kikuchi et al. 2011; Cruciat and Niehrs 2013).

SFRPs were first identified through the discovery of SFRP3's (also known as FRZB) role in cartilage formation (Hoang et al. 1996) and shown to antagonize Wnt (Leyns et al. 1997; Wang et al. 1997). After the discovery of SFRP3, four additional SFRPs were identified, making it the largest family of Wnt inhibitors (Jones and Jomary 2002; Bovolenta et al. 2008). This family is further subdivided into two subgroups, with SFRP1, SFRP2, and SFRP5 forming one subgroup and SFRP3 and SFRP4 forming a second subgroup (Bovolenta et al. 2008). Like many of the other Wnt pathway members,

some redundancy also exists among the SFRP proteins. In particular SFRP1, SFRP2, and SFRP5 are redundant in early development in mice (Satoh et al. 2008).

Several mechanisms have been described for SFRPs' actions on the Wnt pathway, including binding to Wnts, Fzds, and each other (Bovolenta et al. 2008). Exactly how SFRPs interact with the rest of the pathway is likely to be Wnt-, Fzd-, or SFRP-dependent and context specific. While Wnts do not bind exclusively to one SFRP nor do SFRPs bind exclusively to one Wnt, some specificity does exist. One study identified SFRP3 as capable of inhibiting signaling from Wnt1 and Wnt8, but not Wnt3a, Wnt5a, or Wnt11 in *Xenopus* (Wang et al. 1997). In addition, some evidence exists for SFRPs modulating cellular signaling by binding to proteins not normally associated with the Wnt pathway. In one example, SFRP3 bound to EGF to block EGF-induced fibroblast proliferation *in vitro* and interacted with EGF in mouse and *Xenopus* embryogenesis (Scardigli et al. 2008).

Structurally, SFRPs are composed of two domains, a cysteine-rich domain (CRD) which shares 30-50% homology with the CRD domains of the Fzd receptors and a netrin-related motif (NTR) (Cruciat and Niehrs 2013). Which domain(s) are important for SFRPs' effects remains controversial. Some report the CRD domain being necessary and sufficient for Wnt binding and inhibition (Leyns et al. 1997), while others find the NTR domain necessary as well (Bhat et al. 2007; Lopez-Rios et al. 2008).

While SFRPs were originally identified as inhibitors of the Wnt pathway, more recently, the Wnt pathway was shown to be finely tuned to SFRP levels (Xavier et al. 2014). Low levels of SFRP1 activate the Wnt pathway while higher levels inhibit. Further, this enhancement or suppression of Wnt signaling varied by cell context, particularly cell-type and the presence or absence of particular frizzled receptors. In addition, SFRPs have also been shown to inactivate the PCP pathway, which in turn would result in activation of the canonical pathway (Satoh et al. 2008). Consistent with these observations, SFRP-mediated activation of the canonical pathway has been shown in *Xenopus* (Swain et al. 2005).

1.3 The Wnt pathway's role in skeletal myogenesis

1.3.1 Skeletal myogenesis

Understanding myogenesis may provide clues to RMS tumor biology as RMS demonstrates features of skeletal muscle and expresses many of the same proteins as myoblasts and myotubes. As described in section 1.1.2 most evidence suggests a myogenic cell of origin for RMS, particularly for aRMS.

Skeletal myogenesis differs depending on the stage of development: embryonic, fetal/neonatal, and adult (Murphy and Kardon 2011; Belyea et al. 2012). In the embryonic phase, the primary myotome, an embryonic structure derived from somites that gives rise to the skeletal muscles of the trunk and limbs (Parker et al. 2003), and basic muscle pattern are established. Fetal and neonatal myogenesis generate the adult

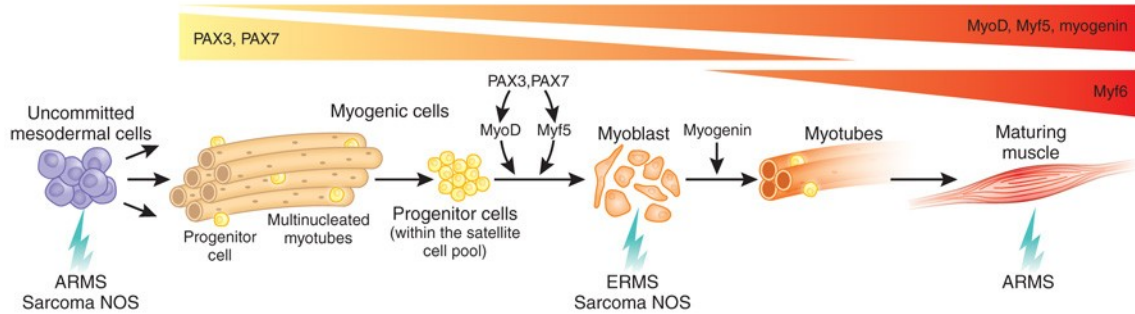


Figure 2: Model of skeletal myogenesis, with possible cellular origins of rhabdomyosarcoma as suggested experimentally.

Muscle specification from the mesoderm depends on myogenic transcription factors (such as PAX3, PAX7, MyoD, Myf5, myogenin and Myf6). Postnatal muscle maintenance and regeneration invokes quiescent muscle precursor cells within the satellite cell pool that proliferate, terminally differentiate and fuse to generate multinucleated myotubes. Depending on the set of oncogenes used and the developmental age of the cells, low-passage MSCs can generate alveolar rhabdomyosarcomas and undifferentiated sarcomas, whereas low-passage myoblasts can form embryonal rhabdomyosarcomas and undifferentiated sarcomas. Alternatively, it has been suggested that alveolar rhabdomyosarcomas arise from maturing muscle. ARMS, alveolar rhabdomyosarcoma; ERMS, embryonal rhabdomyosarcoma; NOS, not otherwise specified. (Katie Vicari) Reprinted by permission from Macmillan Publishers Ltd: NATURE MEDICINE Hettmer, S. and A. J. Wagers (2010). "Muscling in: Uncovering the origins of rhabdomyosarcoma." *Nat Med* 16(2): 171-173, copyright 2010.

musculature and allow for growth and development of muscle. Finally, adult myogenesis is responsible for postnatal growth and repair (Belyea et al. 2012). During muscle development and postnatal muscle regeneration, mononucleated progenitor cells undergo amplification and asymmetric differentiation along a myogenic lineage to form multinucleated myotubes and ultimately myofibers, which are the terminally differentiated unit of skeletal muscle (**Fig. 2**). In both fetal and postnatal development, a small population of mononuclear muscle stem cells (fetal) or satellite cells (postnatal) remains undifferentiated and retains the ability to proliferate and differentiate in response to growth signals or tissue damage (Belyea et al. 2012).

Myogenesis is controlled through a series of Myogenic Regulatory Factors (MRF), including MyoD, Myf5, Myf6 (Mrf4), and Myogenin (**Fig. 2**). The roles for the MRF family members differ by stage of myogenesis. MyoD and Myf5 are both required for the formation of skeletal muscle in embryos, while myogenin plays a critical role during fetal myogenesis, as without it undifferentiated myoblasts are unable to form muscle fibers. In adult myogenesis, satellite cells, upon activation and commitment to the myogenic lineage, express either or both MyoD and Myf5 prior to entering the cell cycle. Expression of Myf5 continues in myoblasts, while MyoD continues into myoblasts and myofibers. Myogenin and Myf6 are expressed in myocytes and myofibers and are associated with terminal differentiation and fusion (Parker et al. 2003).

Paired box transcription factors, Pax3 and Pax7, also play important roles in myogenesis. Pax3 is expressed at the embryonic stage, decreasing after E12.5, although occasionally it has been found expressed in the satellite cell population (Parker et al. 2003; Bentzinger et al. 2012). Pax7 is not expressed until later in development; however, it labels satellite cells and is necessary for maintaining the satellite cell pool and postnatal growth and regeneration (Parker et al. 2003).

While satellite cells are the most common progenitors for adult myogenesis, many other cells have been shown to have myogenic potential and the ability to form myotubes (Bentzinger et al. 2012). These include bone marrow derived progenitors, skeletal muscle side population cells, mesoangioblasts, pericytes, CD133 (Prom)+ progenitors, and PW1 (Peg3)+ interstitial cells. However, none of these appear to be able to replenish the satellite cell pool or repair tissue following injury (Bentzinger et al. 2012).

1.3.2 The Wnt pathway's function in skeletal myogenesis

This section was adapted from Brian Belyea, Julie Grondin Kephart, Jordan Blum, David G. Kirsch, and Corinne M. Linardic, "Embryonic Signaling Pathways and Rhabdomyosarcoma: Contributions to Cancer Development and Opportunities for Therapeutic Targeting," Sarcoma, vol. 2012, Article ID 406239, 13 pages, 2012. doi:10.1155/2012/406239. It was written by Julie Kephart and was published under a Creative Commons Attribution License, which permits

unrestricted use, distribution, and reproduction in any medium, provided the original work is properly cited.

During skeletal myogenesis, Wnt has various roles in embryonic, fetal, and neonatal myogenesis. At the onset of embryonic myogenesis, MyoD is activated in the presomitic mesoderm by Wnt7a signaling through a β -catenin independent pathway (Brunelli et al. 2007). In contrast, Myf5 expression in somites is dependent on β -catenin signaling, and expression of β -catenin is sufficient to induce Myf5 expression in the somites (Borello et al. 2006). Interestingly, in the presomitic mesoderm, both β -catenin signaling and sonic hedgehog/Gli signaling are required for Myf5 expression (Borello et al. 2006). During somite patterning, Wnt1 and Wnt3 are secreted from the dorsal neural tube and Wnt4, Wnt6, and Wnt7a from the surface ectoderm (Bentzinger et al. 2012). Further, Wnt1 preferentially activates Myf5, and Wnt7a and Wnt3a preferentially activate MyoD; however, Wnt4, Wnt5a, and Wnt6 can moderately activate both MyoD and Myf5 expression (Tajbakhsh et al. 1998; Parker et al. 2003). Wnt7a's effects depend on PKC (non-canonical Wnt) signaling (Bentzinger et al. 2012). During embryonic myogenesis, β -catenin is required for dermomyotome and myotome formation, but not required for embryonic axial myogenesis (Hutcheson et al. 2009). SFRPs, if expressed in explanted somatic mesoderm or newly formed somites or injected into the placenta of pregnant females, can inhibit embryonic myogenesis (Borello et al. 1999; Parker et al.

2003). However, during embryonic myogenesis, cells were no longer sensitive to β -catenin signaling once they had entered the limb (Murphy and Kardon 2011).

Fetal myogenesis, consistent with having different myogenic progenitors than embryonic myogenesis, has different requirements for β -catenin. In contrast to embryonic myogenesis, β -catenin is important for fetal limb myogenesis, particularly in the formation of slow fibers. Further, β -catenin positively regulates the number of Pax7+ myogenic progenitors (Hutcheson et al. 2009; Murphy and Kardon 2011).

In adult myogenesis, the role of the Wnt pathway and β -catenin is multifaceted, as activated β -catenin promotes myogenic lineage progression and differentiation, while non-canonical Wnt signaling promotes satellite cell proliferation and inhibits differentiation. In regenerating muscle, a transition from Notch to Wnt signaling is important for the progression along the myogenic lineage from quiescent satellite cell to fully differentiated muscle (Brack et al. 2008). Consistent with this requirement, four days after satellite cells were placed in culture, members of the Wnt pathway, including canonical Wnts (particularly Wnt3a), Fzd1, Fzd2, and Axin2, were upregulated. In addition, activating or inhibiting the Wnt pathway early (two days) following injury did not alter myogenesis; however, activating the Wnt pathway late (four days) following injury increased myogenic differentiation (Brack et al. 2008). In hematopoietic (non-myogenic) CD45+ stem cells, activation of the Wnt pathway, using LiCl, an inhibitor of GSK3 β , is sufficient to allow these cells to enter the myogenic lineage and undergo

myogenic differentiation (Polesskaya et al. 2003). This myogenic differentiation can be blocked by inhibition of the Wnt pathway using SFRP1, SFRP2, or SFRP3 in satellite cells and CD45+ stem cells (Polesskaya et al. 2003; Brack et al. 2008; Descamps et al. 2008). Interestingly, increased Wnt signaling in the myogenic progenitor cells of aged mice (~24 months) leads to their conversion from a myogenic to fibrogenic lineage and contributes to tissue fibrosis (Brack et al. 2007). Finally, growth of muscle (hypertrophy) following muscle overload appears to require β -catenin expression (Armstrong et al. 2006).

In contrast to its role in promoting differentiation, β -catenin increased proliferation of Pax7+ satellite cells and inhibited their differentiation (Otto et al. 2008; Perez-Ruiz et al. 2008; Murphy and Kardon 2011). In addition, Wnt7a expression through the planar cell polarity pathway (non-canonical Wnt signaling) contributes to the expansion of the satellite stem cell population through symmetric divisions (Le Grand et al. 2009). Expanding the satellite cell pool allows for a greater regenerating capacity following muscle injury. Further, demonstrating the complexity of this pathway in regulating myogenesis, only Wnt1, Wnt3a, and Wnt5a promoted satellite cell proliferation, while Wnt4 and Wnt6 were inhibitory (Otto et al. 2008). Finally, during muscle regeneration Wnt1, Wnt3a, Wnt7a, and Wnt11, the Wnts most often associated with embryonic myogenesis, are not induced, but SFRP1, SFRP2, and SFRP3, antagonists of the Wnt pathway, are induced, suggesting a downregulation of the pathway (Zhao and Hoffman 2004).

SFRP's role in differentiation is not limited to myogenic differentiation, but extends into other mesenchymal cell differentiation pathways. During osteoblastic differentiation, SFRP3 promoted, while SFRP4 inhibited the differentiation of multipotent mesenchymal stromal cells. Interestingly, SFRP3 appeared to signal through inhibition of non-canonical Wnt (Yamada et al. 2013). In addition, SFRP3 also promoted adult mesenchymal stem cells (MSC) to begin osteogenesis (Boland et al. 2004). Finally, it plays an important role in cartilage and joint homeostasis (Lodewyckx et al. 2012).

1.4 The Wnt pathway's role in cancer

This section was adapted from Brian Belyea, Julie Grondin Kephart, Jordan Blum, David G. Kirsch, and Corinne M. Linardic, "Embryonic Signaling Pathways and Rhabdomyosarcoma: Contributions to Cancer Development and Opportunities for Therapeutic Targeting," Sarcoma, vol. 2012, Article ID 406239, 13 pages, 2012. doi:10.1155/2012/406239. It was written by Julie Kephart and was published under a Creative Commons Attribution License, which permits unrestricted use, distribution, and reproduction in any medium, provided the original work is properly cited.

The Wnt/ β -catenin pathway was first identified as protumorigenic when an inactivating mutation in APC was described in human colon cancer (Kinzler et al. 1991; Nishisho et al. 1991; Powell et al. 1992). Wnt signaling's contributions to oncogenesis are unsurprising, as Wnt plays a critical role in cell proliferation, differentiation, and

determination, all pathways whose deregulation can lead to or support oncogenesis. Since the identification of mutant APC in colon cancer, many human cancers have been shown to harbor changes in the Wnt pathway, resulting in upregulated β -catenin activity and target gene expression (Logan and Nusse 2004; Clevers 2006; MacDonald et al. 2009). A number of different mutations lead to pathway deregulation and oncogenesis. The mutations in Wnt pathway members that contribute to tumorigenesis do so in diverse ways including increasing proliferation, preventing apoptosis, and supporting motility and invasion (Weeraratna et al. 2002; Clevers 2006). Also diverse are the proteins that are mutated or otherwise contribute to tumorigenesis including GSK3 in leukemia (Wang et al. 2008) and pancreatic cancer (Ougolkov et al. 2005), Axin2 in colon cancer (Clevers 2006), and LEF1 inactivation in sebaceous (hair follicle) tumors (Clevers 2006). While in some malignancies, Wnt's role is limited to only a subset of tumors, in others Wnt contributes to a large subset of tumors such as in non-small-cell lung cancer, 50% of which contain Wnt activation, which supports proliferation and inhibits differentiation (Akiri et al. 2009). Furthermore, secreted Wnt inhibitors can also contribute to tumorigenesis such as upregulation of SFRP3 is in metastatic renal carcinoma (Hirata et al. 2010). The prevailing view had been that upregulation of the Wnt/ β -catenin pathway was tumorigenic; however, recent evidence suggests the role of Wnt signaling is more complex as Wnt pathway members such as GSK3 interact with other signaling pathways and Wnt signaling is cell or tissue specific.

1.4.1 SFRPs' role in cancer

Similarly to the Wnt pathway, the role of SFRPs in cancer depends on tumor type. In fibro- and liposarcomas (Guo et al. 2008) and carcinomas including breast, prostate, cervical, gastric, and hepatocellular (Zi et al. 2005; Bovolenta et al. 2008; Surana et al. 2013), SFRP1 or SFRP3 was found to be downregulated. Further in fibrosarcomas, overexpression of SFRP3, through the c-met pathway, reduced cellular invasion, motility, soft-agar colony formation, *in vitro* and tumor growth *in vivo* (Guo et al. 2008). The variety of SFRP3-suppressed cancers is unsurprising, knowing SFRPs' inhibitory effect on the Wnt pathway and the role Wnt plays in many malignancies in supporting cell proliferation, inhibition of apoptosis, invasion, and metastasis. SFRP downregulation can occur through allelic loss at the SFRP1 and SFRP3 loci or hypermethylation of the SFRP's promoter area. However, the SFRP3 promoter lacks dense CpG islands, often the site of methylation in other SFRPs, suggesting this is not a likely mechanism of downregulation for SFRP3 (Bovolenta et al. 2008).

In contrast SFRP4 is upregulated in the stroma of endometrial and breast carcinomas and SFRP1 and SFRP2 are overexpressed in glioma cells lines (Jones and Jomary 2002). However, contrasting to their normal role, SFRP1 and SFRP2 in the glioma cell lines appeared to be increasing the signaling of β -catenin. Further, metastatic renal cell carcinoma shows high levels of SFRP3, which is necessary for cell

growth, suppression of apoptosis, and invasion (Hirata et al. 2010). This suggests that SFRPs can both inhibit and promote tumorigenesis in a context-dependent manner.

1.5 The Wnt pathway's role in RMS

This section was adapted from Brian Belyea, Julie Grondin Kephart, Jordan Blum, David G. Kirsch, and Corinne M. Linardic, "Embryonic Signaling Pathways and Rhabdomyosarcoma: Contributions to Cancer Development and Opportunities for Therapeutic Targeting," Sarcoma, vol. 2012, Article ID 406239, 13 pages, 2012. doi:10.1155/2012/406239. It was written by Julie Kephart and was published under a Creative Commons Attribution License, which permits unrestricted use, distribution, and reproduction in any medium, provided the original work is properly cited.

The role of Wnt signaling in RMS is only beginning to be understood. Unlike in many cancers, β -catenin activity is downregulated, despite an increase in Wnt2, in a p53^{-/-}/c-fos^{-/-} mouse model of eRMS and in human eRMS cells (RD). Furthermore, increasing β -catenin activity pharmacologically in these cells induced MyoD expression and promoted differentiation (Singh et al. 2010). A separate study also found that increased Wnt signaling inhibited eRMS cell proliferation and induced MF20, a marker of myogenic differentiation (Chen et al. 2014). In contrast, Wnt3a treatment did not affect the proliferation rate of eRMS cell lines Rh18 and RD, despite increasing levels of active β -catenin (Annavarapu et al. 2013). Additional work may be needed to reconcile these

differences; however, the majority of the evidence does suggest that activated Wnt decreases proliferation and enhances differentiation in eRMS.

In aRMS, GSK3 inhibitors, which result in the activation of β -catenin, appeared to preferentially inhibit cell proliferation and induce apoptosis when compared with eRMS cells (Zeng et al. 2010). Further, GSK3 inhibitors appeared to reduce the activity of the PAX3-FOXO1 protein, as PF is phosphorylated by GSK3. Previous work had demonstrated that inhibiting PF activity through the use of a PAX3-KRAB does inhibit growth of aRMS cells in conditions of low serum or soft agar and inhibits tumor xenograft formation in immunodeficient mice (Fredericks et al. 2000) as well as more recent work showing that inhibition of PF also allows for regression of aRMS tumor xenografts, although in this instance, the inhibition of PF phosphorylation was achieved through a PLK1 inhibitor (Thalhammer et al. 2015). This suggests that PF inhibition, for example through inhibition of GSK3, may provide a therapeutic approach. However, that approach is not likely to offer a permanent solution as preliminary data suggest that the regression of aRMS tumors following inhibition of PF is only temporary (Pandey et al. 2015). Finally, treatment of aRMS cell lines (Rh18 and Rh30) with Wnt3a decreased cell proliferation and increased the markers of skeletal muscle differentiation MyoD1, Myf5, and myogenin (Annavarapu et al. 2013). This was accompanied by morphological changes associated with differentiation.

A number of different studies have also queried human tumor samples for β -catenin activation. In the first study, a small set of samples from patients' tumors, aRMS, eRMS, and sclerosing RMS (sRMS) all show cytoplasmic localization of β -catenin, suggesting that a downregulation of the Wnt pathway is a common feature of RMS tumors; however this downregulation is not due to a mutation in β -catenin (Bouron-Dal Soglio et al. 2009). This was also observed in a different set of patient tumor samples, in which no RMS contained over 25% of cells staining positive for nuclear β -catenin and only 15% of RMS contained any cells staining positive for nuclear β -catenin (Ng et al. 2005). In a study investigating multiple sarcoma subtypes, 50% of sarcomas and 65% of sarcoma derived cell lines showed autocrine canonical Wnt signaling (Vijayakumar et al. 2011), suggesting that Wnt signaling may be important in many subtypes of sarcomas. Of the 45 tumors, 1 was RMS and was positive for β -catenin. Of the 23 cell lines, 1 (RD) was eRMS and positive for β -catenin. A second cell line was listed as RMS (A204), but has subsequently found to be a rhabdoid line (Hinson et al. 2013). Finally, in a set of patient tumor samples, 9 out of 14 (64%) aRMS samples demonstrated membrane or cytoplasmic β -catenin, with 0 out of 14 (0%) of those demonstrating nuclear β -catenin. These samples were further divided into PAX3/7-FOXO1-positive aRMS (5 out of 7 demonstrating membrane or cytoplasmic staining) and PAX3/7-FOXO1-negative aRMS (4 out of 7 demonstrating membrane or cytoplasmic staining). For eRMS, 17 out of 30 (57%) demonstrated membrane or cytoplasmic staining and 2 out of 30 (7%)

demonstrated nuclear staining. This suggests that while β -catenin is present in RMS, Wnt pathway signaling is diminished. Finally, this decrease is not due to inability to be activated, as stimulating the pathway with Wnt3a results in activation (Annavarapu et al. 2013).

In an effort to understand the genomic changes occurring in RMS, several large genome screens and other unbiased approaches have also queried human RMS tumors for mutations. Overall, aRMS tumors harbor fewer mutations than eRMS tumors (Shukla et al. 2012; Chen et al. 2013; Shern et al. 2014). Most hypothesize this is due to PF and other fusion genes' strong tumorigenic ability. All three studies identified activating β -catenin mutations in eRMS samples, ranging from 3-7% of eRMS samples, but not in PF-positive aRMS samples. Further, 20% of eRMS samples demonstrated nuclear β -catenin staining, suggesting active β -catenin (Chen et al. 2013). Taken together, these data indicate a possibility for active β -catenin to be contributing to a small subset of eRMS tumors, but showed no evidence for a role for active β -catenin in aRMS.

1.6 Targeting the Wnt pathway in cancer

This section was adapted from Brian Belyea, Julie Grondin Kephart, Jordan Blum, David G. Kirsch, and Corinne M. Linardic, "Embryonic Signaling Pathways and Rhabdomyosarcoma: Contributions to Cancer Development and Opportunities for Therapeutic Targeting," Sarcoma, vol. 2012, Article ID 406239, 13 pages, 2012. doi:10.1155/2012/406239. It was written by Julie

Kephart and was published under a Creative Commons Attribution License, which permits unrestricted use, distribution, and reproduction in any medium, provided the original work is properly cited.

Regarding the Wnt pathway, most drugs being developed as cancer therapeutics are aimed at inhibiting the pathway (Barker and Clevers 2006; Watanabe and Dai 2011; Madan and Virshup 2015) since as described above when Wnt signaling is mutated in human cancer it is usually upregulated. These inhibitors work at different levels of the Wnt pathway; for example, XAV939 inhibits Axin, while iCRT-3, 5, and 14 inhibit the β -catenin-TCF interaction (Huang et al. 2009; Gonsalves et al. 2011). Recently, a phase I trial evaluating a chimeric humanized monoclonal antibody against FZD10 (Frizzled Family Receptor 10) has opened for patients with synovial sarcoma, so inhibiting the Wnt pathway at the level of a Frizzled receptor may be a possibility. The anthelmintic compound niclosamide also downregulates Wnt signaling through Dvl2 and has been effective in inhibiting colorectal cancer cells *in vitro* and controlling tumor growth in a murine xenograft model of colorectal cancer *in vivo* (Osada et al. 2011).

For RMS, current evidence suggests that one would need to activate the Wnt pathway. Such drugs include lithium chloride and lithium salts, which are known to activate the Wnt pathway through inhibition of GSK3 (Klein and Melton 1996). Underscoring the relative safety record of lithium salts, they are used to treat bipolar disorder not only in adulthood but during older childhood and adolescence (Thomas et

al. 2011), and even during pregnancy, with limited risk to the fetus despite equilibration across the placenta (Newport et al. 2005; Pearlstein 2008). Lithium chloride was also studied in adult patients with low-grade neuroendocrine tumors (NET), as GSK3 β regulates growth and hormone production in NETs; however, it was ineffective at inhibiting NET growth (Lubner et al. 2011).

In recent years, other drugs that activate the Wnt pathway have been developed. Maleimide derivatives SB216763 and SB415286 and indirubin analogs BIO and INO all selectively inhibit GSK3 (Yost et al. 1996; Coghlan et al. 2000; Park et al. 2009). Further, indirubin derivatives are being developed for the treatment of Alzheimer's disease as they inhibit GSK3 β and CDK5. BIO is the main active ingredient of a traditional Chinese medicine used for cancer treatment (Yost et al. 1996; Park et al. 2009). WAY-316606, a small-molecule inhibitor of SFRP1, was shown to stimulate bone formation in an *in vitro* model of osteoporosis (Bodine et al. 2009).

1.7 Collaborative work

Some of the work discussed in this dissertation was collaborative. Any figure or data containing collaborative work has been noted along with the role of the collaborator. Much of the collaborative work was performed by several students I had the great fortune of mentoring: Dr. Rosanne Tiller (Duke University medical student), Yi Zhang (Duke University undergraduate student), Dayoung Ko (Duke University undergraduate student), Margaret DeMonia (Elon University undergraduate student),

and Eric Lin (Duke University undergraduate student). I have chosen to include their work as it contributes important information regarding the role of SFRP3 or the Wnt pathway in aRMS. Furthermore, I was involved in the conception of the experiments and in many cases continued the project once the student completed his or her time in the laboratory.

2. Material and methods

2.1 *Microarray*

Microarray analysis (**Fig. 4**) of PAX3-FOXO1-expressing human skeletal muscle myoblast cells (HSMMs; Lonza) was conducted by expressing pK1-PAX3-FOXO1 (previously referred to as pK1-PAX3-FKHR (Galili et al. 1993)) or an empty vector in early passage HSMM cells and grown in defined medium (Clonetics SkGM-2 bullet kit) (Naini et al. 2008). Populations of HSMMs containing an empty vector or PF were harvested prior to senescence and a population containing PF were harvested after senescence bypass. RNA was isolated using an RNeasy kit (QIAGEN) according to the manufacturer's protocol. The Duke University Microarray Facility hybridized Affymetrix U133A arrays according to the manufacturer's instructions. CEL files of all samples were normalized by RMA using Expression Console software (Affymetrix), zero transformed against the average expression levels of the same probe sets of the vector-expressing control HSMMs, filtered by indicated criteria, clustered using Cluster 3.0 software, and displayed with TreeView as previously described (Chen et al. 2010; Tang et al. 2012). This microarray can be found in the Gene Expression Omnibus database (GEO accession number GSE40543). Sample preparation was performed by Lisa Crose (Department of Pediatrics, Duke University Medical Center). All microarray analyses were performed by Jen-Tsen Ashley Chi (Department of Molecular Genetics and Microbiology, Duke University).

Microarray analysis of SFRP3 shRNA-expressing Rh28 cells was performed as follows: Rh28 cells (human PF-positive aRMS cell line) were transduced with an empty vector (V) or SFRP3 shRNAs (SFRP3 sh3 and SFRP3 sh5). Cells were maintained in RPMI + 10% tetracycline-screened FBS (Hyclone). 1×10^6 cells at population doubling (PD) 18 were plated in 6 cm dishes on day 0, treated with growth media (RPMI + 10% tet-screened FBS) or growth media supplemented with 4 $\mu\text{g}/\mu\text{L}$ doxycycline on days 1-5, and harvested on day 6. Growth media or growth media supplemented with doxycycline was replaced daily. Cells were detached using trypsin followed by pelleting by centrifugation, media was removed, and pellets were frozen at -80°C until use.

RNA quality was verified by the Duke University Microarray facility. Affymetrix U133A arrays were hybridized by the Duke University Microarray Facility according to the manufacturer's instructions. Jen-Tsan Ashley Chi and Po-Han Chen (Department of Molecular Genetics and Microbiology, Duke University) performed the microarray analysis. CEL files of all samples were normalized by RMA using Expression Console software (Affymetrix), zero transformed against the average expression levels of the same probe sets of the empty vector expressing, doxycycline treated control Rh28 cells, filtered by indicated criteria, clustered using Cluster 3.0 software. The robust multi-array average (RMA)-normalized data were selected by significance analysis (SAM) to identify genes that were consistently induced or

repressed by both SFRP3 shRNAs and displayed with TreeView. All the microarray data have been submitted to the Gene Expression Omnibus database (GEO accession number GSE67999).

2.2 Cell Lines

Human RMS cell lines RD, Rh28, and Rh30 were gifts from Tim Triche (Children's Hospital of Los Angeles, CA, USA) in 2005; Rh36, SMS-CTR, and Rh3 were gifts from Brett Hall (Columbus Children's Hospital, OH, USA) in 2006; and Rh41 were obtained from Children's Oncology Group in 2013. Rh28, Rh3, and Rh30 cells demonstrate aRMS histology and express PF. RD, Rh36, SMS-CTR, and Rh41 cells demonstrate eRMS histology. Rh28 and Rh3 originate from the same patient and ought to be considered related (Barr et al. 1998). Identity of cell lines (except Rh41) was confirmed using cell line authentication performed in 2011 using STR analysis (Promega PowerPlex 1.2) conducted by the Fragment Analysis Facility at the Johns Hopkins Genetic Resources Core Facility (Baltimore, MD, USA) and in 2014 (Promega Powerplex 18D) conducted by the Duke University DNA analysis facility (Durham, NC, USA). Rh41 cells were STR verified by the Children's Oncology Group prior to distribution.

RMS cell lines were maintained in RPMI 1640 media (Sigma) supplemented with 10% FBS (Gibco), unless they contained a doxycycline-inducible shRNAs, in which case the 10% FBS was replaced by tetracycline-screened FBS (Hyclone).

HT1080 and 293T cells were obtained from ATCC through the Duke University Cell Culture facility and were maintained in DMEM media (Sigma) supplemented with 10% FBS (Gibco). WI-38 cells were obtained from ATCC through the Duke University Cell Culture facility and were maintained in MEM media (Gibco) supplemented with 10% FBS (Gibco), 1.0 mM sodium pyruvate (Gibco), and 0.1 mM non-essential amino acids (Gibco).

2.3 Expression of shRNAs and cDNAs in cells

2.3.1 Expression of SFRP3 shRNAs and HA*-SFRP3

SFRP3 shRNA sequences (**Table 1**) were obtained from the RNAi consortium (Broad Institute, Cambridge, MA) and annealed oligos were ligated into pLKO.1 puro (Addgene 8453), Tet-pLKO-puro (Addgene 21915), and Tet-pLKO-neo (Addgene 21916) plasmids.

Table 1: SFRP3 shRNAs sequences

	Mature Antisense Sequence (5' to 3')
SFRP3 sh1 forward	ATAAGGCTGTAATTAGATCGG
SFRP3 sh2 forward	AATAGGCTTACATTACAGCG
SFRP3 sh3 forward	ATCTTAGTCATGTTCCAGGGC
SFRP3 sh4 forward	TTCCTCATTAACATTAAGTGG
SFRP3 sh5 forward	TTTACTGAGTCCAAGATGACG

HA*-SFRP3 was a gift from Ugo Borello (INSERM/Stem Cell and Brain Research Institute, Bron Cedex, Lyon, France) and was subcloned into the EcoRI and Sall sites in the pBABE puro retroviral backbone (Borello et al. 1999). HA*-SFRP3 is the murine

homolog of human SFRP3 and contains an HA-tag between the CRD and NTR domains (Fig. 3). Nucleotide mismatches between the shRNA sequences (two in SFRP3 sh3, three in SFRP3 sh5) and HA*-SFRP3, rendering it shRNA-resistant.



Figure 3: Diagram of SFRP3 and HA*-SFRP3

For generation of virus containing the SFRP3 shRNAs, a lentiviral packaging plasmid [psPAX2 (Addgene plasmid #12260)], VSV-G envelope plasmid [PMD2 (Addgene plasmid #12259)], and an empty vector (pLKO.1, tet-pLKO-puro, tet-pLKO-neo) or shRNA containing plasmid were transfected into 293T cells using Fugene on day 0. On day 1, the media was replaced with fresh media. On days 2 and 3, the media was harvested from the 293T plates, filtered through a 0.45 μm filter (Corning), combined with polybrene, and added to the cells' media for transduction. A pore size of 0.45 μm permits virus particles to pass through the filter while preventing the passage of most pathogens, including bacteria and fungi. On day 4 the media was replaced, and on day 5 selection with an appropriate agent was initiated. Once selection was complete, as

indicated by death of a non-transduced control plate, the selection agent was removed from the media.

For generation of virus containing HA*-SFRP3, a retroviral packaging plasmid (pCL-10A1) and an empty vector (pBABE puro) or HA*-SFRP3 were transfected into 293T cells using Fugene on days 0 and 1. On day 2, the media was replaced with fresh media. On day 3, the media was harvested from the 293T plates, filtered through a 0.45 μ M filter (Corning), combined with polybrene, and added to the cells to be transduced. On day 4 the media was replaced, and on day 5 selection with an appropriate agent was initiated. Once selection was complete, as indicated by death of a non-transduced control plate, the selection agent was removed from the media.

2.3.2 Expression of oncogenic pathway activating cDNAs, including Notch 1 ICD

Oncogenic pathway activating cDNAs were obtained from Kris Wood (Department of Pharmacology and Cancer Biology, Duke University) and have been previously described (Martz et al. 2014). For the oncogenic pathway screen, virus media containing all of the cDNAs was obtained from Kris Wood and allowed to infect Rh28 cells containing doxycycline-inducible shRNAs. For the pathway verification and expression of Notch1 ICD, individual cDNAs in lentiviral vectors for Luciferase, MEK-1 WT, and Notch1 ICD were obtained from the Wood laboratory. Lentiviral particles for the expression of these cDNAs were generated and transduced into cells as described above for SFRP3 shRNAs. As the oncogenic pathway cDNA plasmids contain a

puromycin selection marker, any SFRP3 shRNA plasmid used in conjunction with an oncogenic pathway cDNA contained a neomycin selection marker.

2.4 PCR

RNA was extracted from cell pellets using RNA-Bee reagent (Tel-Test), which is based on a phenol/chloroform method of extraction. RNA for the microarray was extracted using an RNeasy kit (Qiagen), according to the manufacturer's protocol. The RNA was subsequently used to generate cDNA using an Omniscript Reverse-Transcription Kit (Qiagen).

2.4.1 RT-PCR

RT-PCR (semi-quantitative PCR) was performed by combining 5 μ L of cDNA with 30.5 μ L of water, 5 μ L of 10X Red Taq buffer, 2.5 μ L of 2.5 mM dNTPs, 2.5 μ L each of 20 μ M forward and reverse primers, and 2 μ L of RedTaq (Sigma) for a total volume of 50 μ L. Cycling conditions were 95°C for 10 minutes, followed by 25, 28, or 35 cycles of 95°C for 45 seconds, 55°C for 45 seconds, and 72°C for 1 minute, followed by 72°C for 10 minutes. Reactions were kept at 4°C until run on a 2% agarose gel. Primers for RT-PCR are listed in **Table 2**.

Table 2: Primers for semi-quantitative PCR

	Sequence (5'-3')
SFRP1 FW	GTGCGAGCCGGTCATGCAGT
SFRP1 REV	ACACCGTTGTGCCTTGGGGC
SFRP3 FW	GGGGCAAGCAGTGAACGCTGT
SFRP3 REV	TAGTTGCGTGCTTGCCGGGG
SFRP4 FW	CAGCACGCAGGAGAACGCCA
SFRP4 REV	CACCGATCGGGGCTTAGGCG
DKK2 FW	CCAAGGAGGTGCGGGGCAAG
DKK2 REV	GGTAGGCCTGCCCCAGGTTT
WNT5A FW	CGGTCGCTCCGCTCGGATTC
WNT5A REV	CCGTCTCGCGGCTGCCTATC
WNT5B FW	TGAAGCAGAAGGTGGACAGCTTCAGT
WNT5B REV	GGCGGTCTCTCGGCTGCCTAT
FZD5 FW	GCGGGATCCGTGGAGAGTCCT
FZD5 REV	AGCAGCAGCAACAGCGAGGG
GAPDH FW	GAGAGACCCTCACTGCTG
GAPDH REV	GATGGTACATGACAAGGTGC
P21 FW	ACTCAGAGGCGCCATGTCA
P21 REV	GCCGCCGTTTTTCGACCCTGA
Luciferase FW	CAGTATGGGCATTTCCGAGC
Luciferase REV	AGCGACACCTTTAGGCAGAC

2.4.2 qPCR

Quantitative PCR (qPCR) was performed by combining 1 μ L of cDNA with 8.5 μ L of water, 3 μ L of forward and reverse primer mix (5 μ M each), and 12.5 μ L of Universal Sso Advanced SYBR (BioRad) or SYBR Green (BioRad), depending on the PCR machine used (BioRad iQ5 or BioRad CFX, respectively), for a total volume of 25 μ L. Cycling conditions were 95°C for 10 minutes, followed by 40 cycles of 95°C for 45 seconds, 55°C for 45 seconds, and 72°C for 1 minute, followed by 72°C for 10 minutes. This was followed by melt curve, from 55°C to 95°C in 0.5°C increments. A melt

curve was used to confirm that each PCR reaction only resulted in one PCR product, thus confirming that the primers did not amplify off targets. Primers were not used if they produced more than one PCR product. Each sample was run in triplicate. For each primer, a dilution curve was used to calculate the efficiency based on the following formula:

$$Efficiency = 10^{\left(\frac{-1}{slopes}\right)} - 1$$

If the efficiencies of the target gene (gene of interest) primer and the reference gene primer were not different, efficiency was not included in the fold change calculation.

The following equations were used to calculate fold change:

$$Fold\ change = 2^{-\Delta\Delta Cq}$$

$$\Delta\Delta Cq = \Delta Cq\ sample - \Delta Cq\ control$$

$$\Delta Cq = Cq\ target - Cq\ reference$$

If the efficiencies of the target gene primer and the reference gene primer were different, efficiency was included in the fold change calculation and the following equation was used:

$$Fold\ change = \frac{E\ target(\Delta Cq\ target\ (MEAN\ control-sample))}{E\ ref\ (\Delta Cq\ ref\ (MEAN\ control-sample))}$$

Table 3: Primers for qPCR

	Sequence (5'-3')
MYOD FW	GGTCCCTCGCGCCCAAAGAT
MYOD REV	CAGTTCTCCCGCCTCTCCTAC
MYOG FW	CAGTGCACTGGAGTTCAGCG
MYOG REV	TTCATCTGGGAAGGCCACAGA
MYF6 FW	CCCCTTCAGCTACAGACCCAA
MYF6 REV	CCCCTTGGAATGATCGGAAAC
AXIN2 FW	ACAACAGCATTGTCTCCAAGCAGC
AXIN2 REV	GCGCCTGGTCAAACATGATGGAAT
SFRP3 FW	GAGGAGCTGCCAGTGTACGAC
SFRP3 REV	GAAAATCAGCTCCGTCGG
HEY1 FW	GTTCGGCTCTAGGTTCCATGT
HEY1 REV	CGTCGGCGCTTCTCAATTATTC
HES1 FW	TCAACACGACACCGGATAAAC
HES1 REV	GCCGCGAGCTATCTTTCTTCA
CTBP2 FW	ATCCACGAGAAGGTTCTAAACGA
CTBP2 REV	CCGCACGATCACTCTCAGG
CCND1 FW	AACTACCTGGACCGCTTCTCT
CCND1 REV	CCACTTGAGCTTGTTACCA
WNT6 FW	GGCTGTGGGCAGCCCCTTGGTTAT
WNT6 REV	CGAGCTAGCTCTGCCACCACT
NAV2 FW	GCTGCTTCCTTGTGGCTATC
NAV2 REV	TAACCCCGTCTGTCAACTCC
APC FW	GGAAGCAGAGAAAGTACTGGA
APC REV	CTGAAGTTGAGCGTAATACCAG
SNAI2 FW	TGTTGCAGTGAGGGCAAGAA
SNAI2 REV	GACCCTGGTTGCTTCAAGGA
GAPDH FW	ATGGGGAAGGTGAAGGTCG
GAPDH REV	GGGGTCATTGATGGCAACAATA

Samples were always run in triplicate and the average of the fold change of the triplicates was used for analyses. Sequences for qPCR primers are located in **Table 3**. Equations for efficiency and fold change were obtained from IDT's qPCR Applications Guide (<http://www.idtdna.com/pages/docs/default-source/user-guides-and-protocols/primetime-qpcr-application-guide-3rd-ed-.pdf?sfvrsn=20>)

2.5 Immunoblotting

A mixture of protease and phosphate inhibitors was added to a Tris/RIPA lysis buffer prior to use. Cells were lysed either by adding buffer to a cell pellet and pipetting to resuspend the pellet or directly onto a dish of washed cells then scraped using a cell scraper. The lysate was passed through a 21g needle to shear DNA. The protein concentration of the lysate was determined by a DC assay (BioRad). 50 µg of lysate per sample was loaded onto a SDS-PAGE acrylamide gel. Acrylamide gels varied from 8% to 15% acrylamide, depending on the size of the proteins of interest. Proteins were transferred to a polyvinylidene difluoride membrane (PVDF, Millipore) and immunoblotted with primary antibodies. Secondary HRP-labeled antibodies (goat anti-rabbit or goat anti-mouse, Invitrogen) were added to the membrane. Chemoluminescence (Amersham, GE Healthcare) was used to exposed film and visualize the protein. Membranes were stripped of antibodies using a guanidine chloride solution before probing for a different protein.

The following antibodies were used for immunoblotting: anti-p21 (Santa Cruz #sc-6246), anti-HA (Roche #11583816001), anti-cleaved caspase 3 (Cell Signaling #9661), and anti-actin (Sigma #A5441).

2.6 MTT, BrdU, cell cycle analysis, and cell growth assays

The MTT assay was used as a surrogate for measuring cell growth. Succinate dehydrogenase enzyme found in mitochondria converts yellow 3-(4,5-Dimethyl-2-thiazolyl)-2,5-diphenyl-2H-tetrazolium bromide methylthiazolyldiphenyl-tetrazolium bromide (MTT) to purple formazan. The intensity of the purple formazan is measured using a spectrophotometer based plate reader. The amount of purple formazan is proportional to the activity of mitochondria, which we assume is proportional to the number of mitochondria and number of cells. However, this assay is not an appropriate measure of cell growth if a change alters the activity of mitochondria disproportionately to the number of cells.

For the MTTs measuring the effects of genetic interventions on growth (either shRNAs or expression of a cDNA), cells were counted and plated at five densities in replicates of six in a 96-well plate. The number of cells plated per well varied by cell line and duration of the assay and are listed for individual experiments in **Table 4**. Media was replaced after 3 days, except for doxycycline-inducible constructs in which half the media was replaced daily. After 3-7 days, depending on the growth rate and confluency of the cells, 1 mg/mL MTT was added to each well. After a 3.5 hour incubation at 37°C,

the media was removed, the cells and purple formazan solubilized in DMSO, and absorbance measured at 540 nm.

Table 4: Conditions for MTT assays with genetic interventions

Figure	Cell Line	Genetic Interventions	Cells plated	Duration
Fig. 5C	Rh28	V, SFRP3 sh3, SFRP3 sh5	10,000	4 days
Fig. 5D	Rh30	V, SFRP3 sh3, SFRP3 sh5	5,000	3 days
Fig. 5G	Rh28	Doxycycline inducible V, SFRP3 sh3, SFRP3 sh5 and V and HA*-SFRP3	10,000	4 days
Fig. 6C	Rh28	Doxycycline inducible V, SFRP3 sh3, SFRP3 sh5	10,000	4 days
Fig. 6D	Rh30	Doxycycline inducible V, SFRP3 sh3, SFRP3 sh5	5,000	4 days
Fig. 7A	SMS-CTR	V, SFRP3 sh3, SFRP3 sh5	5,000	5 days
Fig. 7B	RD	V, SFRP3 sh3, SFRP3 sh5	2,500	4 days
Fig. 7C	HT1080	V, SFRP3 sh3, SFRP3 sh5	2,500	5 days

In order to measure the effects of drug interventions (vincristine, LiCl, or AR-A014418), cells were counted and plated at a known density in replicates of six per treatment condition. The next day, drug was added to all the wells and allowed to incubate with the cells for 48-72 hours. After which, the MTT was read as described for a genetic intervention. **Table 5** contains details of individual MTT experiments.

Table 5: Conditions for MTT assays with drug interventions

Figure	Cell Line	Drug	Genetic Interventions	Cells plated	Duration of drug treatment
Fig. 11A	Rh28	LiCl (0, 1, 3, 10, 30, 100, and 300 mM)	None	12,500	72 hours
Fig. 11D	Rh28	AR-A014414 (0, 1, 3, 10, 30 μ M)	None	15,000	72 hours
Fig. 16	Rh28	Doxycycline (0, 0.5, 1, 2, 4 μ g/mL)	Doxycycline inducible V, SFRP3 sh3, SFRP3 sh5, Luciferase (Control), Notch1 ICD, and MEK-1	8,000	5 days
Fig. 19A	Rh28	Vincristine (0, 0.1, 0.3, 1, 3, 10, 30 nM)	Luciferase (Control) and Notch1 ICD	20,000	48 hours
Fig. 19B	Rh30	Vincristine (0, 0.1, 0.3, 1, 3, 10, 30 nM)	Luciferase (Control) and Notch1 ICD	8,000	48 hours
Fig. 19C	Rh41	Vincristine (0, 0.1, 0.3, 1, 3, 10, 30 nM)	Luciferase (Control) and Notch1 ICD	5,000	48 hours
Fig. 25A	Rh28	Vincristine (0, 0.1, 0.3, 1, 3, 10 nM)	Doxycycline inducible V, SFRP3 sh3	20,000	48 hours

A BrdU assay was used to measure cell proliferation. Cells were grown, counted, and plated at a known density (20,000 cells per well and 10,000 cells per well for Rh28 and Rh30, respectively) in a 96-well plate as described in the MTT assay. After 48 hours of growth, the cells were labeled with BrdU and allowed to incubate for 3.5 hours at 37°C. BrdU incorporation was measured using Cell Proliferation ELISA BrdU

kit (Roche). Absorbance was measured at 370 nm using a spectrophotometer plate reader.

For the cell cycle analysis, cells were genetically manipulated or incubated with drug. On the day of harvest, cells were detached from the dish with trypsin and 1×10^6 cells were counted. Cells were washed in PBS, fixed in ice-cold 70% ethanol in PBS for 15 minutes, and washed again in PBS. The cells were then stained with a PI solution (20 $\mu\text{g}/\text{mL}$ PI and 50 $\mu\text{g}/\text{mL}$ RNaseA in PBS with 0.05% Triton-X) for 30 min at 37°C. Samples were analyzed by flow cytometry by Michael Cook of the Duke University Flow Cytometry Facility.

For cell growth assays, on day -1, Rh28 cells were trypsinized, manually counted using a hemocytometer, and plated at a known density (50,000 cells per dish) in 6 cm dishes in triplicate per treatment condition. On day 0, the cells' media was replaced with media containing either drug or vehicle (water or 25 mM LiCl or DMSO or 30 μM AR-A014414). On days 1, 3, and 5, 3 plates for each dose were trypsinized and counted. The media for day 5 plates was replaced on day 3.

2.7 Differentiation and senescence assays

For the differentiation assay, 3.5×10^6 Rh28 cells expressing an empty vector, SFRP3 sh3, or SFRP3 sh5 were plated in 6 cm dishes. The next day, the media was replaced with either standard growth media (RPMI supplemented with 10% FBS) or differentiation media (DMEM/F12 supplemented with 2% normal horse serum).

Differentiation or fusion media allows normal human skeletal muscle myoblast cells to differentiate and fuse into myotubes (Linardic et al. 2007). Media was replaced every other day for 5 days, after which cells were fixed and stained for MF-20, a marker of myogenic differentiation. MF-20, an anti-sarcomere-myosin hybridoma, (Developmental Studies Hybridoma Bank) was used at a dilution of 1:5. Cells were imaged at 200X magnification (Microscope: Nikon DIAPHOT 200, Camera: Nikon DS-Fi1, Software: NIS-Elements F 3.0).

For the senescence assay, 2.5×10^6 Rh28 cells expressing an empty vector, SFRP3 sh3, or SFRP3 sh5 were plated in 6 cm dishes. WI-38 cells (primary fetal lung fibroblast cells) at population doubling (PD) 54 served as a positive control. The next day the cells fixed and labeled with X-gal staining solution for approximately 22 hours at 37°C in accordance with the manufacturer's directions of the senescence detection kit (Calbiochem). Cells were imaged at 200X magnification (Microscope: Nikon DIAPHOT 200, Camera: Nikon DS-Fi1, Software: NIS-Elements F 3.0). Blue color indicates β -galactosidase (β -gal) activity, a marker of senescent cells.

2.8 *Wnt3a conditioned media*

L/Wnt3a cells and L/Neo cells (control for L/Wnt3a cells) were obtained from Wei Chen (Duke University) and grown in DMEM supplemented with 10% FBS. To generate the conditioned media, cells were plated and media harvested on days 4 and 7, with fresh media added on day 4 after harvest. Cells were plated at approximately the

same density to maintain the consistency of the conditioned media. After harvest, the media was sterile filtered (0.22 μm , VWR) and stored at -80°C until use. Once thawed the media was stored at 4°C for up to a month. For use, growth media was removed from the target cells, the target cells were washed once with PBS, and 100% conditioned media added to the cells.

2.9 Mouse xenograft studies

2.9.1 Genetic suppression of SFRP3 in aRMS xenograft tumors

Rh28 cells stably expressing doxycycline-inducible SFRP3 shRNAs (or empty vector) were implanted subcutaneously into the flanks of SCID/*beige* mice. Mice were monitored twice weekly, and upon observing palpable tumors (**Fig. 20 and 25**) or a 150 mm³ tumor (**Fig. 21, 22**), the drinking water was supplemented with 1 mg/mL doxycycline (Sigma-Aldrich) in 5% w/v sucrose or 5% w/v sucrose (control). Tumors were measured using calipers and tumor volume calculated as $[(\text{width} \times \text{length})^2] / 2$. Mice were sacrificed at 23-24 days (**Fig. 20**), at 14 days (**Fig. 21, 22**), or upon reaching an IACUC-defined maximum tumor burden or decline in health (**Fig. 20-22, 25**). This duration of therapy (23-24 days) was chosen as some of the control mice were reaching the maximum tumor burden. For **Fig. 21, 22**, the later initiation and shorter duration of treatment were chosen to allow for the greatest observation of effects due to SFRP3 suppression before the emergence of resistant cell population. Portions of tumors were

preserved in RNAlater (Qiagen) for PCR or formalin-fixed for IHC. All animal studies were conducted in accordance with policies set forth by the Duke University IACUC.

2.9.2 Activation of Wnt signaling using oral LiCl in aRMS xenograft tumors

1×10^7 Rh28 cells were implanted subcutaneously into the flanks of SCID/*beige* mice. Mice were monitored twice weekly, and upon observing palpable tumors mice began receiving either 200 mg/kg LiCl or vehicle (water) orally 5 days per week. An appropriately sized gavage needle (20g 1.5 curved 2.25 mm ball, Braintree Scientific) was used, based on the weight of the mice. All mice were sacrificed when most of the cohort of mice had received 21 days of treatment. Tumors were removed and weighed. All animal studies were conducted in accordance with policies set forth by the Duke University IACUC.

2.10 Immunohistochemistry

Paraffin-embedded formalin-fixed xenograft tumor samples were sectioned and stained with hematoxylin and eosin (H&E, Sigma) to assess morphology. Tumor sections were also labeled with Ki67 (Dako #M7240) and TUNEL (Trevigen #4810-30-K) to assess proliferation and apoptosis, respectively. Slides were evaluated by a pathologist (Rex Bentley, Department of Pathology, Duke University) with experience in the evaluation of pediatric sarcomas. Ki67 and TUNEL slides were photographed (Microscope: Leica Microsystems #DMLB, Camera: Leica Microsystems #DFC425, Software: Leica Microsystems #LAS V 3.7), and positive and negative cells were counted

manually with the aid of cell counting software (ImageJ, NIH, Bethesda, Maryland). Three tumor sections per treatment condition were labeled with β -catenin (1:200, BD Biosciences #610154). β -catenin slides were photographed (Microscope: Leica Microsystems #DMLB, Camera: Leica Microsystems #DFC425, Software: Leica Microsystems #LAS V 3.7), and the staining intensity of individual cells was counted manually with the aid of cell counting software (ImageJ, NIH, Bethesda, Maryland). The protocol for β -catenin staining was obtained from Heather Whetstone (Benjamin Alman's laboratory, University of Toronto) and Benjamin Alman (Department of Orthopedic Surgery, Duke University and University of Toronto) provided assistance reviewing the slides.

2.11 Drug treatments

For *in vitro* work, lithium chloride (Sigma) was dissolved in water, sterile filtered (0.22 μ m, VWR), and added to the cells' media to achieve final concentrations of 10mM and 25mM. For *in vivo* work, LiCl (Sigma, 62478) was dissolved in autoclaved drinking water provided by DLAR staff to working concentration of 17 mg/mL and sterile filtered (0.22 μ m, VWR). Mice received 200 mg/kg LiCl daily for 5 days a week for a period of 21 days. For both *in vitro* and *in vivo* work, LiCl solutions were freshly made and frozen at -20°C until use.

AR-A014418 was obtained dissolved in DMSO from Oren Becher's laboratory (Department of Pediatrics, Duke University). It was further diluted in growth media and added to cells.

For *in vitro* work, vincristine sulfate (Sigma) was dissolved in methanol, diluted in growth media, and added to culture media for final concentrations as indicated. For *in vivo* work, mice were treated with vincristine sulfate (1 mg/mL, Hospira) or PBS via intraperitoneal injection at a dose of 1 mg/kg weekly for 10 weeks. Assistance with selecting an appropriate vincristine dose and dosing schedule was provided by Peter Houghton (Greehey Children's Cancer Research Institute, University of Texas Health Science Center). For *in vitro* and *in vivo* work, dilutions of vincristine were freshly made and stored at -20°C and 4°C, respectively, until use.

2.12 Statistics

Unless otherwise noted, data is presented as the mean and SE. Statistical analysis was performed using GraphPad Prism (GraphPad). One-way ANOVA, two-way ANOVA, Log-Rank (Mantel-Cox) Test, and unpaired T-test were used as appropriate. IC50 calculations were performed using GraphPad Prism. P values were considered significant under 0.05.

3. SFRP3 is required for aRMS tumorigenesis *in vitro*

This section, including figures, was adapted from Kephart JJ, Tiller RG, Crose L, Slemmons KK, Chen PH, Hinson AR, Bentley RC, Chi JT, and Linardic CM, "Secreted frizzled related protein 3 (SFRP3) is required for tumorigenesis of PAX3-FOXO1-positive alveolar rhabdomyosarcoma," Clin Cancer Res. 2015 Jun 12. pii: clincanres.1797.2014. AACR, the publisher of Clinical Cancer Research, permits authors to reproduce parts of their articles including tables and figures without seeking AACR's permission.

3.1 Introduction

Tumorigenesis in PF-positive tumors is primarily driven through the actions of PF; however as a transcription factor, PF is not an ideal candidate for inhibition through small molecule inhibitors. In addition, PF-positive tumors show very few other genetic changes, limiting the list of candidates for targeted therapy (Shukla et al. 2012; Chen et al. 2013; Shern et al. 2014). This has led our laboratory to approach inhibiting PF-positive aRMS by identifying and targeting pathways downstream from or cooperating with PF to support tumorigenesis. Previously, we have shown FGFR4 (Crose et al. 2012) and RASSF4 (Crose et al. 2014) to be downstream of PF and contribute to tumorigenesis. In this work, we demonstrate that the secreted Wnt antagonist SFRP3 also cooperates with PF to support aRMS tumorigenesis.

3.2 Secreted Wnt inhibitors, including SFRP3, are upregulated in PAX3-FOXO1-expressing primary human myoblasts and in human aRMS cell lines.

Prior work from our laboratory identified a role for the *PAX3-FOXO1* fusion gene in permitting bypass of HSMM cells past the senescence checkpoint (Linardic et al. 2007), thus priming cells for additional genetic changes that generate the aRMS phenotype (Naini et al. 2008). To identify genes that are downstream from or cooperate with PF in this event, we performed gene expression analysis of HSMM cells ectopically expressing the *PAX3-FOXO1* fusion cDNA as they transitioned through pre-senescent and post-senescent stages (Croese et al. 2014). These cell populations were compared to pre-senescent HSMM cells expressing an empty vector. While approximately 1,000 genes were found to be upregulated over 3-fold, one of the pathways that emerged from the analysis was the Wnt pathway.

Review of the gene list revealed changes in both Wnt receptors and ligands, including secreted Wnt activators and inhibitors. In total, seven Wnt pathway members were identified: the secreted inhibitors SFRP1, SFRP3, SFRP4, and DKK2; the canonical and non-canonical Wnt WNT5B (Westfall et al. 2003; Kanazawa et al. 2005); and two non-canonical members WNT5A and FDZ5 (**Fig. 4A,D**). Other genes known to be altered in PF-positive aRMS, including CXCR4, FGFR4, MYOD, MEF2A, served as internal controls for the array (**Fig. 4A**). Expression of the Wnt family genes was verified by RT-PCR of cDNA generated from the original cell set analyzed in

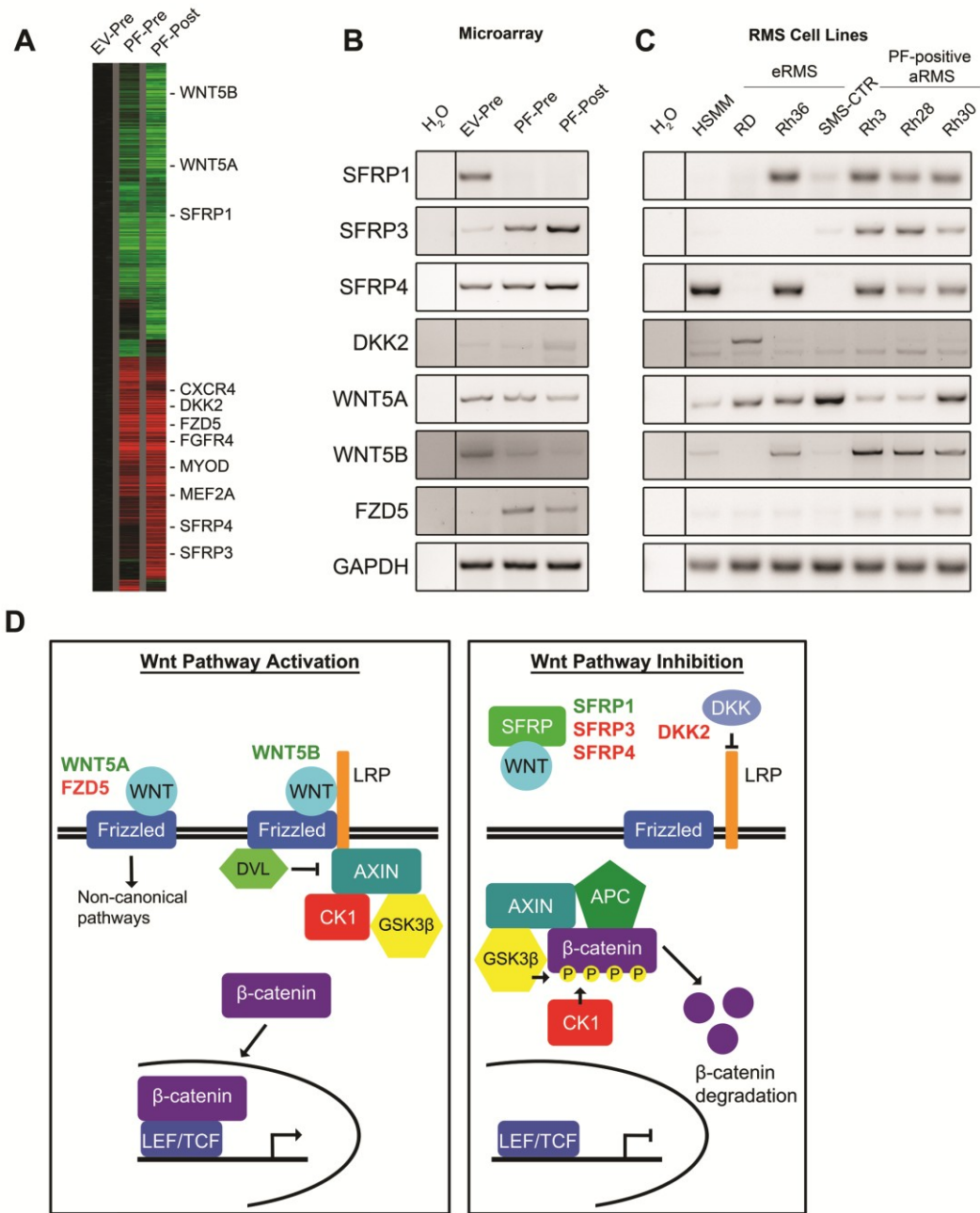


Figure 4: Secreted Wnt inhibitors, including SFRP3, are upregulated in PAX3-FOXO1-expressing primary human myoblasts and in human aRMS cell lines.

(A) Wnt pathway genes identified through transcriptome profiling to be differentially regulated in the PF pre-senescence bypass (PF-Pre) or PF post-senescence bypass (PF-Post) groups when compared to the empty vector pre-senescence (EV-Pre) group. *CXCR4*, *MYOD*, *MEF2A*, and *FGFR4* are known to be upregulated in response to PF and served as internal controls. Portions of these expression data were previously reported (Croese et al. 2014) and this image is modified with permission from the *Journal of Clinical Investigation*. Expression patterns of Wnt pathway genes identified in the array were (B) verified through RT-PCR and (C) assayed in HSMM, eRMS, and aRMS cells using RT-PCR. SFRP3 was chosen for further analysis due to its expression pattern. (D) Diagram of the canonical Wnt pathway. Wnt pathway genes identified in the microarray from (A) are labeled in green (downregulated) or red (upregulated). WNT5B is both a canonical and non-canonical Wnt. Microarray performed by Lisa Croese and analyzed by Jen-Tsen Ashley Chi.

the microarray (**Fig. 4B**). Because these genes were found upregulated in the setting of ectopic expression of PF in HSMM cells, their expression was next evaluated in three human aRMS cell lines (Rh3, Rh28 and Rh30) and compared to a panel of three human eRMS cell lines (RD, Rh36, SMS-CTR). While we found SFRP1, SFRP3 and SFRP4 to all be upregulated in aRMS cell lines, SFRP3 was most interesting since its pattern of expression in aRMS cell lines mirrored that in the HSMM cells expressing PF, and it was preferentially upregulated in aRMS compared to eRMS cells (**Fig. 4C**).

3.3 Genetic suppression of SFRP3 inhibits aRMS cell growth.

To probe the role of SFRP3 in aRMS, we used a loss-of-function approach and generated five lentivirally-delivered shRNA sequences against human SFRP3. Upon stable infection into Rh28 and Rh30 cells, two of the shRNAs reproducibly suppressed SFRP3 expression as measured by RT-PCR (**Fig. 5 A,B**). Monitoring of endogenous SFRP3 at the protein level was not feasible since commercially-available antibodies did not detect SFRP3 protein in our system. As measured by MTT assay, stable expression of the shRNAs in both Rh28 and Rh30 aRMS cells inhibited cell population growth (**Fig. 5 C,D**).

To verify that the growth inhibitory actions of the shRNAs were not due to off-target effects, we sought to concurrently rescue the decreased cell growth with a gain-of-function approach using an ectopically expressed SFRP3. To this end, we took

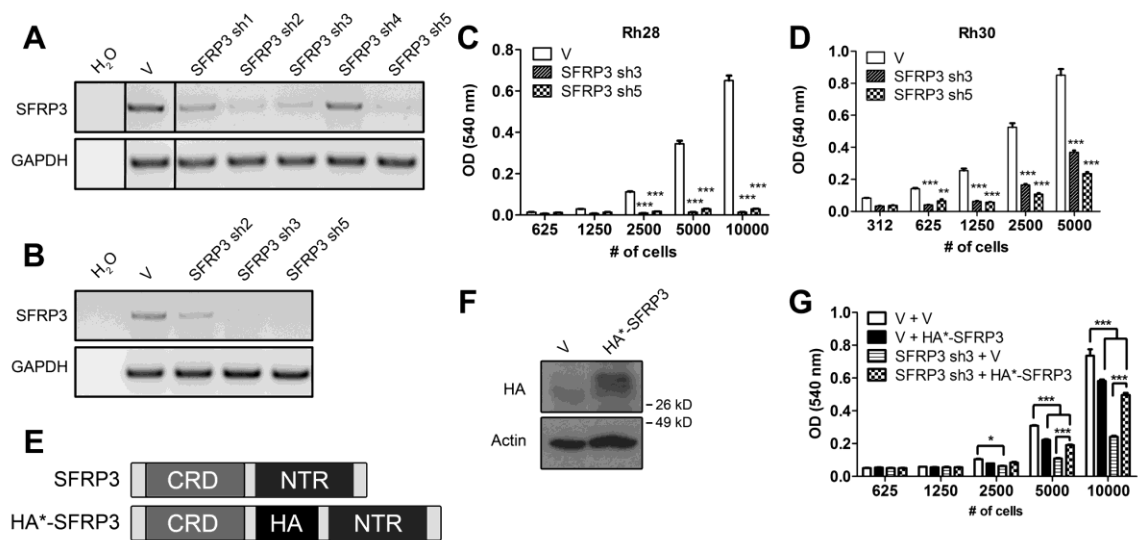


Figure 5: SFRP3 suppression inhibits aRMS cell growth.

shRNAs against SFRP3 were stably expressed in aRMS cell lines Rh28 (A) and Rh30 (B) using a lentiviral vector. SFRP3 sh3 and sh5 consistently showed robust suppression of SFRP3 as measured by RT-PCR; therefore, were chosen for further study. Both SFRP3 sh3 and sh5 reduced cell growth of Rh28 (C) and Rh30 (D) cells as measured by a standard MTT assay. (E) To confirm that the decrease in cell growth is not due to shRNA off-target effects, a murine SFRP3 containing an HA tag (HA*-SFRP3) was used as a rescue construct. (F) HA*-SFRP3 was stably expressed in Rh28 cells and detected by immunoblot. (G) HA*-SFRP3, when co-expressed with a doxycycline-inducible version of SFRP3 sh3, partially rescued the SFRP3 sh3-mediated decreased cell growth. * $p < 0.05$, ** $p < 0.01$, *** $p < 0.001$ Rosanne Tiller performed the HA western blot for F and the experiment for G.

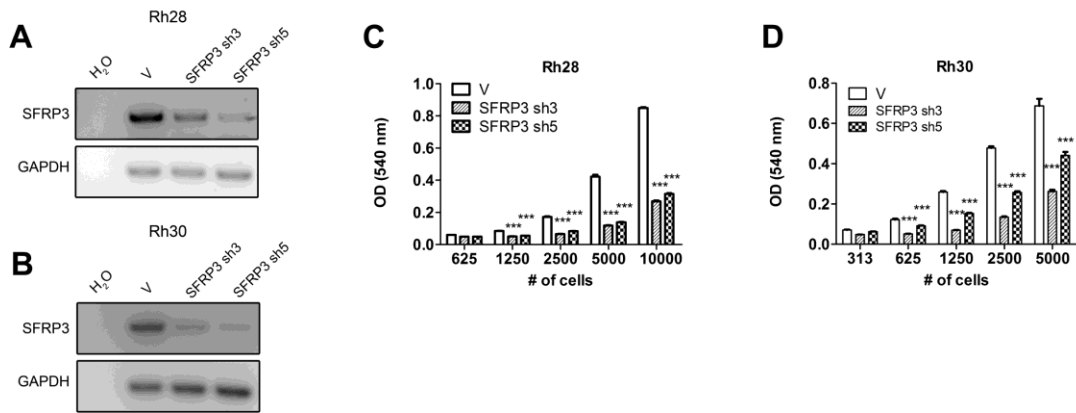


Figure 6: Doxycycline-inducible SFRP3 shRNA inhibit cell growth.

SFRP3 sh3 and sh5 were sub-cloned into a doxycycline-inducible vector, stably expressed in Rh28 (A) and Rh30 (B) cells, and tested for their ability to suppress SFRP3 mRNA in the presence of doxycycline as measured by RT-PCR. In the presence of doxycycline (4 μ g/mL), both SFRP3 sh3 and sh5 reduced cell growth of Rh28 (C) and Rh30 (D) cells as measured by a standard MTT assay. ***p<0.001

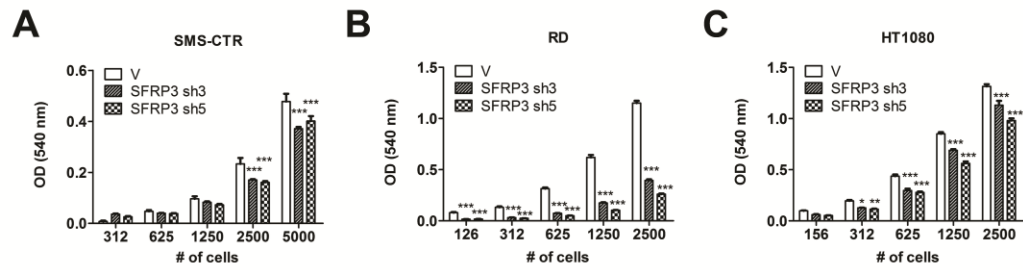


Figure 7: SFRP3 suppression reduces cell growth in eRMS and fibrosarcoma cells

shRNAs against SFRP3 were stably expressed in eRMS cell lines SMS-CTR (A), RD (B), and in a fibrosarcoma cell line, HT1080 (C). Cell growth was measured by a standard MTT assay. SFRP3 sh3 and sh5 reduced cell growth of SMS-CTR by 22% and 17%, respectively. In RD cells, SFRP3 sh3 and SFRP3 sh5 reduced cell growth by 66% and 77%, respectively. In HT1080 cells, SFRP3 sh3 and SFRP3 sh5 reduced cell growth by 14% and 19%, respectively. * $p < 0.05$, ** $p < 0.01$, *** $p < 0.001$

advantage of an shRNA-resistant murine SFRP3 construct with an HA (epitope) tag (Borello, Coletta et al. 1999). Since SFRP3 is proteolytically cleaved at both the N and C-termini (Leyns, Bouwmeester et al. 1997), the HA tag is positioned between the CRD and NTR domains and the construct termed HA*-SFRP3 (**Fig. 5E**). Using immunoblot to the HA epitope, we verified the ability of the cDNA to be expressed (**Fig. 5F**), then stably co-expressed it in Rh28 cells containing an empty vector or a doxycycline-inducible shRNAs against SFRP3 (inducible system shown in **Fig. 6 A-D**). As predicted, the decreased cell growth observed in the cells expressing SFRP3 shRNAs was largely rescued in the presence of HA*-SFRP3 (**Fig. 5G**). Taken together, these data suggest that SFRP3 has a pro-growth role in human PF-positive aRMS cell lines.

As SFRP3 is expressed at lower levels in eRMS cell lines when compared with aRMS cell lines (**Fig. 4C**), we predicted that suppressing SFRP3 in eRMS cell lines would have minimal effect on cell growth. Contrary to our prediction, SFRP3 suppression in eRMS cell lines SMS-CTR (**Fig. 7A**) and RD (**Fig. 7B**) reduced cell growth. However, the decrease was greater in RD cells (66-77%) than in SMS-CTR (17-22%). It is unclear why eRMS cells, particularly RD cells, are sensitive to SFRP3 suppression. While off-targets are a possibility with shRNAs, **Fig. 5G** demonstrated exogenous SFRP3 expression rescues SFRP3 suppression-mediated decreased cell growth, suggesting these shRNAs have minimal off-target effects. Alternatively, while eRMS cells express lower levels of SFRP3, suppressing the SFRP3 that is present may still affect cell growth, as increasing

Wnt signaling (which we would predict with SFRP3 suppression) has been shown to increase differentiation in eRMS cells (Singh et al. 2010).

SFRP3 suppression was also investigated in a fibrosarcoma cell line, HT1080 (**Fig. 7C**). This cell line was selected as it demonstrates low SFRP3 expression and exogenously expressing SFRP3 decreased growth and invasiveness due to inhibition of Met-mediated signaling (Guo et al. 2008). Expressing SFRP3 in HT1080 cells also suppressed β -catenin (Guo et al. 2008). In HT1080s, SFRP3 suppression decreased cell growth 14-19%. This decrease is smaller than that seen in aRMS cell lines, suggesting that SFRP3 suppression-mediated decreased cell growth is specific to aRMS cells. However, the small decrease in cell growth observed in the HT1080 cells could be due either to off-target effects or HT1080 cells are sensitive to even small changes in SFRP3 levels.

3.4 Suppression of SFRP3 in aRMS inhibits cell proliferation and causes a G₁ arrest.

To investigate the etiology of the decreased cell growth, we first investigated the possibility that SFRP3 suppression was interfering with cell proliferation. We found that in aRMS cells stably expressing SFRP3 shRNAs, BrdU incorporation declined (**Fig. 8 A,B**), suggesting that loss of function of SFRP3 did inhibit cell proliferation. Since a decrease in cell proliferation can reflect unrecognized differentiation, senescence, or cell cycle arrest, all three processes were further investigated. No consistent or robust

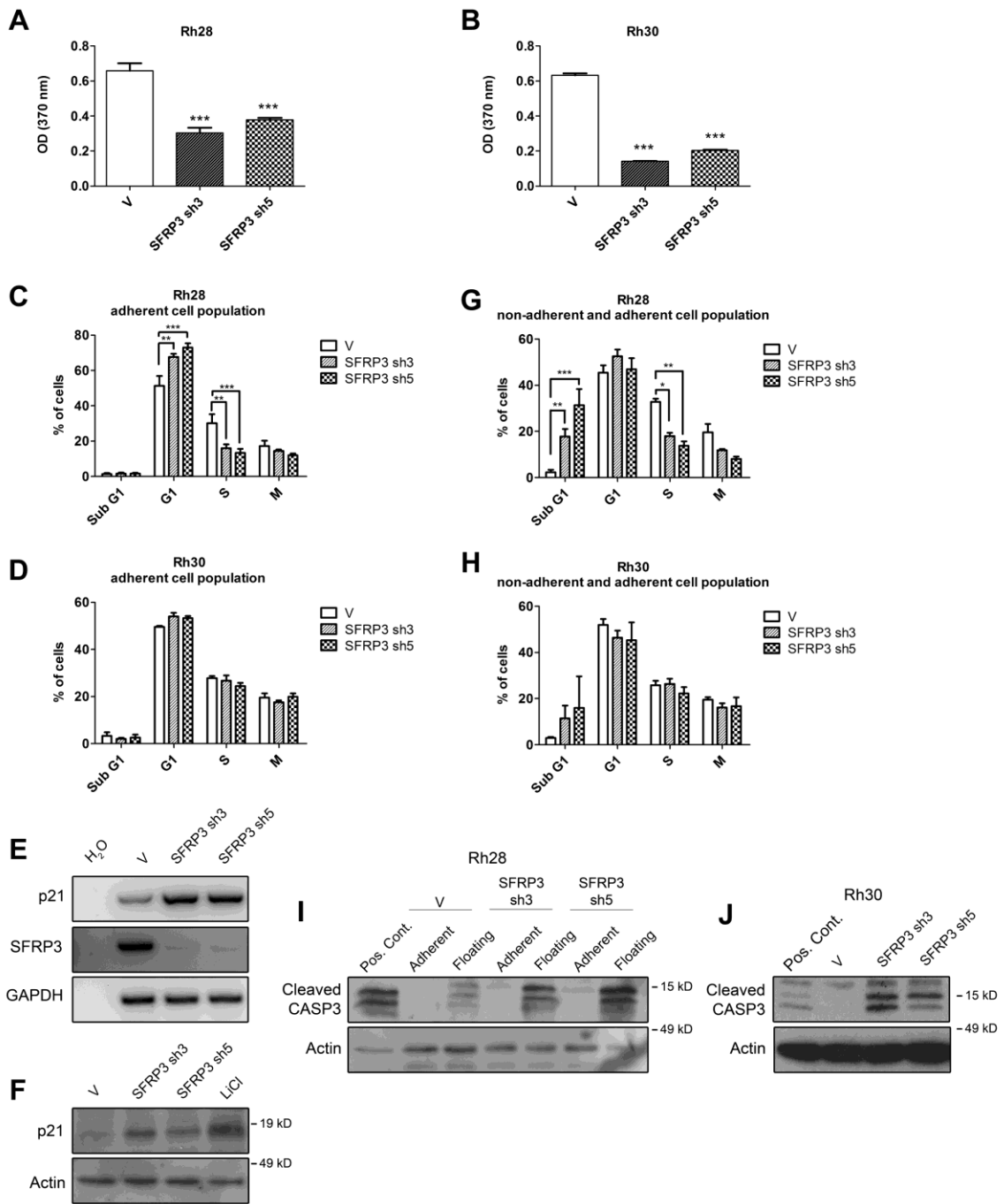


Figure 8: SFRP3 suppression inhibits cell proliferation, causes a G₁ arrest, and increases apoptosis.

SFRP3 suppression inhibits cell proliferation of Rh28 (A) and Rh30 (B) cells as measured by BrdU incorporation. SFRP3 suppression causes a G₁ arrest in Rh28 (C) and Rh30 (D) cells as measured by cell cycle analysis using PI staining and flow cytometry, although statistically significant only in Rh28 cells. Cell cycle data shown are the averages of three (Rh28) or four (Rh30) independent experiments. Consistent with a G₁ arrest, SFRP3 suppression elevates p21 levels in Rh28 cells as measured by RT-PCR (E) and immunoblot (F). LiCl served as a positive control. While no evidence of apoptosis was observed in the adherent cell population assayed in (A) through (F), when non-adherent cells were included in the analysis, apoptosis in response to SFRP3 suppression was detected in Rh28 (G) and Rh30 (H) cells. Data shown are the averages of three (Rh28) or five (Rh30) independent experiments. (I) Apoptosis in response to SFRP3 suppression was confirmed in Rh28 cells using immunoblots for cleaved caspase-3. (J) Rh30 cells stably expressing SFRP3 shRNAs also showed increased cleaved caspase-3. This analysis was performed on the total cell population (adherent and non-adherent). *p<0.05, **p<0.01, ***p<0.001

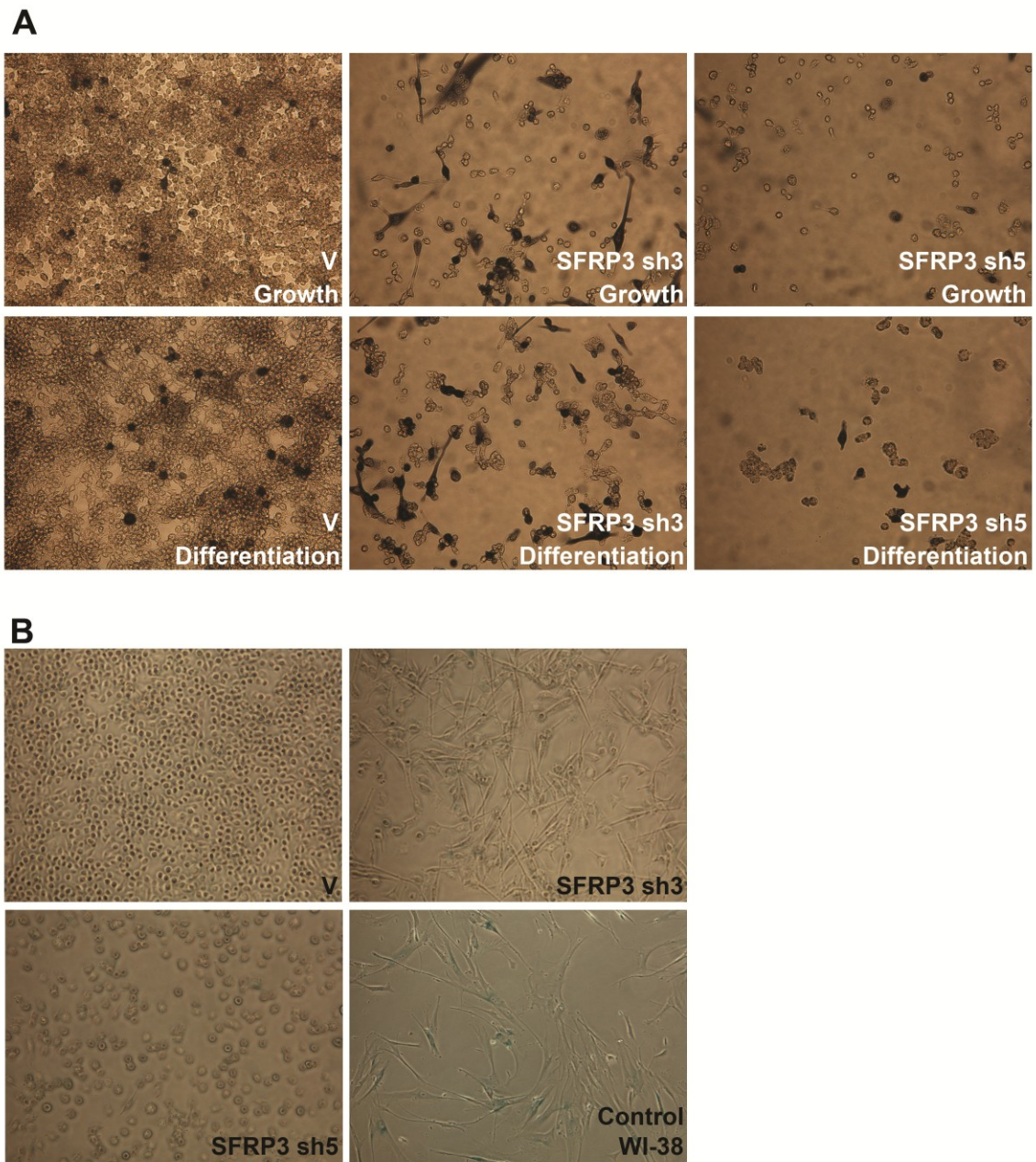


Figure 9: SFRP3 suppression does not alter myogenic differentiation or senescence.

(A) Rh28 cells containing an empty vector (V), SFRP3 sh3, or SFRP3 sh5 were grown in growth media (RPMI supplemented with 10% FBS) or differentiation media (DMEM/F12 supplemented with 2% normal horse serum) for five days, fixed, and stained for MF-20, a marker of myogenic differentiation. SFRP3 suppression does not appear to be increasing MF-20 staining in either growth or differentiation conditions. (B) Rh28 cells containing an empty vector (V), SFRP3 sh3, or SFRP3 sh5 were assessed for β -galactosidase (β -gal) activity, a marker of senescence. Positive cells are blue. WI-38 cells (primary lung fibroblasts) served as a positive control. Senescent cells were not observed in Rh28 cells, regardless of SFRP3 suppression. Images for (A) and (B) are 200X magnification.

differences in the number of differentiated [as assessed by ability to form myotubes and express the myogenic marker MF20 (**Fig. 9A**)] or senescent cells were observed in response to the stable expression of SFRP3 shRNAs in Rh28 cells (**Fig. 9B**). Similarly, we saw no consistent evidence of Wnt pathway activation (which is required for terminal myogenic differentiation) in aRMS cells stably expressing SFRP3 shRNAs, although in response to Wnt3a-conditioned media and LiCl (a GSK3 β inhibitor) they retain the ability to activate β -catenin signaling, similarly to seen previously (Annavarapu, Cialfi et al. 2013). This is discussed in greater detail in **section 4.2**.

In Rh28 cells both shRNAs caused a 16-22% increase in the percentage of cells accumulated in the G₁ phase of the cell cycle (**Fig. 8C**). In Rh30 cells, the effect of the shRNAs was more modest, with a 3-5% increase in the percentage of cells at G₁ (**Fig. 8D**). To investigate mechanism, levels of the cell cycle inhibitor p21 (Harper et al. 1993) were measured by semi-quantitative RT-PCR and immunoblot. We found p21 upregulated at both the mRNA (**Fig. 8E**) and protein (**Fig. 8F**) levels. Together, these data suggest that inhibition of SFRP3 in aRMS cells inhibits cell proliferation via a G₁ cell-cycle arrest that is partially mediated through p21.

3.5 Suppression of SFRP3 in aRMS cells also induces apoptosis.

The decrease in cell proliferation observed in aRMS cells expressing SFRP3 shRNAs was much less than the profound decrease observed in overall cell growth. This suggested that another mechanism such as cell death might be contributing. While

the previous cell cycle analysis (**Fig. 8C,D**) showed no change in the sub-G₁ peak (reflective of apoptosis), that analysis had only included adherent cells. And, since cells with SFRP3 shRNAs morphologically demonstrated an increase in the number of floating (non-adherent) cells, to capture possible missed sub-G₁ signal, we next assayed the entire (adherent and non-adherent) cell population by flow cytometry. Rh28 cells expressing SFRP3 shRNAs showed a large increase in the percentage of cells in sub-G₁ (**Fig. 8G**), while Rh30 cells again showed a more modest increase (**Fig. 8H**). For confirmation of an apoptotic effect of SFRP3 suppression, we measured cleaved caspase-3 by immunoblot. While no increase in apoptosis as measured by cleaved caspase-3 was observed in the adherent cell population, a significant increase in apoptosis was observed in non-adherent Rh28 cells expressing both SFRP3 shRNAs (**Fig. 8I**). SFRP3 suppression also increased cleaved caspase 3 in Rh30 cells (**Fig. 8J**). In summary, suppression of SFRP3 causes decreased cell proliferation, a cell cycle arrest at G₁, increased p21 expression, and an increase in apoptosis, suggesting that a combination of these mechanisms is responsible for the observed decreased aRMS cell growth.

3.6 Discussion

In PF-expressing HSMM cells and PF-positive cell lines, SFRP3 is elevated and cooperates with PF to support tumorigenesis. SFRP3 appears to support the increased proliferation and decreased apoptosis necessary for tumorigenesis. This is similar to other proteins identified in our laboratory: FGFR4 prevents apoptosis and RASSF4

supports increased proliferation in aRMS cells (Croese et al. 2012; Croese et al. 2014).

However, RASSF4 also prevents senescence, a function in which SFRP3 does not appear to participate.

It is also interesting that apoptosis, measured by increases in cleaved caspase-3 and an increase in the sub-G₁ peak, was only observed in the non-adherent cell population. This could be occurring because once the cells undergo apoptosis, they lose adherence to the tissue culture dish and become suspended in the media. Alternatively, the cells could be losing adherence while still alive, but once they are non-adherent undergo anoikis. While not investigated in this project, understanding why SFRP3 suppression induces apoptosis may be important to predict if SFRP3 suppression will result in apoptosis *in vivo*. Based on mouse xenograft experiments (**Fig. 20,21**), SFRP3 suppression does appear to modestly increase apoptosis, as measured by TUNEL staining, in at least one instance.

4. SFRP3 suppression alters the Wnt, Notch, and TGF β embryonic signaling pathways

4.1 Introduction

In an effort to understand the mechanism underlying the SFRP3 suppression-mediated decreased cell growth, we aimed to identify pathways altered by this change in SFRP3 levels. As SFRP3 is usually described as Wnt pathway antagonist, capable of altering Wnt signaling by binding to Wnt, Frizzled, and other SFRPs, we first attempted to observe changes in canonical Wnt signaling (Bovolenta et al. 2008).

4.2 Crosstalk between SFRP3 and the Wnt signaling pathway

Prior to investigating SFRP3 suppressed aRMS cells for alterations in Wnt signaling, we sought an assay capable of identifying changes in Wnt signaling in our cells. As Wnt signaling has been extensively studied, numerous assays currently exist. Of these, a luciferase reporter assay, immunofluorescence for localization of β -catenin in cells, and measuring the levels of Axin2 through qPCR were selected.

A luciferase reporter plasmid with TCF binding sites (TOPflash) is commonly used to measure the activation of the canonical Wnt pathway (Molenaar et al. 1996; Veeman et al. 2003). Rh28 cells were unsuitable for this assay due to technical difficulties with transfection of the plasmids. Transfection was achieved with native Rh30 cells and signal from the luciferase reporter was induced through the use of LiCl (a GSK3 β inhibitor) or Wnt3a conditioned media to activate Wnt signaling. However,

constitutively expressed SFRP3 shRNAs decreased the viability of Rh30 cells, preventing transfection. Doxycycline-inducible SFRP3 shRNAs were also unsuitable as the doxycycline media also prevented transfection.

Immunofluorescence can also be used to monitor changes in Wnt signaling activity as active β -catenin will translocate from the cytoplasm to nucleus. However, we were never able to observe increases in nuclear β -catenin following treatment with LiCl. Further, we did not observe differences in the localization of β -catenin after SFRP3 suppression.

Finally, transcriptional targets of TCF/LEF genes can be used as indicators of Wnt pathway activation, particularly Axin2. Axin2 is induced by β -catenin/TCF along with DKK1 and Naked as part of a negative feedback loop dampening Wnt signaling. To this end, we measured levels of Axin2 by qPCR. SFRP3 sh5 and SFRP3 sh3 do increase Axin2 levels 1.6 to 2-fold in Rh28 and Rh30 cells, respectively (**Fig. 10A**). While we observed this increase in Axin2 in several experiments, the increase was not observed in all experiments. In addition, for both cell lines, both shRNAs produced effects on cell growth, but only one appeared to be altering Wnt signaling. We questioned whether the magnitude change in Axin2 could be increased through serum starvation and the addition of Wnt ligand (Chen et al. 2014). The addition of Wnt3a conditioned media did increase the levels of Axin2 overall, but the change was not greater in SFRP3 suppressed cells (**Fig. 10B**). Similarly, serum starvation followed by activation with Wnt3a

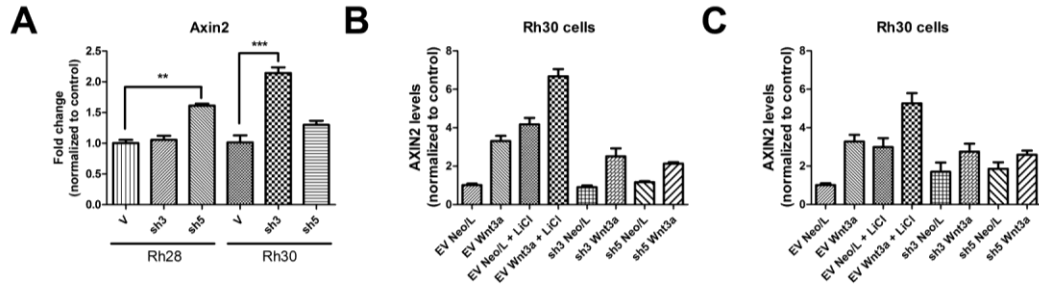


Figure 10: SFRP3 suppression modestly elevates AXIN2 levels

(A) Rh28 or Rh30 cells constitutively expressing an empty vector (V), SFRP3 sh3, or SFRP3 sh5 were assessed for levels of Axin2 by qPCR. SFRP3 sh3 and sh5 elevated Axin2 levels in Rh30 and Rh28 cells, respectively. (A) is shown again as Fig. 18A. (B) Both 24 hours of 100% Wnt3a conditioned media treatment and 24 hours of 25 mM LiCl treatment induced expression of Axin2 in Rh30 cells, with the combination (added concomitantly) increasing expression more than with either treatment alone. Wnt3a conditioned media did increase expression of Axin2 in SFRP3 suppressed cells, but not by more than in empty vector cells. (C) Cells were serum starved for 24 hours prior to 24 hours 100% Wnt3a conditioned media treatment. Again Wnt3a increases Axin2 levels, but the magnitude of the change does not appear to depend on SFRP3 suppression. qPCR for (A) performed by Margaret DeMonia.

conditioned media also increased the levels of Axin2, but the change was not greater in SFRP3 suppressed cells (**Fig. 10C**). As neither serum starvation nor stimulation with Wnt3a conditioned media amplified the expression of Axin2 following SFRP3 suppression, we could not conclude with great confidence that SFRP3 suppression did in fact increase Axin2 levels. Further, we questioned whether such small changes in Wnt signaling could account for the profound phenotypical changes observed with SFRP3 suppression.

The Wnt pathway status can be difficult to assess in cells as TCF and β -catenin are capable of regulating Wnt signaling components in a cell-specific manner (Logan and Nusse 2004; MacDonald et al. 2009). In many cell types, a negative feedback loop allows active β -catenin to induce expression of the negative regulators Axin2, DKK1, and Naked, dampening Wnt signaling. In other cell types, including colon carcinogenesis, a positive feedback reinforces Wnt signaling through the induction of Rspo and TCF/LEF. However, Axin2 induction is near universal, thus is one of the most reliable methods for assessing Wnt pathway activation. Indeed, in a SFRP3 knockout mouse, the Wnt pathway was only modestly activated (Lodewyckx et al. 2012).

4.2.1 Activation of the Wnt pathway partially phenocopies SFRP3 suppression

While the changes in Wnt signaling we observed following SFRP3 suppression were modest, we hypothesized that if the phenotypic changes observed were mediated

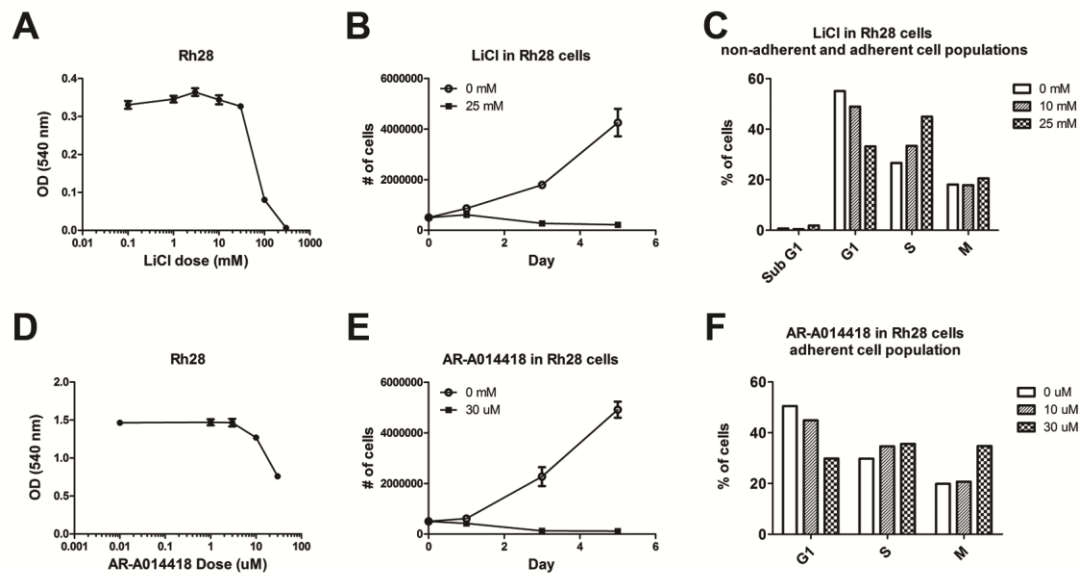


Figure 11: Activation of the Wnt pathway decreases cell growth and cause a cell cycle arrest.

(A) Cell growth of Rh28 cells treated with LiCl (0, 1, 3, 10, 30, 100, and 300 mM) was measured using an MTT assay. LiCl decreases cell growth at doses of 100 and 300 mM. (B) LiCl (25 mM) decreases Rh28 cell growth. (C) LiCl (10 mM and 25 mM) arrests Rh28 cells at S phase as measured by cell cycle analysis using PI staining and flow cytometry. (D) Cell growth of Rh28 cells treated with AR-A014418 (0, 1, 3, 10, 30 μM) was measured using an MTT assay. AR-A014418 decreases cell growth at doses of 10 and 30 μM. (E) Similarly, AR-A014418 (30 μM) decreases Rh28 cell growth, but unlike LiCl, AR-A014418 causes an M phase cell cycle arrest, with only a 4-5% increase in S (F). Experiments in panels A-F were performed once. Experiments in panels B-F were performed by Dayoung Ko.

by an activation in Wnt signaling, we could replicate those changes through pharmacological activation of the pathway. GSK3 inhibitors LiCl (Klein and Melton 1996) and AR-A014414 (Bhat et al. 2007) were chosen. LiCl is widely available and has safely been used in humans for over 50 years for the treatment of bipolar disorder. AR-A014414 is a newer GSK3 inhibitor designed to be more specific to GSK3, which is reflected in its lower IC₅₀ when compared to LiCl (Tighe et al. 2007). Optimal doses of LiCl (**Fig. 11A**) and AR-A014414 (**Fig. 11D**) were identified using an MTT then assess for their ability to decrease cell growth. Both 25 mM LiCl (**Fig. 11B**) and 30 μ M (**Fig. 11E**) decreased cell growth. Finally, while neither LiCl (**Fig. 11C**) nor AR-A014414 (**Fig. 11F**) arrested the cell cycle at G₁ as observed with SFRP3 suppression, both did cause a cell cycle arrest at S and G₂/M, respectively. This is unsurprising as GSK3 inhibitors have previously been reported to delay mitotic exit without affecting progression through G₁/S (Tighe et al. 2007). Interestingly, activation of Wnt signaling is also known to suppress proliferation of aRMS cells (Rh4 and Rh30) about 20%, without altering eRMS proliferation (Annarapu et al. 2013). This suggests that Wnt activation, not only through inhibition of GSK3, is capable of suppressing cell growth in aRMS.

As LiCl inhibited cell growth and induce a cell cycle arrest, we hypothesized that it would have the potential to inhibit tumor growth *in vivo*. Xenograft tumors arising from Rh28 cells were generated, and mice received either control treatment (water) or

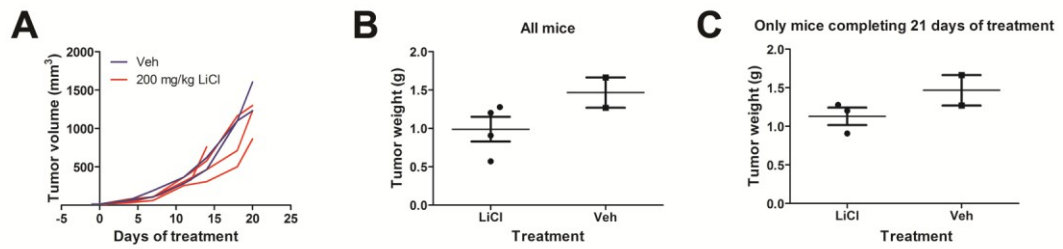


Figure 12: LiCl does not affect growth of Rh28 cells murine xenograft as measured by tumor volume, but trends towards a decrease in tumor weight

Rh28 cells were injected subcutaneously into the flanks of SCID/*beige* mice. Once tumors were palpable, mice were randomly assigned to LiCl (200 mg/kg) or water (control) group. Tumor dimensions were measured twice a week using calipers. LiCl did not alter tumor volume (A), but appeared to non-significantly reduce tumor volume (B), even when only mice completing 21 days of treatment are included in the analysis (C).

200 mg/kg LiCl. This dose was selected as it was shown to activate Wnt signaling, increasing bone formation and bone mass in mice (Clement-Lacroix et al. 2005). Mice receiving LiCl showed no difference in tumor growth (as measured by tumor volume) when compared to the control mice, thus the study was terminated, regardless of how many days of treatment the mice received (**Fig. 12A**). However, when the tumors were removed, we observed a non-significant trend towards LiCl reducing tumor weight (**Fig. 12B**). One of the mice received fewer days of LiCl than the others, and even when that mouse's tumor is excluded, we still observe a non-significant trend towards a reduction in tumor weight (**Fig. 12C**).

4.3 Screen to uncover oncogenic signaling pathways capable of rescuing SFRP3 suppression-mediated decreased cell growth

As we were unable to identify any robust changes in Wnt signaling in SFRP3-suppressed cells, we turned to an unbiased approach, a screen of oncogenic signaling pathway activators described in Martz et al (2014). Kris Wood and his laboratory (Department of Pharmacology and Cancer Biology, Duke University) developed this technology and identified mechanisms of resistance to 13 different targeted therapies used in 7 cancer types. The screen consists of 36 known activators, representing 17 different oncogenic pathways, and 3 controls (**Fig. 13**). Of these, 5 pathways, RAS-MAPK (mitogen-activated protein kinase), Notch1, PI3K (phosphoinositide 3-kinase)-mTOR (mechanistic target of rapamycin), and ER (estrogen receptor) emerged as the

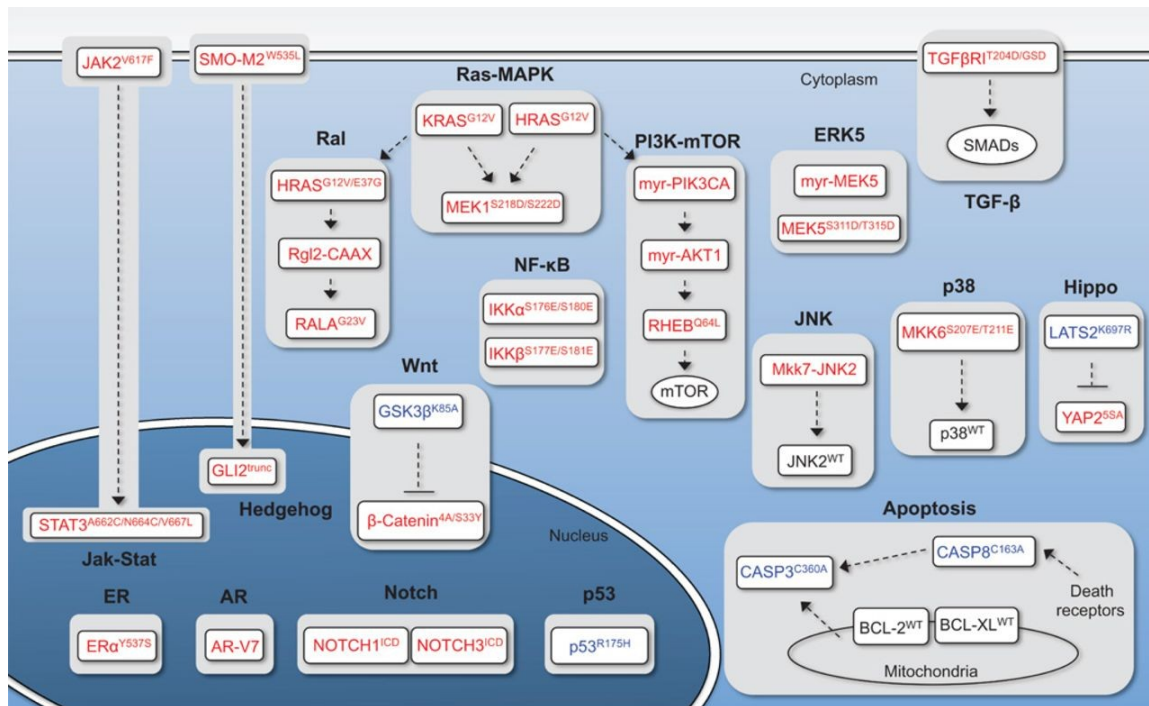


Figure 13: Strategy for manipulating oncogenic signaling pathways

Pathway names are in bold and situated in the cellular context in which they function. The engineered cDNA constructs in each pathway are denoted as either wild type (WT; black), constitutively active mutants (red), or dominant-negative mutants (blue). From C. A. Martz, K. A. Ottina, K. R. Singleton, J. S. Jasper, S. E. Wardell, A. Peraza-Penton, G. R. Anderson, P. S. Winter, T. Wang, H. M. Alley, L. N. Kwong, Z. A. Cooper, M. Tetzlaff, P.-L. Chen, J. C. Rathmell, K. T. Flaherty, J. A. Wargo, D. P. McDonnell, D. M. Sabatini, and K. C. Wood, Systematic identification of signaling pathways with potential to confer anticancer drug resistance. *Sci. Signal.* 7, ra121 (2014). AAAS, the publisher of *Science Signaling*, permits use of published figures in dissertations without requesting permission.

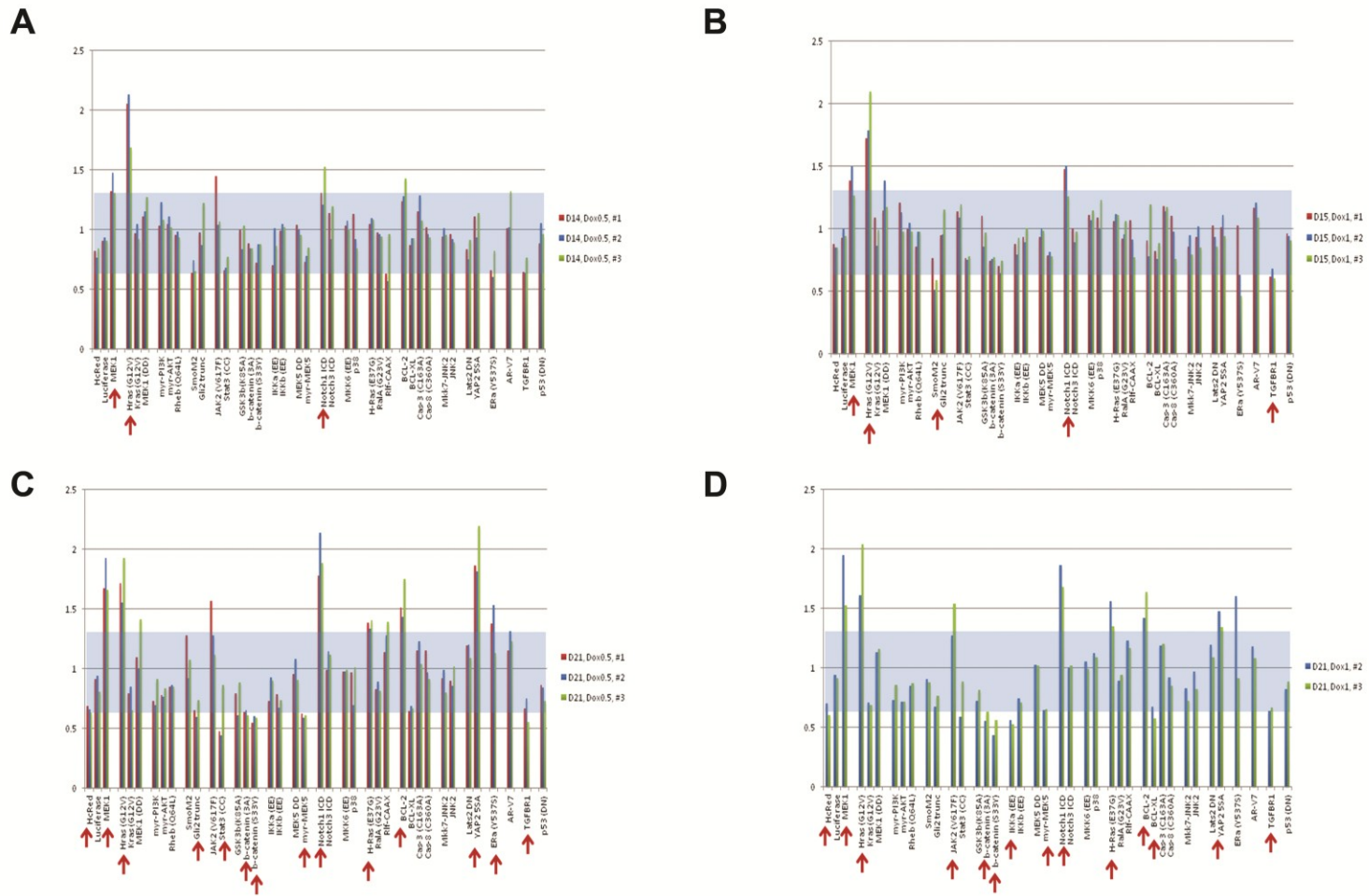


Figure 14: Screen of oncogenic pathways in SFRP3 suppressed cells

Rh28 cells containing a doxycycline-inducible SFRP3 sh3 and constitutively active cDNA for an oncogenic pathway activator or control were treated with 0.5 $\mu\text{g}/\text{mL}$ (A,C) or 1 $\mu\text{g}/\text{mL}$ (B,D) doxycycline for 14 or 15 days (A,B) or 21 days (C,D). Any change greater than 30% (outside of the shaded area) was considered significant. Of these, MEK-1, HRas (G12V), and Notch1 ICD provided resistance to SFRP3 sh3-mediated decreased cell growth, while TGFBR1 sensitized. Luciferase is used as a control. Samples in A-D were generated by Julie Kephart, prepared for sequencing by Julie Kephart and members of the Wood laboratory, and analyzed by Kris Wood.

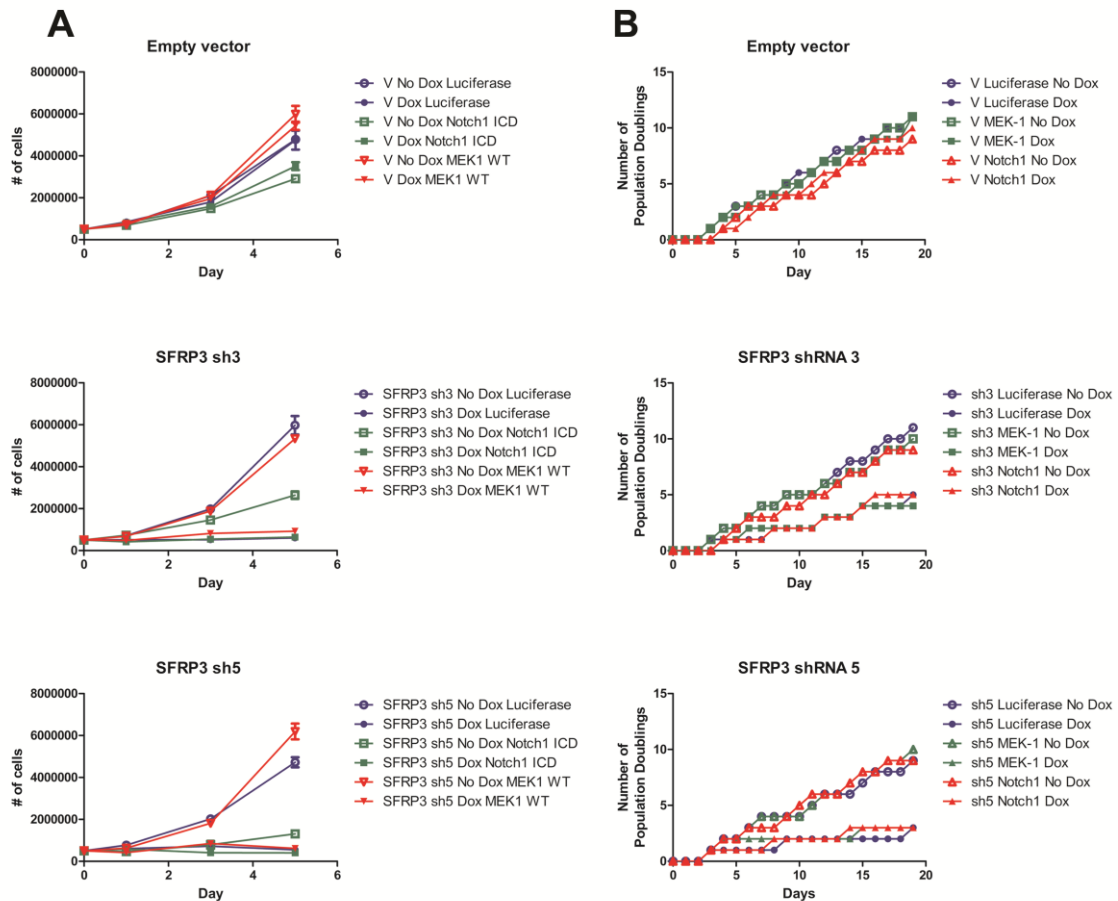


Figure 15: Attempts to confirm results from screen of oncogenic pathways in SFRP3 suppressed cells

In the screen of oncogenic pathways in SFRP3 suppressed cells (Fig. 14), MEK-1, HRas (G12V), and Notch1 ICD provided resistance to SFRP3 sh3-mediated decreased cell growth, while TGFBR1 sensitized. However, neither MEK-1 nor Notch1 ICD rescued SFRP3 suppression-mediated decreased cell growth as measured by either a 5-day growth curve (A) or a 21-day population doubling assay (B), thus we are unable to validate the results of the screen. Luciferase is used as a control.

most common for conferring resistance to the targeted therapies. We hypothesized that we could apply this technology to identify pathways potentially downstream from- or cooperating with SFRP3, as a pathway conferring resistance to SFRP3 suppression-mediated decreased cell growth may be downstream of SFRP3.

In our screen, each Rh28 cell contains a doxycycline-inducible SFRP3 shRNA (SFRP3 sh3) and a barcoded pathway-activating mutant complementary DNA (cDNA) or barcoded control cDNA. The cells were treated with media containing 0, 0.5, or 1 $\mu\text{g}/\mu\text{L}$ doxycycline and harvested after 14 or 21 days. Due to doxycycline's short half-life in media, the media was replaced daily to ensure cells were exposed to the correct dose of doxycycline. Upon harvest, the genomic DNA was extracted (DNeasy Blood and Tissue Kit, Qiagen) and sequenced. The cDNAs were barcoded, allowing for measurement of the relative abundance of individual cDNAs in the population. Abundant cDNAs contain an activating mutant conferring a growth advantage, while rare cDNAs confer a growth disadvantage. By comparing the relative abundance of individual cDNAs in the cells treated with doxycycline to the cells without, we can identify activating mutants which confer a growth advantage in the presence of SFRP3 suppression, rather than conferring a non-specific growth advantage.

Activating mutants were considered for further studies if their levels were altered more than 30% when comparing the doxycycline to the non-doxycycline condition. A threshold of 30% was used as it is the standard threshold for analyzing this

type of screen, as determined by its developer, Kris Wood. Many more activating mutants were altered at the 21 day time-point, suggesting the possibility that some of them may be conferring resistance to doxycycline rather than SFRP3 suppression. Previous experiments have found that doxycycline can inhibit Rh28 cells, with 8 $\mu\text{g}/\mu\text{L}$ killing more than 50% of cells within 5 days (personal communications with Rosanne Tiller). No decreased cell growth has been observed at 5 days with the doses used in the screen; however, the cells were not tested for doxycycline-mediated decreased cell growth after 21 days of treatment. For this reason, we focused on activating mutants identified at the 14 day timepoint.

Three cDNAs were considered as conferring resistance to the SFRP3 suppression-mediated decreased cell growth: MEK-1 (wild-type), HRas (G12V), and Notch1 ICD (**Fig. 14 A-D**). One cDNA was considered as enhancing the SFRP3 suppression-mediated decreased cell growth: TGFBR1. HRas (G12V) was not considered for further studies as it induces senescence when expressed in native Rh28 cells (personal communications with Corinne Linardic and Candy Chen). Of these, MEK-1 and Notch1 ICD were selected for further studies as MEK (Rottinger et al. 2004; Yun et al. 2005; Kim et al. 2007) and Notch (Katoh 2007; Kwon et al. 2011; Andersen et al. 2012; Collu et al. 2012; Kim et al. 2012; Collu et al. 2014) signaling have been shown to interact with Wnt signaling.

It is surprising that we identified wild-type MEK-1 (originally included in the screen as a control), but not the oncogenic MEK-1 DD as capable of rescuing SFRP3 suppression-mediated decreased cell growth. However, it is likely that only the right amount of MAPK pathway activation (through which MEK-1 signals) is beneficial to the cells, as a strong activation, such as that resulting from oncogenic Ras, induces senescence (personal communications with Corinne Linardic and Candy Chen). The MAPK pathway also contains numerous positive and negative feedback loops, allowing for tight regulation of the pathway (Avraham and Yarden 2011). MEK-1 and MEK-1 DD may be affecting these feedback loops differently, allowing for only one to rescue SFRP3 suppression-mediated decreased cell growth.

Based on our hypothesis of SFRP3 suppression increasing Wnt signaling, we had predicted that activated β -catenin would enhance SFRP3 suppression-mediated decreased cell growth. β -catenin cDNA containing cells were decreased more than 30% at both doses of doxycycline at day 21, but not at day 14, where the decrease was approximately 10% and 25% at doses of 0.5 μ g/mL and 1 μ g/mL doxycycline, respectively, with both activated β -catenin cDNAs.

We attempted to validate the screen first using a growth curve in which we compared cells with an SFRP3 shRNA or control and barcoded plasmid in the presence of absence of doxycycline (**Fig. 15A**). Luciferase served as a control for the MEK-1 and Notch1 ICD barcoded plasmids. We observed that MEK-1 increased and Notch1 ICD

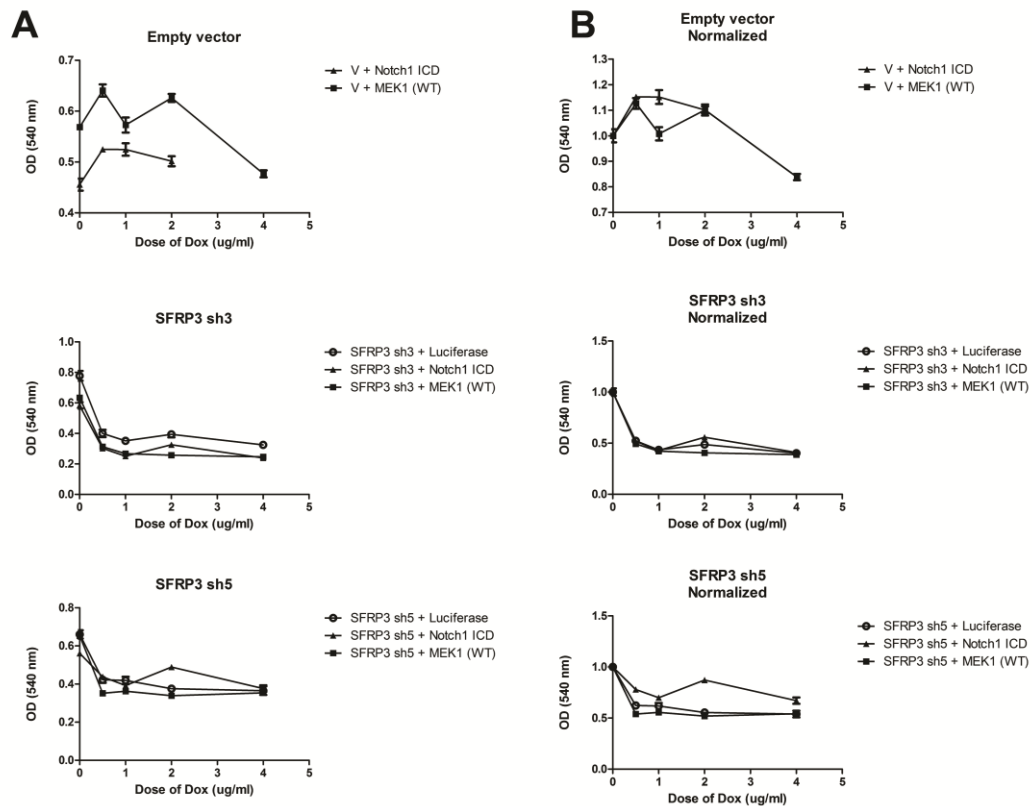


Figure 16: Validation of the oncogenic pathway screen results using GI50 curves

Rh28 cells containing a doxycycline-inducible empty vector (V), SFRP3 sh3, SFRP3 sh5 and luciferase (control), Notch1 ICD, or MEK-1 were plated at a known density and treated with varying doses of doxycycline (0, 0.5, 1, 2, 4 $\mu\text{g}/\text{mL}$) for 5 days. Notch1 ICD and MEK-1 both affected overall cell growth (A); therefore the data were normalized to 0 $\mu\text{g}/\text{mL}$ doxycycline (B) for analysis. Neither Notch1 ICD nor MEK-1 rescued the decreased cell growth with the exception of Notch1 ICD in the SFRP3 sh5 condition. The empty vector with luciferase condition was omitted from the assay due to bacterial or fungal contamination.

decreased overall cell growth when compared to Luciferase. However, neither MEK-1 nor Notch1 ICD appeared to rescue any of the SFRP3 suppression-mediated decreased cell growth, suggesting we were not able to validate either result from the screen. We hypothesized that this may be due to the shorter duration of the growth curve.

To address the possibility that the growth curve was too short of a duration to validate the assay, we next attempted to validate the results using a 21-day population doubling assay (**Fig. 15B**). Again, we did not observe either MEK-1 or Notch1 ICD rescuing the SFRP3 suppression-mediated decreased cell growth.

Normally, the screen is validated through a GI50 (half-maximal growth inhibition) curve, in which the curve of a particular targeted therapy is shifted by the presence of the barcoded activating mutant cDNA. As we are using a genetic-based approach for the suppression of SFRP3, rather than a pharmacological one, we performed the GI50 curves with increasing doses of doxycycline (**Fig. 16A**). Due to Notch1 ICD and MEK-1 affecting the growth of the cells, the data were also analyzed after normalization to the 0 $\mu\text{g/mL}$ doxycycline condition (**Fig. 16B**). We did not observe either Notch1 ICD or MEK-1 rescuing SFRP3 suppression-mediated decreased cell growth (as evidenced by the curve shifting to the right), with the exception of Notch1 ICD following SFRP3 sh5. However, in this experiment, no dose of doxycycline produced an intermediate level of decreased cell growth, making it difficult to visualize the GI50 curve and observe potential shifts. Due to doxycycline and the shRNAs

mechanism of action, it is unclear whether it is possible to observe a dose dependent response for decreased cell growth rather than a binary response. In the future, we plan on repeating this study with lower doses of doxycycline in an attempt to define a GI50 curve more clearly, allowing for a greater possibility of uncovering shifts in the GI50 curve in response to Notch1 ICD or MEK-1.

4.4 The role of Notch in RMS

Unsurprisingly, based on its role in muscle differentiation, the Notch pathway has been described to play important roles in both eRMS and aRMS tumorigenesis. In eRMS, Notch receptors are expressed at higher levels than in skeletal muscle cells (Belyea et al. 2011; Raimondi et al. 2012; De Salvo et al. 2014). Further, the pathway supports proliferation and inhibits differentiation (Belyea et al. 2011; Raimondi et al. 2012; De Salvo et al. 2014). Similar to eRMS, Notch receptors are also expressed at higher levels in aRMS levels (Roma et al. 2011). In aRMS, Notch signaling supports increased proliferation in addition to supporting increased mobility and invasiveness (Roma et al. 2011; De Salvo et al. 2014)

4.5 Crosstalk between the Wnt and Notch signaling pathways

As Notch1 ICD was identified in the screen identifying oncogenic pathways interacting with SFRP3, we wanted to confirm that the Wnt and Notch pathways did interact in aRMS cells. To this end, in PF-positive aRMS cell lines (Rh28 and Rh30) lentivirally transduced with Notch1ICD, we measured the levels of AXIN2, a

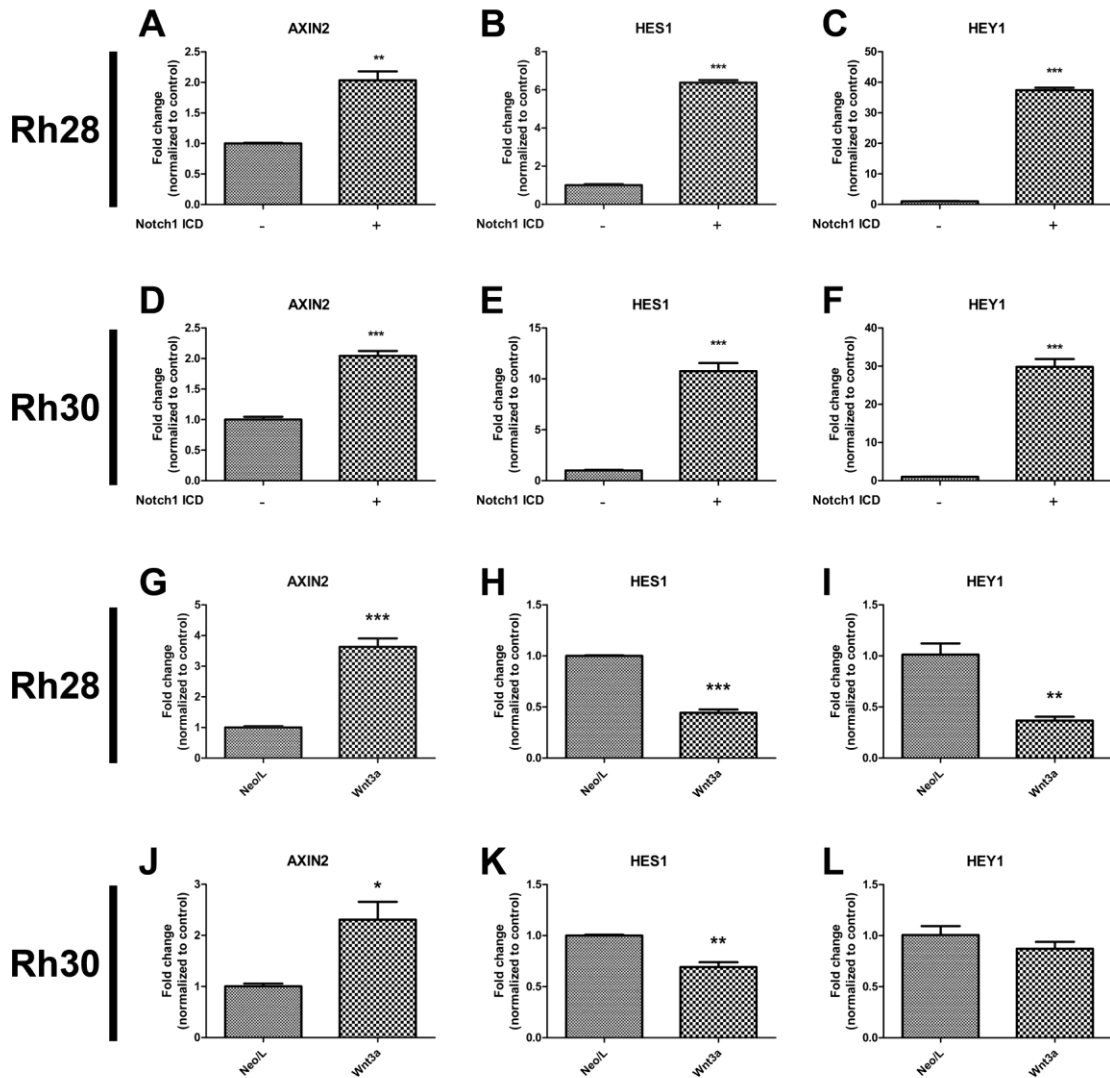


Figure 17: The Wnt and Notch pathways interact in aRMS cells

Expression of Notch1 ICD in Rh28 (A) and Rh30 (D) cells activates Wnt signaling as measured by Axin2 mRNA levels. Notch1 ICD-mediated activation of the Notch pathway is confirmed through increased Hes1 (B, E) and Hey1 (C, F) mRNA levels. Wnt3a conditioned media is confirmed to activate Wnt signaling in Rh28 (G) and Rh30 (J) cells. Further, it suppressed both Hes1 (H) and Hey1 (I) in Rh28 cells and Hes1 (K), but not Hey1 (L) in Rh30 cells. * $p < 0.05$, ** $p < 0.01$, *** $p < 0.001$ qPCR for Rh28 with Wnt3a conditioned media was performed by Margaret DeMonia.

downstream target of canonical β -catenin signaling (**Fig. 17 A,D**). The Notch1 ICD plasmid is the same as was included in the oncogenic pathway activation screen.

Activation of Notch signaling through the gain-of-function mutant Notch1 ICD activated β -catenin signaling. Notch pathway activation was confirmed by increases in both HES1 and HEY1, two downstream targets of Notch signaling (**Fig. 17, B-C, E-F**). This suggests that the Notch pathway does activate β -catenin signaling in aRMS cells and crosstalk does occur.

We also investigated the reverse, whether activation of the Wnt pathway in aRMS cells could also alter the activity of the Notch pathway. To activate the Wnt pathway, we treated the cells with Wnt3a conditioned media and observed an increase in AXIN2 (**Fig. 17 G,J**). Interestingly, activation of the Wnt pathway suppressed levels of HES1 and HEY1 (**Fig. 17 H-I, K-L**), suggesting a suppression of the Notch pathway.

4.6 Crosstalk between SFRP3 and the Notch signaling pathway

Since we have some evidence (**Fig. 10A, Fig. 18A**) that SFRP3 suppression may activate Wnt signaling and activated Wnt signaling inhibits Notch (**Fig. 17 G-L**), we predicted that SFRP3 suppression would also inhibit Notch signaling. As we had previously described, we saw modest 1.6 to 2-fold increases in AXIN2 following SFRP3 suppression, but not in all conditions (**Fig. 10A, Fig. 18A**). However, contrary to what we had predicted, SFRP3 sh3 increased both HES1 (**Fig. 18B**) and HEY1 (**Fig. 18C**) in

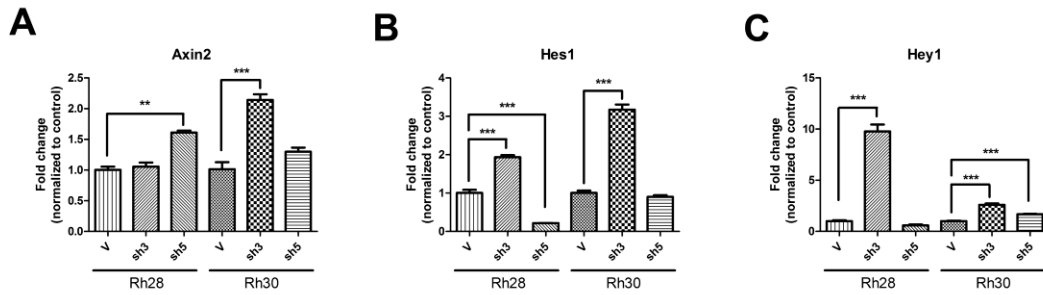


Figure 18: SFRP3 suppression, particularly SFRP3 sh3, activates the Notch pathway.

(A) Stable expression of SFRP3 sh3 in Rh30 and SFRP3 sh5 in Rh28 elevate Axin2 mRNA levels. Fig. 18 A is also shown as Fig. 10A. SFRP3 sh3 increases expression of Hes1 (B) and Hey1 (C) mRNA in aRMS cells; however SFRP3 sh5 only elevates Hey1 in Rh30 cells. **p<0.01, ***p<0.001 qPCR performed by Margaret DeMonia.

both Rh28 and Rh30 cells. SFRP3 sh5 produced conflicting results, decreasing HES1 in Rh28 cells (**Fig. 18B**), but increasing HEY1 in Rh30 cells (**Fig. 18C**). This suggests that while SFRP3 suppression does appear to affect the Notch pathway, the interaction is likely to be more complicated than the proposed hypothesis of SFRP3 activating Wnt signaling, which in turn, suppresses Notch signaling. Future work should investigate if SFRP3 interacts with the Notch pathway independently of the Wnt pathway.

4.7 Crosstalk between SFRP3 and the TGF β signaling pathway

Wnt and TGF β interactions during development have been well documented. Initially described in *Xenopus*, β -catenin, LEF1/TCF, and SMAD4 form a complex during the establishment of the Spemann's organizer (the dorsal lip of the *Xenopus* gastrula and generates signals imparting dorsoventral and anteroposterior patterning to nearby cells (Leyns et al. 1997)) (Nishita et al. 2000) and Smad3 and LEF1 interact to cooperatively regulate LEF1/TCF target genes (Labbe et al. 2000). Further, SFRP is also present in the Spemann's organizer, where it acts as an antagonist by binding Wnt8 (Leyns et al. 1997; Wang et al. 1997). Since then numerous interactions between TGF β and Wnt have been described in mammalian cells in which members of the SMAD family bind DVL1, AXIN, β -catenin, LEF1, and TCF4 (Minoo and Li 2010). The role of TGF β signaling in skeletal myogenesis has also been characterized. Expression of the ligand TGF β 1 allows for the development of myoblasts into fast fibers and without it myoblasts develop into slow fibers. In addition TGF β signaling inhibits skeletal muscle regeneration through

inhibiting satellite cell proliferation, myofiber fusion, and expression of some muscle specific genes (Burks and Cohn 2011). While TGF β signaling is only beginning to be understood in RMS, its role appears to differ by RMS subtype. In eRMS, TGF β promotes cell growth and inhibit differentiation, similar to its role in skeletal myogenesis.

Differentiation does occur, when a critical amount of TGF β signaling is present (Bouche et al. 2000). In contrast, another study found reduced eRMS cell growth following the addition of exogenous TGF β , but aRMS cells were resistant to the addition of exogenous TGF β , showing no changes in downstream targets of TGF β signaling. This resistance was determined to be caused by PF inhibiting interactions between FOXO1 and SMAD family members, and indeed when PF was suppressed, aRMS cells were once again sensitive to exogenous TGF β (Schmitt-Ney and Camussi 2015). The contrasting data presented in these studies suggest that more information is needed to fully understand the role of TGF β signaling in eRMS and aRMS; however, both studies do demonstrate a connection between TGF β signaling and cell growth and differentiation of RMS cells, consistent TGF β signaling contributing to skeletal myogenesis.

Based on the literature describing an interaction between Wnt and TGF β , the oncogenic pathways screen (**Fig. 14 A-D**) and SFRP3 suppression microarray (**Fig. 22E**) were queried for evidence for a role for the TGF β pathway. In the oncogenic screen, TGF β R1, in the presence of SFRP3 suppression further inhibited cell growth. In the SFRP3 suppression microarray, SFRP3 suppression demonstrated a pathway signature

of active TGF β signaling (**Fig. 23**). While this will require further confirmation and investigation, these preliminary results suggest that SFRP3 suppression, in addition to increasing Wnt signaling, may also be increasing TGF β signaling. In the oncogenic pathway screen (**Fig. 14**), expression of TGF β signaling further inhibited cell growth specifically in SFRP3 suppressed cells, suggesting that the phenotype observed following SFRP3 suppression may be partly due to changes in TGF β signaling. As the literature is unclear on the role of TGF β signaling in RMS cells, further studies are needed to determine if our findings in the oncogenic pathways screen and SFRP3 suppression microarray are consistent with the literature. In addition, in the oncogenic pathway screen, the receptor TGF β R1 was identified, while most previous studies had investigated the ligand. TGF β signaling is a complex pathway with numerous receptors and ligands so it is unclear if different receptors or ligands will affect RMS cells differently.

4.8 Activated Notch confers resistance to vincristine

In the initial work describing the oncogenic screen, Notch1 ICD was able to confer resistance to 10 out of 13 targeted therapies in at least one cell line tested per cancer type tested (Martz et al. 2014). As such, we hypothesized that Notch1 ICD resistance may not be specific to SFRP3-suppression-mediated decreased cell growth. To this end, we performed an MTT with increasing doses of vincristine in three aRMS cell lines: Rh28 (**Fig. 19 A,D**), Rh30 (**Fig. 19 B,E**), and Rh41 (**Fig. 19 C,F**). In all three cell

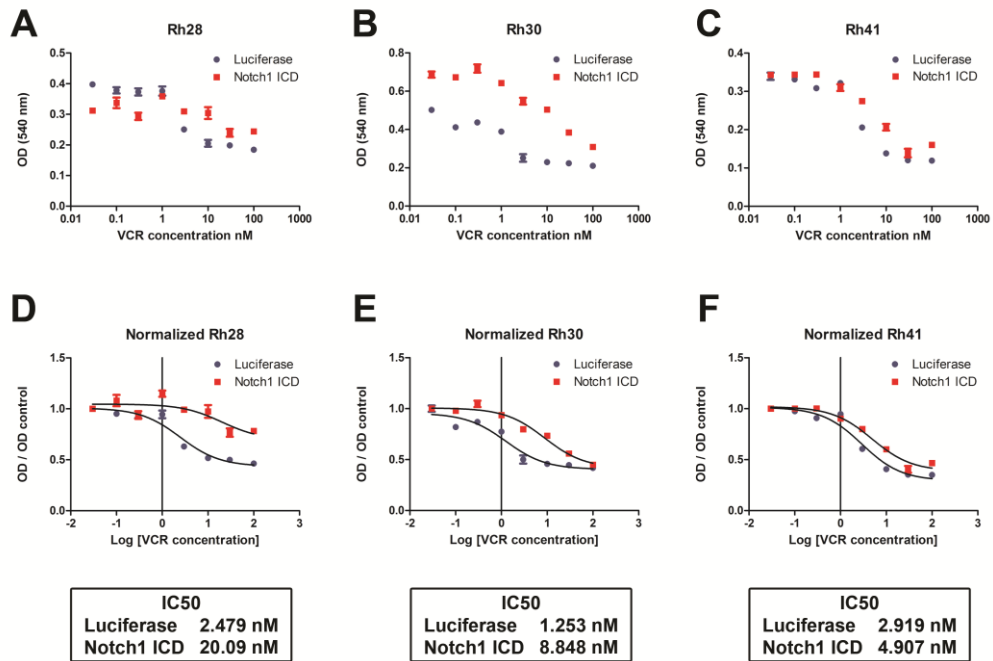


Figure 19: Notch confers resistance to vincristine

aRMS cells Rh28 (A), Rh30 (B), and Rh41 (C) stably expressing Notch1 ICD or a control (luciferase) were treated for 48 hours with increasing doses of vincristine (0, 0.1, 0.3, 1, 3, 10, 30, and 100 nM). As Notch1 ICD altered the cell growth of some cell lines, all were normalized to the luciferase control. Notch1 ICD conferred resistance to vincristine in Rh28 (D), Rh30 (E), and Rh41 (F) cells as evidenced by the increases in IC50.

lines, the expression of Notch1 ICD in the cells shifted the IC50 curve to the right, suggesting the Notch1 ICD was conferring resistance to vincristine. Notch1 ICD also had differing effects on the cell growth of aRMS. In Rh28 cells, Notch1 ICD modestly decreases cell growth (**Fig. 19A**). In Rh30 cells, Notch1 ICD increases cell growth (**Fig. 19B**). In Rh41 cells, Notch1 ICD had no effect on cell growth (**Fig. 19C**). While Notch pathway activation had previously been reported to support aRMS cell proliferation, this suggests that the effect appears to be cell type specific (De Salvo et al. 2014). The ability of the Notch pathway to confer resistance to vincristine, part of the backbone of chemotherapy used in RMS, should be investigated further. Specifically, tumors resistant to vincristine should be analyzed for increased Notch signaling. In addition Notch inhibitors should be investigated as potential tools for resensitizing tumors to vincristine.

4.9 Conclusions

Based on these data, the signaling network in aRMS cells is very complex with crosstalk likely between SFRP3, Wnt, Notch, and TGF β signaling. As such it is unlikely that a change in only one pathway is responsible for the phenotype observed following SFRP3 suppression. Activation of Notch only inhibited cell growth in Rh28 cells and increased cell growth in Rh30 cells, suggesting it is not likely to be the sole mechanism of action for SFRP3 suppressed decreased cell growth. In addition, it was able to rescue vincristine-mediated decreased cell growth in all cell lines, suggesting it may allow

aRMS cells to survive better to a wide variety of insults. As a result it should be further investigated as a potential mechanism of resistance to current aRMS therapies.

5. SFRP3 is required for aRMS tumorigenesis *in vivo*

This section, including figures, was adapted from Kephart JJ, Tiller RG, Crose L, Slemmons KK, Chen PH, Hinson AR, Bentley RC, Chi JT, and Linardic CM, "Secreted frizzled related protein 3 (SFRP3) is required for tumorigenesis of PAX3-FOXO1-positive alveolar rhabdomyosarcoma," Clin Cancer Res. 2015 Jun 12. pii: clincanres.1797.2014. AACR, the publisher of Clinical Cancer Research, permits authors to reproduce parts of their articles including tables and figures without seeking AACR's permission.

5.1 Introduction

In Chapter 3, we described SFRP3 suppression decreasing cell growth *in vitro* and characterized the mechanisms of this decreased cell growth, identifying a combination of decreased proliferation and increased apoptosis. In this chapter, we examine the role of SFRP3 suppression in a murine xenograft model of aRMS and combine SFRP3 suppression with vincristine in the same murine model of aRMS. As expected based on the *in vitro* data, SFRP3 suppression does reduce aRMS tumor growth. Further, SFRP3 suppression sensitizes the tumors to vincristine, causing 100% tumor regression (as assessed using external measurements made by calipers) and 71% ablation (as measured at necropsy).

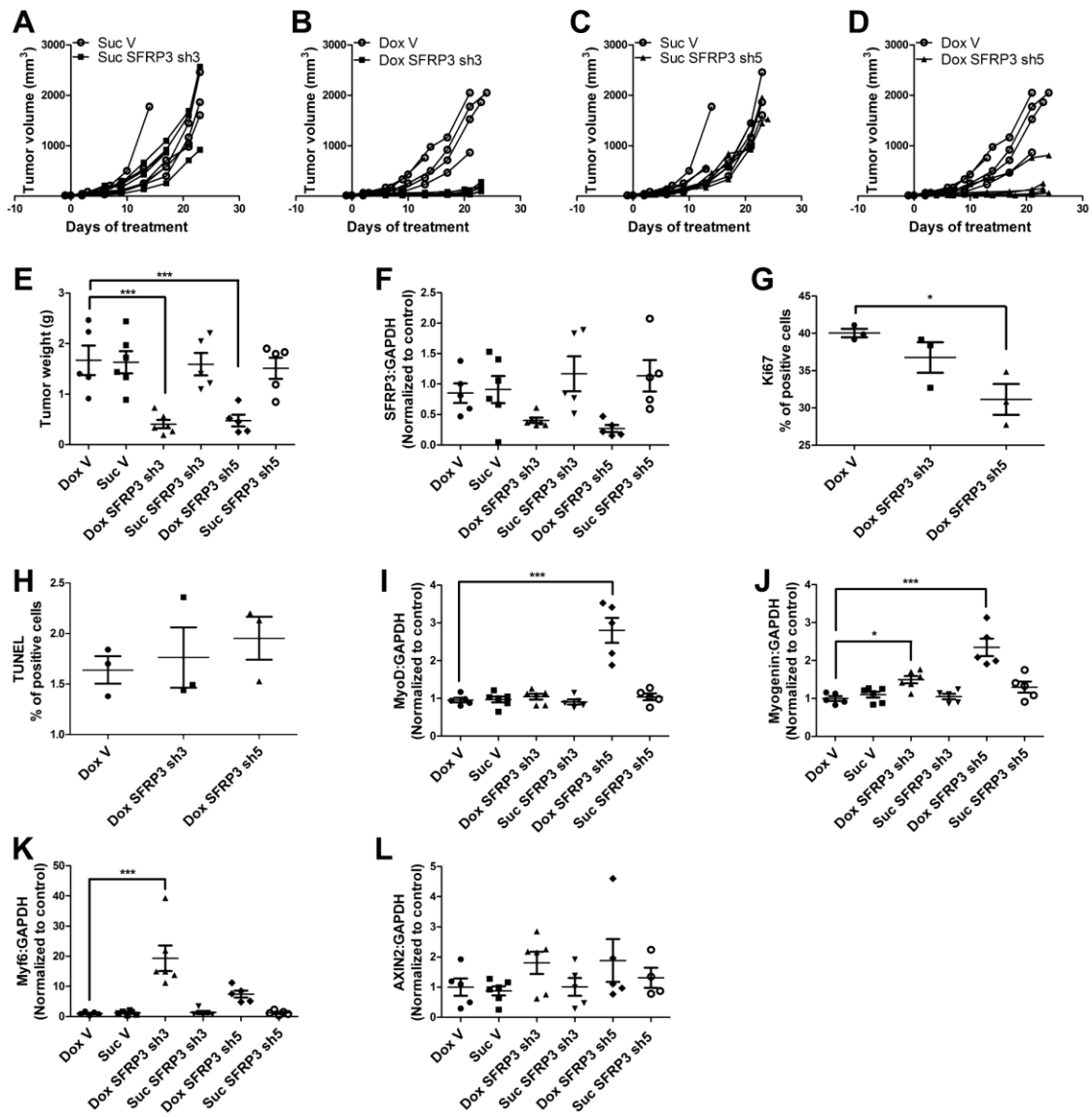


Figure 20: SFRP3 suppression inhibits tumor growth *in vivo*.

Rh28 cells expressing doxycycline-inducible shRNAs against SFRP3 (or vector) were injected subcutaneously into the flanks of SCID/*beige* mice. Once tumors were palpable, mice were randomly assigned to doxycycline or sucrose (control) group. Tumor dimensions were measured twice a week using calipers. In mice treated with sucrose, SFRP3 sh3 (A) and sh5 (C) showed no reduction in growth. In the doxycycline treated groups, SFRP3 suppression due to sh3 (B) or sh5 (D) reduced tumor growth. (E) Following 23 days of exposure to doxycycline or sucrose or when an IACUC-defined endpoint was reached, mice were sacrificed and tumors were excised and weighed. SFRP3 suppression reduced tumor weight. (F) SFRP3 levels within the tumors were measured by RT-PCR to confirm knockdown. Tumors were fixed, embedded in paraffin, sectioned, and analyzed using IHC for cell proliferation (Ki67) and apoptosis (TUNEL). (G) SFRP3 sh5 significantly reduced, while SFRP3 sh3 showed a trend towards reducing, cell proliferation. (H) Both SFRP3 sh3 and sh5 show a trend towards increasing apoptosis, although not statistically significant. SFRP3 shRNAs also elevated levels of markers of muscle differentiation, MYOD1 (I), MYOG (J), and MYF6 (also known as MRF4) (K), as measured by qPCR. (L) SFRP3 shRNAs also non-significantly increased levels of AXIN2, a transcriptional target of β -catenin, as measured by qPCR. * $p < 0.05$, *** $p < 0.001$ when compared to Dox V. Katrina Slemmons performed the qPCR for panels I-K.

5.2 Suppression of SFRP3 inhibits aRMS tumorigenesis *in vivo*.

We assessed the role of SFRP3 in supporting tumorigenesis *in vivo* using a conditional subcutaneous xenograft model of aRMS. Since SFRP3 suppression causes aRMS cells to grow poorly, we used a doxycycline-inducible shRNA system to control for effects on tumor implantation. This allowed for expression of the shRNAs after a tumor had formed. SFRP3 sh3 and sh5 were cloned into an inducible vector and tested for their ability to suppress SFRP3 mRNA expression following three days of 4 $\mu\text{g/mL}$ doxycycline (**Fig. 6A,B**). The ability of the inducible shRNA to reduce Rh28 and Rh30 cell growth was also verified (**Fig. 6 C,D**).

Xenograft tumors arising from Rh28 cells with a doxycycline-inducible shRNA against SFRP3 or an empty vector were generated, and mice received either control treatment (sucrose water) or doxycycline. Mice receiving the control treatment showed no difference in tumor growth, regardless of SFRP3 shRNA status, showing that in the absence of doxycycline the shRNAs were not leaky (**Fig. 20 A,C**). Mice receiving doxycycline and bearing xenograft tumors from cells expressing empty vector similarly showed robust tumor growth (**Fig. 20 B,D**). However, mice receiving doxycycline and bearing xenografts expressing SFRP3 shRNA3 or shRNA5 showed an inhibition of xenograft growth (**Fig. 20 B,D**), with an associated decrease in tumor weight (**Fig. 20E**). To prove target knockdown after necropsy, levels of human SFRP3 mRNA were measured in the tumors by semi-quantitative RT-PCR and analyzed using densitometry

(Fig. 20F). While there was some variation, tumors in which SFRP3 was suppressed using the shRNAs showed lower levels of SFRP3 than the controls.

To understand the mechanism of decreased tumor growth and identify changes caused by SFRP3 suppression, tumors were embedded, sectioned, and stained for H&E, Ki67, and TUNEL to assess tumor cell morphology, proliferation, and apoptosis, respectively. While H&E showed no obvious changes, there was a trend towards a reduction in Ki67 and an increase in apoptosis in tumors bearing SFRP3 shRNAs (Fig. 20 G,H), mirroring the observed decrease in proliferation and increase in apoptosis observed *in vitro*.

5.3 Suppression of SFRP3 in vivo induces markers of differentiation and Wnt pathway activation

While we had not observed a consistent or robust increase in differentiation in RMS cells under conditions of SFRP3 suppression *in vitro*, we nevertheless examined the SQ tumor xenografts for evidence of such, and found that tumors expressing the doxycycline-inducible SFRP3 shRNA constructs under conditions of doxycycline treatment had evidence of myogenic differentiation. Specifically, the early differentiation marker MyoD (Fig. 20I) was upregulated in response to SFRP3 sh5, while the intermediate and late markers Myogenin (Fig. 20J) and Myf6 (Fig. 20K) were upregulated in response to both SFRP3 sh3 and sh5. Given the requirement for Wnt signaling during myogenic differentiation, we next examined the same tumors for

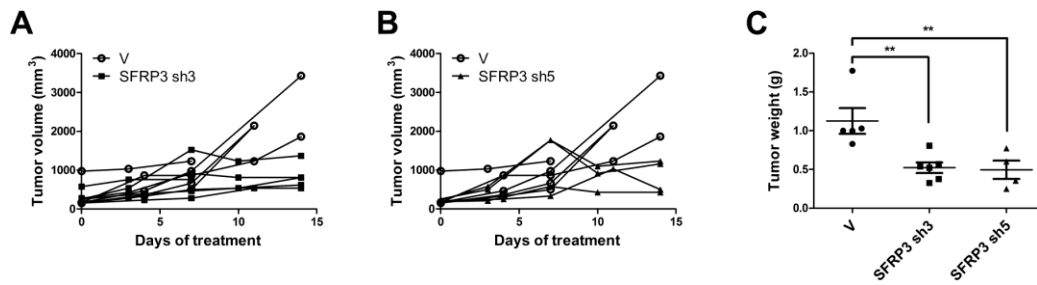


Figure 21: Shorter duration of SFRP3 suppression inhibits tumor growth *in vivo*.

Rh28 cells expressing doxycycline-inducible shRNAs against SFRP3 (or vector) were injected subcutaneously into the flanks of SCID/beige mice. Once tumors reached 150 mm³, mice began doxycycline treatment. Tumor dimensions were measured twice a week using calipers. SFRP3 suppression due to sh3 (A) or sh5 (B) reduced tumor growth. (C) Following 14 days of exposure to doxycycline or when an IACUC-defined endpoint was reached, mice were sacrificed and tumors were excised and weighed. SFRP3 suppression reduced tumor weight. * $p < 0.05$, ** $p < 0.01$ when compared to V.

evidence of Wnt pathway activation using Axin2 expression (Yan et al. 2001; Jho et al. 2002; Lustig et al. 2002; Annavarapu et al. 2013). In tumors bearing the SFRP3 shRNAs under conditions of doxycycline treatment, we did find Axin2 modestly upregulated (**Fig. 20L**).

Since these xenograft tumors were harvested over 20 days after initiation of doxycycline, potentially permitting tolerance to shRNA expression, we repeated the xenograft experiment but harvested the tumors after only 14 days doxycycline exposure in order to capture early events. As before, those tumors expressing the SFRP3 shRNAs under conditions of doxycycline showed decreased tumor volume and weight (**Fig. 21A-C**), decreased Ki67 (**Fig. 21A**) and increased TUNEL staining (**Fig. 22B**). However they also demonstrated an altered morphology (statistically significant fewer cells per field (**Fig. 22C**)) and an increase in nuclear β -catenin staining (**Fig. 22D**). Taken together these results suggest that in the *in vivo* setting, suppression of SFRP3 in aRMS promotes myogenic differentiation and Wnt pathway activation.

Given the findings in the xenograft tumors, to gain additional insight into the molecular consequences of SFRP3 suppression we used microarrays to analyze global gene expression after SFRP3 suppression by the two doxycycline-inducible SFRP3 shRNAs (**Fig. 6 A,B**) in triplicate. The robust multiarray average (RMA)-normalized data were selected by significance analysis of microarrays (SAM) to identify genes that were consistently induced or repressed by both SFRP3 shRNAs. With the false discovery

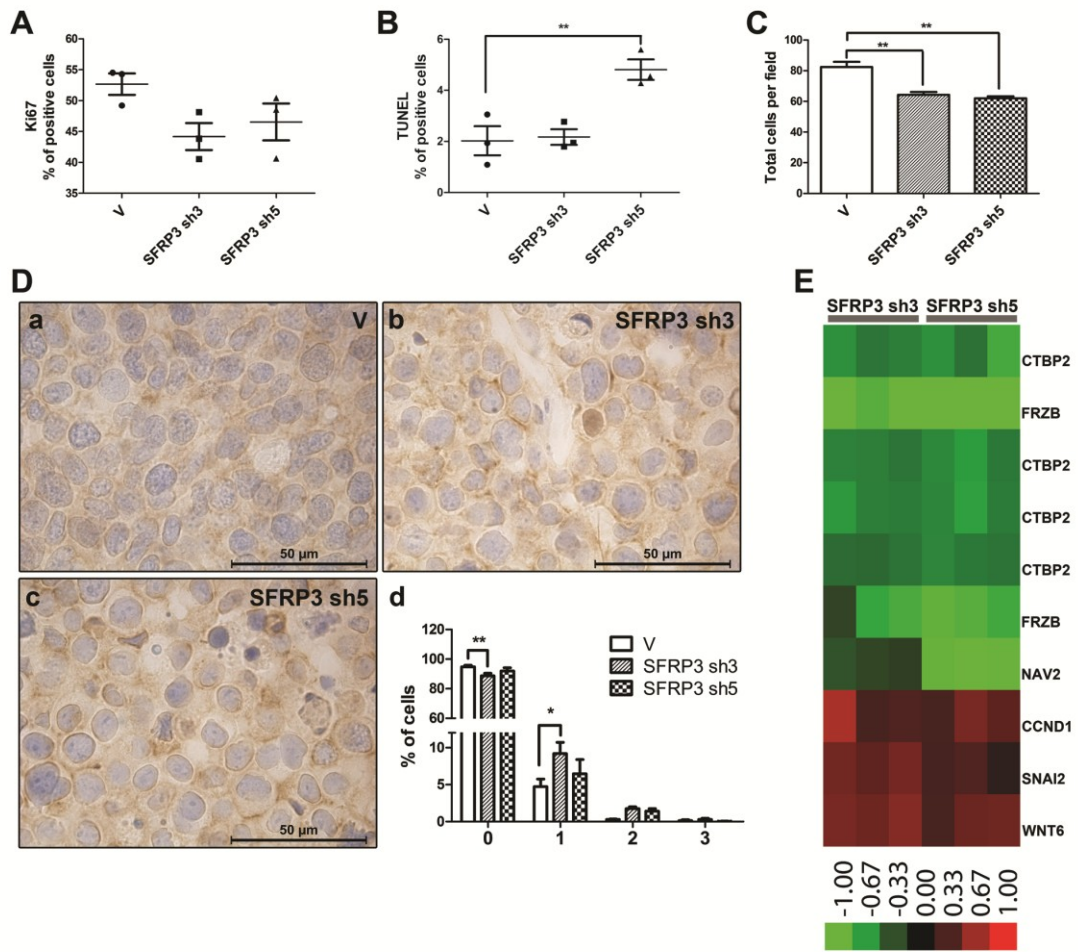


Figure 22: SFRP3 suppression increases β -catenin expression.

Tumors were generated and harvested as described in Fig. 20, except that they were harvested after only 14 days to capture early events. Tumors were fixed, embedded in paraffin, sectioned, and analyzed using IHC for cell proliferation (Ki67), apoptosis (TUNEL), and β -catenin. SFRP3 suppression shows a trend towards reduced proliferation (A) and increased apoptosis, significant for SFRP3 sh5 (B). SFRP3 suppression reduced the number of cells per field (C) and (D a-c), but increased nuclear β -catenin staining (D a-d), suggesting increased Wnt signaling activity. Representative sections shown in (D a-c). (E) Heatmap of the expression changes of the indicated Wnt-related genes consistently altered by SFRP3 suppression. The filter criteria required at least 4 observations with an abs value of ≥ 0.3 . The color bar has a value of 1. * $p < 0.05$, ** $p < 0.01$ Mircoarray performed by the Duke Microarray Facility based on samples prepared by Julie Kephart. Microarray analysis performed by Dr. Jen-Tsen Ashley Chi and Po-Han Chen.

Table 6: GO enriched and repressed probesets

#	GO enrichment of induced probesets	GO enrichment of repressed probesets
1	GO:0007517 [5]: muscle development	GO:0050874 [3]: organismal physiological process
2	GO:0006936 [3]: muscle contraction	GO:0050896 [3]: response to stimulus
3	GO:0006937 [4]: regulation of muscle contraction	GO:0009605 [4]: response to external stimulus
4	GO:0006941 [4]: striated muscle contraction	GO:0050877 [4]: neurophysiological process
5	GO:0009653 [3]: morphogenesis	GO:0007049 [5]: cell cycle
6	GO:0009887 [4]: organogenesis	GO:0007017 [7]: microtubule-based process
7	GO:0048513 [3]: organ development	GO:0006996 [5]: organelle organization and biogenesis
8	GO:0007275 [2]: development	GO:0008089 [9]: anterograde axon cargo transport
9	GO:0006942 [5]: regulation of striated muscle contraction	GO:0007010 [6]: cytoskeleton organization and biogenesis
10	GO:0050875 [3]: cellular physiological process	GO:0000279 [6]: M phase
11	GO:0008152 [3]: metabolism	GO:0000278 [6]: mitotic cell cycle
12	GO:0044237 [4]: cellular metabolism	GO:0007067 [8]: mitosis
13	GO:0044238 [4]: primary metabolism	GO:0000280 [7]: nuclear division
14	GO:0009987 [2]: cellular process	GO:0000087 [7]: M phase of mitotic cell cycle
15	GO:0030035 [7]: microspike biogenesis	GO:0009581 [5]: detection of external stimulus

Microarray analysis performed by Dr. Jen-Tsen Ashley Chi and Po-Han Chen.

rate (FDR) of 1.13%, we identified 474 induced and 711 repressed probe-sets (Table included in Kephart et al. 2015 supplemental data, GEO accession number GSE67999). We analyzed the Gene Ontology (GO) enrichment and found the induced genes were enriched in striated muscle development/differentiation (15 most induced probesets shown in **Table 6**, Full GO analysis found in Kephart et al. 2015 supplemental data). In contrast, the repressed genes were enriched in response to stimulus and cell cycle/mitosis genes (15 most repressed probesets shown in **Table 6**, Full GO analysis found in Kephart et al. 2015). These results indicate that SFRP3 suppression induced muscle differentiation and repressed proliferation, consistent with the *in vivo* data (**Fig. 20 G-H, Fig. 22 A-D**).

Given the role of SFRP3 in Wnt signaling, we also interrogated the microarray data for effects on Wnt-related genes. 109 genes were chosen for analysis (based on the literature and their inclusion in commercially available Wnt-related signaling arrays.) We were most interested in changes seen across both shRNAs, derived by zero-transformation (Tang, Lucas et al. 2012), and as expected found downregulation of SFRP3 (FRZB) (**Fig. 22E, Table 7**) but also downregulation of Wnt pathway-repressing genes such as CTBP2 (a transcriptional repressor of TCF, similar to CTBP1 (Valenta et al. 2003)) and NAV2 (which is downstream from APC, (Ishiguro et al. 2002)). Interestingly, APC (which promotes the degradation of β -catenin) was also downregulated by the shRNAs, but was not downregulated in enough samples to meet the inclusion criteria

Table 7: Wnt pathway genes identified in SFRP3 suppression microarray

Probe Set ID	Gene Symbol	SFRP3 sh3-1	SFRP3 sh3-2	SFRP3 sh3-3	SFRP3 sh5-1	SFRP3 sh5-2	SFRP3 sh5-3
201218_at	CTBP2	-0.6125133	-0.5045433	-0.5463333	-0.6131733	-0.4905933	-0.7743733
203697_at	FRZB	-1.2770387	-0.8583567	-1.2344207	-1.6813807	-1.5767877	-1.2725587
201220_x_at	CTBP2	-0.5593467	-0.5447067	-0.5032867	-0.5870267	-0.6604267	-0.5182967
210835_s_at	CTBP2	-0.6462	-0.54572	-0.53408	-0.57489	-0.67311	-0.53728
210554_s_at	CTBP2	-0.4646633	-0.4547033	-0.5001133	-0.5713133	-0.5189433	-0.4983933
203698_s_at	FRZB	-0.28328	-0.713888	-0.787856	-0.942111	-0.859609	-0.755287
218330_s_at	NAV2	-0.3505167	-0.2900867	-0.2586667	0.9775167	-1.0584747	-0.9824967
208712_at	CCND1	0.71732733	0.31104133	0.34621533	0.30591633	0.51413133	0.39717933
213139_at	SNAI2	0.489853	0.413014	0.503598	0.302047	0.346313	0.190204
221609_s_at	WNT6	0.52458867	0.47130767	0.57538667	0.31307467	0.45743767	0.48218167

Microarray analysis performed by Dr. Jen-Tsen Ashley Chi and Po-Han Chen.

for **Fig. 22E**. Conversely, we noted upregulation of genes including CCND1 (cyclin D1) and SNAI2 (SLUG), both Wnt signaling target genes (Wu et al. 2012; Ashihara et al. 2015) and WNT6, which is known to inhibit myoblast proliferation but induce myoblast elongation (Hitchins et al. 2013). Taken together, these results suggest that suppression of SFRP3 in part activates β -catenin/Wnt signaling pathway as we had seen in the tumor xenografts.

While SFRP3 suppression does appear to increase Wnt signaling, the changes are less than 2-fold, leading us to hypothesize that more than one cellular signaling pathway is probably altered and responsible for the striking phenotype. To this end, the microarray was also analyzed for changes in signatures associated with oncogenic pathways (**Fig. 23**). Surprisingly, the signature for active β -catenin was expressed very strongly in the control cells and decreased in the SFRP3 suppressed cells. This is contrary to the literature suggesting low levels of active β -catenin in RMS cells and other evidence suggesting SFRP3 suppression increases β -catenin signaling (**Fig. 10A, 18 D,E**). These pathway signatures were developed in epithelial cells, while RMS cells are of mesenchymal origin. Further, we know that Wnt signaling is cell and context specific, so it is probable that this signature is not an accurate representation of β -catenin activation in RMS cells. The pathway signatures developed in epithelial cells can provide useful information; however, any information must be confirmed with additional experiments or data in mesenchymal or RMS cells.

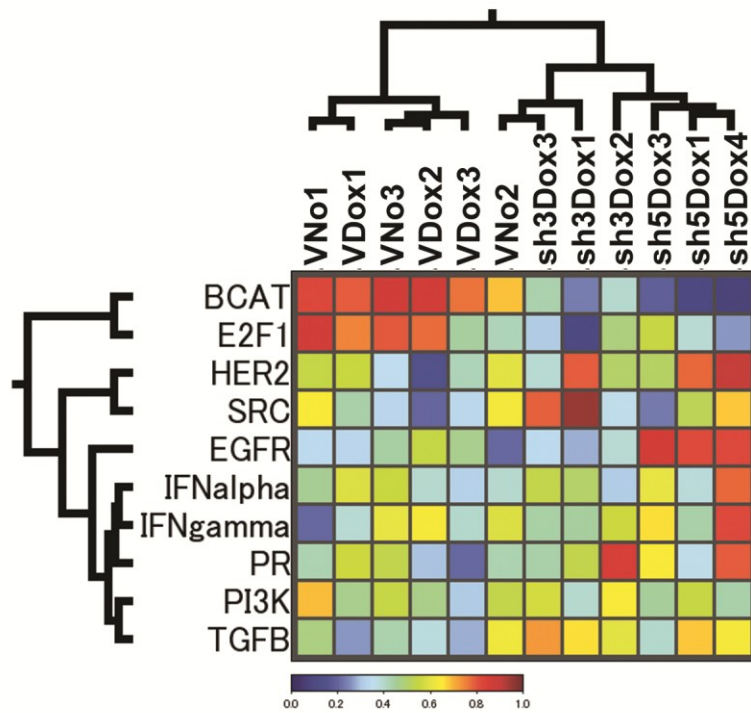


Figure 23: Pathway signature analysis

Heatmap of the changes of signatures associated with oncogenic pathways in the microarray. The development and usage of the signatures have been previously described (Bild et al. 2006; Chang et al. 2011). Analysis performed by Dr. Jen-Tsen Ashley Chi and Po-Han Chen.

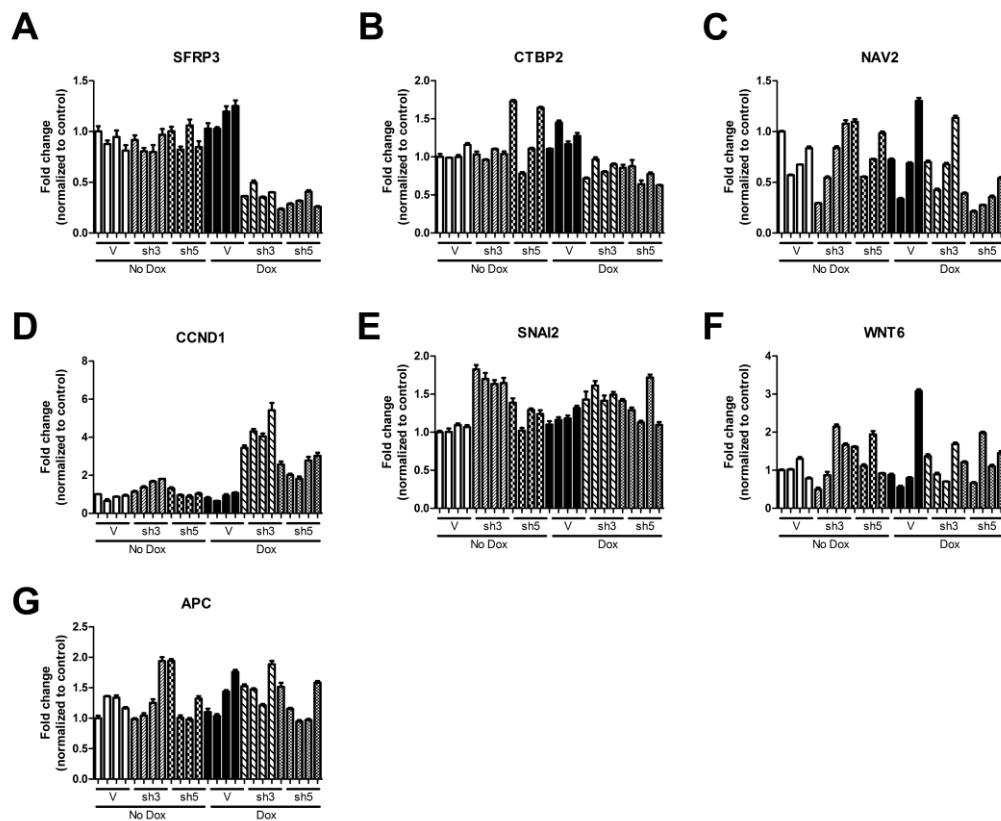


Figure 24: Validation Wnt pathway members identified in the microarray.

Expression patterns of Wnt pathway members SFRP3 (A), CTBP2 (B), NAV2 (C), CCND1 (D), SNAI2 (E), WNT6 (F) were verified through qPCR. For the microarray V, SFRP3 sh3, and SFRP3 sh5 with doxycycline were analyzed in biological triplicate; however, for the microarray verification, V, SFRP3 sh3 and SFRP3 sh5 with and without doxycycline were analyzed in biological replicates of four or five. APC was also analyzed as in the microarray, it was suppressed in response to SFRP3 sh3; however, the qPCR does not reflect that result. Each bar is the average of three technical replicates of a biological replicate.

In addition, we observe a reduction in E2F1 activity, consistent with the downregulation of cell cycle genes (**Table 6**). The binding motifs of these cell cycle related genes also demonstrated enrichment in E2F1 binding sites. Consistent with the results from the oncogenic pathway screen (**Fig. 14**), SFRP3 suppression is also associated with an increase in the TGF β pathway. When the upregulated genes were analyzed, an enrichment for SMAD4 binding sites was noted. Finally, we noted that the empty vector controls treated with (VDox) and without (VNo) doxycycline did not segregate from each other. This suggests that the dose of doxycycline we selected did not alter the expression of oncogenic pathways.

Suppression of SFRP3 in microarray samples was confirmed through qPCR (**Fig. 24A**). The expression levels of Wnt pathway genes CTBP2 (**Fig. 24B**), NAV2 (**Fig. 24C**), CCND1 (**Fig. 24D**), SNAI2 (**Fig. 24E**), WNT6 (**Fig. 24F**) were also measured by qPCR . Of these, SFRP3, CTBP2, and CCND1 demonstrate qPCR levels that were consistent with the result of the microarray. In the remaining genes, NAV2, SNAI2, and WNT6, no clear changes are observed. However, the data for those genes are variable and the changes observed in the microarray are less than two-fold, thus this variability may obscure small changes in expression level. To connect CTBP2 or CCND1 with the SFRP3 suppression-mediated decreased cell growth, overexpression of CTBP2 or suppression of CCND1 would be assessed for its ability to rescue SFRP3 suppression-mediated decreased cell growth. Finally, the expression level of APC (**Fig. 24G**) was analyzed as it

was suppressed in response to SFRP3 sh3 in the microarray and its suppression would be consistent with an increase in Wnt signaling; however, through qPCR, that result could not be confirmed.

5.4 SFRP3 suppression in combination with vincristine abrogates aRMS tumorigenesis.

Finally, as a pre-clinical assessment of SFRP3 suppression in aRMS, we investigated the role of genetic SFRP3 suppression in combination with chemotherapy, as combination therapy approaches have been successful in treating pediatric malignancies. We hypothesized that combining SFRP3 suppression with vincristine, a chemotherapy agent used for aRMS treatment since the 1970s (Crist et al. 1995), would be more effective at inhibiting aRMS cell growth than either alone. To this end, we first performed an MTT assay using Rh28 cells expressing an empty vector or SFRP3 sh3 with vincristine (0-10 nM). While both SFRP3 inhibition and vincristine inhibited cell growth alone, the combination produced the greatest inhibition (**Fig. 25A**), as evidenced by the shRNA-drug dose curve shifting to the left.

While Rh28 cells appeared sensitized to vincristine in the presence of SFRP3 suppression *in vitro*, we next investigated the combination in our *in vivo* xenograft model of aRMS. Xenograft tumors were generated using Rh28 cells containing a doxycycline inducible SFRP3 shRNA (SFRP3 sh3) or empty vector as done previously. Once the tumors were palpable, mice were randomized to treatment with doxycycline plus

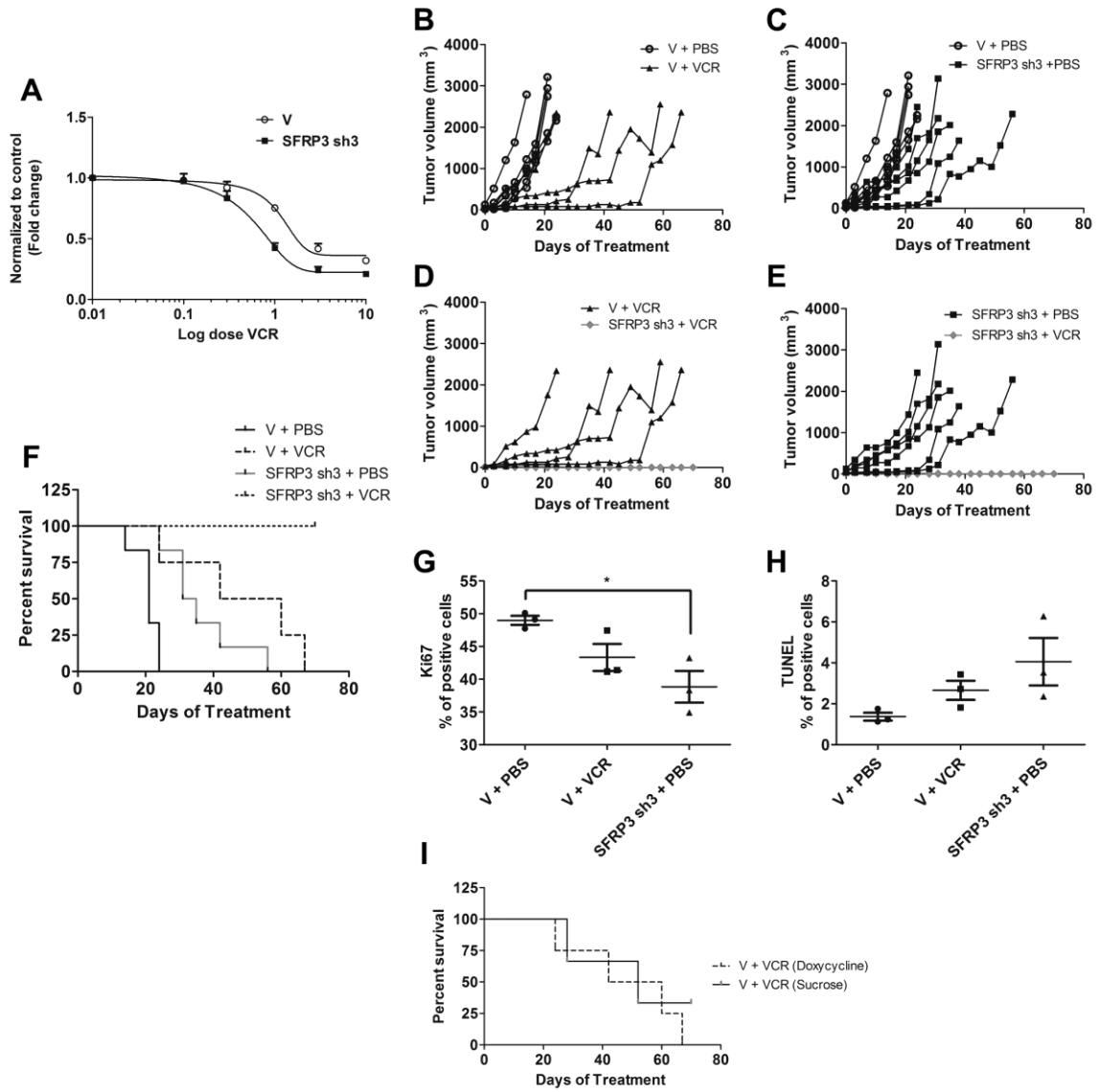


Figure 25: SFRP3 suppression in combination with vincristine inhibits aRMS cell and tumor growth and causes tumor regression.

(A) Rh28 cells stably expressing a doxycycline-inducible shRNA against SFRP3 (SFRP3 sh3) or empty vector (V) were treated with 2 μ g/mL doxycycline and increasing doses of vincristine. As measured by MTT assay, the combination of SFRP3 suppression and vincristine was more effective than vincristine alone at inhibiting cell growth. Rh28 xenograft tumors were generated containing an empty vector (V) or a doxycycline-inducible SFRP3 shRNA (SFRP3 sh3). All mice received doxycycline and either vincristine (VCR) or PBS. Both vincristine (V+PBS) (B) and SFRP3 suppression (SFRP3 sh3+PBS) (C) decreased tumor growth as compared to empty vector (V+PBS). The combination of vincristine and SFRP3 suppression (SFRP3 sh3+VCR) was most effective at decreasing tumor growth, inhibiting more than vincristine (V+VCR) (D) or SFRP3 suppression (SFRP3 sh3+PBS) (E) alone. (F) While both SFRP3 suppression (SFRP3 sh3+PBS) and vincristine (V+VCR) increased survival compared to control (V+PBS), the combination of SFRP3 suppression and vincristine (SFRP3 sh3+VCR) prolonged survival the longest. (G) SFRP3 suppression significantly decreased cell proliferation when compared to empty vector. (H) Both SFRP3 suppression and vincristine show a trend towards an increase in apoptosis. (I) To verify that doxycycline was not interacting with vincristine to suppress tumor growth, mice whose tumors contained an empty vector were treated with vincristine and either doxycycline (V + VCR (Doxycycline)) or sucrose (V + VCR (Sucrose)). There was no significant change in survival between the groups, suggesting that vincristine does not interact with doxycycline to reduce tumor growth.

weekly vincristine (or vehicle) injections. As expected, we found that vincristine alone or SFRP3 suppression alone inhibited tumor growth (**Fig. 25 B,C**). However, the combination of vincristine and SFRP3 suppression was more effective than either treatment alone (**Fig. 25 D,E**), and unexpectedly caused tumor regression. To verify that doxycycline was not interfering with the chemotherapeutic property of vincristine, a shadow control group of mice were treated with vincristine plus the vehicle for doxycycline and compared to those being treated with vincristine. There was no difference between the groups, suggesting that indeed doxycycline was not interfering with vincristine (**Fig. 25I**). In survival analysis, while SFRP3 suppression alone and vincristine alone prolonged survival to an IACUC-approved endpoint, the combination was most effective (**Fig. 25F**).

At necropsy, the tumors arising from the SFRP3 suppression alone or vincristine alone treatment groups showed no notable changes in the histology when stained with H&E. However, both groups showed decreased cell proliferation as measured by Ki67, with the change caused by SFRP3 suppression being significant (**Fig. 25G**). Both also demonstrated a trend towards an increase in apoptosis, as measured by TUNEL staining (**Fig. 25H**). In the SFRP3 suppression plus vincristine group, five of seven mice had no detectable tumors at necropsy. The remaining two mice had tiny remnant subcutaneous masses, the larger of which we embedded in paraffin and found on H&E to be composed mostly of fat cells. In summary, these data demonstrate the pre-clinical utility

of SFRP3 suppression in combination with chemotherapy *in vivo*, suggesting that this approach should be explored further for its potential use in clinical care of patients with aRMS.

5.5 Discussion

Similar to its effects *in vitro*, SFRP3 suppression in a murine xenograft model of aRMS suppressed tumor growth decreased tumor growth and decreased proliferation and increased apoptosis. It was in these xenograft tumors that we were able to find further evidence for SFRP3 suppression increasing Wnt signaling, by measuring an elevation in Axin2 expression. This reaffirms the change in Axin2 we observed *in vitro* (Fig. 10A).

Analysis of the tumors also revealed SFRP3 suppression induced markers of differentiation. SFRP3 suppression was predicted to induce differentiation based on its actions during muscle regeneration (Brack et al. 2008). Activation of the Wnt pathway in aRMS, through the use of Wnt3a, also induces the myogenic markers MyoD1, Myf5, and myogenin and changes cell morphology to that of a differentiated cell (Annavarapu et al. 2013). Despite this evidence, we were unable to identify robust changes in myogenic markers which would indicate differentiation either when SFRP3 was suppressed in growth or differentiation media (Fig. 9A). However, evidence for differentiation in the tumor suggests that the tissue culture environment may not be as conducive for differentiation as an *in vivo* setting.

Finally, SFRP3 suppression sensitizes SFRP3 suppressed cells to vincristine. This is an important finding for the field of RMS, as RMS patients are treated with a multi-modal approach. New therapies are much more likely to be used in combination with current standard-of-care therapies, thus finding a new targeted approach that enhances the effect of a current therapy is promising.

6. Conclusions

This work demonstrates a novel role for the secreted Wnt inhibitor SFRP3 in PF-positive alveolar rhabdomyosarcoma (aRMS) tumorigenesis. While attempts have been made at inhibiting PF through inhibition of its phosphorylation and activity (Fredericks et al. 2000; Thalhammer et al. 2015), PF is not a currently tractable pharmacological target and as a transcription factor is not an ideal candidate for inhibition through small molecules inhibitors. Further, preliminary work suggests that inhibition of PF results in temporary tumor regression (Pandey et al. 2015), suggesting it may not be the ideal target for a new therapy for PF-positive aRMS. As such, we aim to understand proteins downstream from or cooperating with PF to support tumorigenesis. To this end, we conducted a microarray of genes altered by the expression of PF. Among the over 1,000 genes up- or down-regulated more than 3-fold, we chose to focus on the Wnt pathway inhibitor, SFRP3. Already, embryonic developmental pathways including Wnt, Hippo, Notch, and Hedgehog, have been found to be involved in RMS tumorigenesis (Tostar et al. 2010; Belyea et al. 2011; Annavarapu et al. 2013; Crose et al. 2014). This work adds to that body of knowledge by showing that SFRP3 is necessary for *in vitro* and *in vivo* aRMS growth.

6.1 The connection between PF and SFRP3

While SFRP3 levels were increased in PF-containing cells (both aRMS cell lines and HSMs stably expressing PF), SFRP3 most likely cooperates with PF to support

aRMS tumorigenesis, rather than being a direct downstream target. Indeed neither SFRP3, nor any other SFRP family members, appear in a genome-wide screen identifying PF binding sites (Cao, Yu et al. 2010). This is not unusual as other necessary changes for aRMS tumorigenesis, including inactivation of p16INK4a, are also cooperating changes with PF rather than directly downstream changes (Linardic et al. 2007). Future work may elucidate the connection between PF and SFRP3, which may also provide insight into the regulation of as to SFRP3.

6.2 SFRP3 suppression decreases cell and tumor growth

Interestingly, the suppression of SFRP3 decreased cell growth through a combination of mechanisms, decreased proliferation, and increased apoptosis. These phenotypes are likely connected, as cell cycle arrest may lead to secondary apoptosis if specific checkpoints are activated (Orth et al. 2012). The expression of SFRP3 in renal cancer inhibits apoptosis, suggesting that SFRP3 may have a primary role in controlling apoptosis as well (Hirata et al. 2010). Future work identifying the timing of the cell cycle arrest and apoptosis in SFRP3-suppressed aRMS cells may reveal if they are indeed connected.

To further understand the decreased proliferation, we measured the levels of p21, as it is a central sensor and effector of anti-proliferative signals in cells (Abbas and Dutta 2009). An increase in p21 was associated with the SFRP3 suppression-mediated decrease in cell proliferation. Indeed PF-positive aRMS is known to have low levels of

p21, mediated through EGR1 (Hecker et al. 2010). p21 reactivation using the HDAC inhibitor valproic acid (VPA) combined with the small molecule inhibitor PCK412 (midostaurin) induced apoptosis and reduced tumor growth *in vivo*. This suggests that the p21 pathway is still functional in PF-positive aRMS cells and activation of the pathway ought to be considered for future aRMS therapies.

Previous studies have shown that SFRP3 can inhibit the differentiation-inducing effects of Wnt signaling on murine myoblasts, and that the addition of recombinant SFRP3 in regenerating murine skeletal muscle decreases nascent myotube formation, demonstrating that SFRP3 has a clear role in blocking differentiation (Brack et al. 2008). Further, in eRMS, activation of the Wnt pathway induces markers of differentiation (Singh et al. 2010; Chen et al. 2014). To this end we examined both myogenic differentiation and Wnt pathway status following SFRP3 suppression *in vitro* and *in vivo*.

In aRMS cell lines, while we observed a cell cycle arrest in response to SFRP3 suppression, surprisingly, we did not observe changes in terminal differentiation (MF-20 staining). However, SFRP3 suppression induced myogenic differentiation as observed using a microarray approach and examination of markers of differentiation in tumors. It is plausible that the aRMS cell lines used in these studies have the ability to express markers of differentiation, but are unable to achieve terminal differentiation and express MF-20. In addition, should the cells be arrested mid-differentiation, it is also plausible that this arrest would induce the apoptosis we observed.

Interestingly, while both shRNAs promoted myogenic differentiation in the tumors, differences emerged as to which markers of differentiation were induced. Particularly, SFRP3 sh3 appeared to induce markers associated with later events in myogenic differentiation than SFRP3 sh5. Similarly, while we did not see evidence of Wnt pathway activation in the stable suppression system, the microarray analysis and levels of AXIN2 in the tumors did reflect this activation. While we do not fully understand the mechanisms causing these inconsistencies, most likely a combination of effects are responsible including differences in the microenvironment, between the shRNAs, and in the amplitude of SFRP3 suppression. Indeed, Wnt activation and repression has been shown to be finely tuned to SFRP levels (Xavier et al. 2014). Adding to this complexity, the amount of Wnt ligand present also determines which pathway is activated, canonical or non-canonical (Nalesso et al. 2011). Future work will attempt to reconcile these differences.

To further validate the requirement for SFRP3 in aRMS growth, SFRP3 was genetically suppressed in subcutaneous xenografts of aRMS cell lines. This resulted in a decrease in tumor growth and a decrease, although not statistically significant, in cell proliferation. We also observed a trend towards an increase in apoptosis. The magnitude of the effects on cell proliferation and apoptosis are not as large as expected based on the magnitude of the decrease in tumor growth. This is likely due to the tumor consisting of many cells that have overcome the growth inhibition caused by SFRP3.

6.3 The connection between SFRP3 and the Wnt pathway

In both our *in vitro* and *in vivo* studies, suppression of SFRP3 in aRMS cells blocked cell growth both by reducing proliferation and inducing apoptosis. Increased SFRP3 expression has been previously reported in metastatic renal carcinoma, required for cell growth and invasion (Hirata et al. 2010). However, several other malignancies including prostate cancer, breast cancer, and fibrosarcoma demonstrate downregulation or inhibition of SFRPs (Guo et al. 2008; Surana et al. 2013). While SFRPs were originally identified as Wnt signaling inhibitors, recently SFRPs such as SFRP1 have been shown to both potentiate and inhibit canonical Wnt signaling depending on a number of factors including SFRP concentration, cell type, and Frizzled receptor expression (Xavier et al. 2014). This suggests that secreted Wnt inhibitors may have more complex signaling functions than previously thought, and each SFRP will need to be investigated in a cell and cancer-specific context.

We were unable to demonstrate that SFRP3 inhibition consistently altered β -catenin signaling in our cells, despite effective positive controls demonstrating our approach was capable of detecting changes. As has previously been observed, this suggests aRMS cells have the ability to activate β -catenin signaling (Annavarapu et al. 2013). However, in the screen investigating the effects of oncogenic pathway activation on the survival of Rh28 cells with SFRP3 suppression, we observed that SFRP3 suppression synergized with β -catenin pathway activation to decrease survival in 3 out

of 4 conditions investigated. One critique of this screen is its inability to differentiate between downstream targets and cooperative effects, so it is unclear how SFRP3 suppression synergizes with β -catenin activation. Lodewyckx et al. (2012) demonstrated that in a SFRP3 knockout mouse, modest Wnt pathway activation was observed through pathway signatures in a microarray, but not through changes in β -catenin phosphorylation. This tight regulation appears to occur through compensation for the lack of SFRP3 through increased expression of other SFRP family members (Lodewyckx et al. 2012). Finally, another secreted Wnt inhibitor, DKK1 was found to be overexpressed in prostate cancer and caused a G₁ arrest (Hall et al. 2010). However, as with SFRP3, the authors could identify no change in Wnt signaling following inhibition of DKK1. This suggests that secreted Wnt inhibitors may have a broader network of downstream signaling pathways than previously thought.

This work primarily focused on the contribution of SFRP3 to aRMS; however, evidence suggests that other secreted Wnt inhibitors may also modulate tumorigenesis. In particular, in work done by a collaborator (Tim Triche, Children's Hospital of Los Angeles) a microarray of human exon suggested that SFRP4 is upregulated in aRMS when compared with eRMS (personal communications with Tim Triche). In the same array, SFRP3 was also elevated in aRMS compared to eRMS, but was not found significant (personal communication with Stephen Skapek and Lin Xu, University of Texas Southwestern Medical Center). Further, in our microarray, we identified three

other secreted Wnt inhibitors, SFRP1, SFRP4, and DKK2, as altered in response to the presence of PF in HSMMs. All three are expressed in PF-positive aRMS cells lines, and should be considered as other potential modulators of aRMS tumorigenesis. In particular, SFRP3 and SFRP4 are closely related, so may have some overlapping functions in promoting tumorigenesis.

6.4 SFRP3 suppression sensitizes aRMS cells to vincristine and potential for use in aRMS patients

SFRP3 inhibition increased the sensitivity of aRMS cells to vincristine, a chemotherapeutic agent used often in aRMS. This effect was particularly pronounced *in vivo*; however, we do not fully understand the mechanism for this decreased cell and tumor growth. Vincristine, like other vinca alkaloids, disrupts cell proliferation by inhibiting microtubule assembly (Himes et al. 1976). However, more recently, vincristine was also found to inhibit angiogenesis (Mabeta and Pepper 2009). This second mechanism or other changes in the tumor microenvironment may explain the difference observed between vincristine's effects *in vitro* and *in vivo*, as multiple distinct mechanisms have the greatest potential to inhibit tumor growth. It is also possible that *in vitro*, where presumably vincristine's mechanism of action is through inhibiting the cell cycle by inhibiting microtubule assembly, aRMS cells that are already arrested at G₁ due to SFRP3 inhibition are insensitive to vincristine. While genetic inhibition of SFRP3 is not be feasible for treatment of aRMS patients, a monoclonal antibody against SFRP2 is effective in a murine model of breast cancer (Fontenot et al. 2013). Therefore, a similar

monoclonal antibody against SFRP3 could be developed and tested for clinical efficacy in patients.

While these data suggest that a combination of SFRP3 suppression, possibly through a monoclonal SFRP3 antibody, and vincristine has great potential to suppress aRMS tumors, the data suggesting SFRP3 suppression modestly upregulates Wnt signaling are also worth considering. Treatment of aRMS xenografts with LiCl had little effect on tumor growth, but the possibility that activation of the pathway could sensitize the tumors to vincristine was never explored. As such, the combination of LiCl, AR-A014418, or another Wnt activator with vincristine is worth exploring.

The oncogenic pathway screen also provided three cDNAs (MEK-1, Notch1 ICD, and HRAS) and TGFBR1 that rescued or enhanced SFRP3 suppression-mediated decreased cell growth, respectively. While we were not able to validate any of these results, we did show that Wnt signaling, SFRP3, and Notch signaling do interact in aRMS. Further, TGF β signaling was identified in a separate microarray as one of the pathways most suppressed in response to SFRP3. As such, both of these pathways should be explored further for their potential for treatment of PF-positive aRMS. In addition, Notch1 ICD rescued SFRP3 suppression and vincristine mediated decreased cell growth, thus the combination of Notch pathway inhibitors, such as GSI inhibitors, and vincristine should be explored. The disadvantage of GSI inhibitors is their toxicity, particularly in the gastrointestinal tract (Imbimbo 2008). Unfortunately, vincristine also

demonstrates gastrointestinal tract toxicity (Carbone et al. 1963), so any combination will have to address this dilemma. Finally, two independent screens suggested that SFRP3 suppression altered TGF β signaling and that an increase in TGF β signaling could sensitize cells to SFRP3 suppression-mediated decreased cell growth. While this data is preliminary, the combination of SFRP3 suppression and TGF β activation should be further explored.

6.5 Conclusions and future directions

In this work we demonstrated that SFRP3 is upregulated in response to PF expression, in both PF-expressing human myoblasts and human aRMS cell lines. Genetic suppression of SFRP3 reduced aRMS growth both *in vitro* and *in vivo*, suggesting that SFRP3 is necessary for aRMS tumorigenesis. This is associated with an increase in differentiation and a modest increase in Wnt signaling. Further, SFRP3 suppression sensitized aRMS cells and tumors to vincristine, suggesting that SFRP3 inhibition is a promising strategy for further investigation. This suggests that SFRPs may play an important role in aRMS. These results provide insights into the molecular mechanisms underlying aRMS and may inform new directions for aRMS treatment.

References

1. Abbas, T. and A. Dutta (2009). "p21 in cancer: intricate networks and multiple activities." Nat Rev Cancer **9**(6): 400-414.
2. Abraham, J., Y. Nunez-Alvarez, et al. (2014). "Lineage of origin in rhabdomyosarcoma informs pharmacological response." Genes Dev **28**(14): 1578-1591.
3. Akiri, G., M. M. Cherian, et al. (2009). "Wnt pathway aberrations including autocrine Wnt activation occur at high frequency in human non-small-cell lung carcinoma." Oncogene **28**(21): 2163-2172.
4. Andersen, P., H. Uosaki, et al. (2012). "Non-canonical Notch signaling: emerging role and mechanism." Trends Cell Biol **22**(5): 257-265.
5. Annavarapu, S. R., S. Cialfi, et al. (2013). "Characterization of Wnt/beta-catenin signaling in rhabdomyosarcoma." Lab Invest **93**(10): 1090-1099.
6. Armstrong, D. D., V. L. Wong, et al. (2006). "Expression of beta-catenin is necessary for physiological growth of adult skeletal muscle." Am J Physiol Cell Physiol **291**(1): C185-188.
7. Ashihara, E., T. Takada, et al. (2015). "Targeting the canonical Wnt/beta-catenin pathway in hematological malignancies." Cancer Sci **106**(6): 665-671.
8. Avraham, R. and Y. Yarden (2011). "Feedback regulation of EGFR signalling: decision making by early and delayed loops." Nat Rev Mol Cell Biol **12**(2): 104-117.
9. Barker, N. and H. Clevers (2006). "Mining the Wnt pathway for cancer therapeutics." Nat Rev Drug Discov **5**(12): 997-1014.
10. Barr, F. G., L. E. Nauta, et al. (1998). "Structural analysis of PAX3 genomic rearrangements in alveolar rhabdomyosarcoma." Cancer Genet Cytogenet **102**(1): 32-39.
11. Belyea, B., J. G. Kephart, et al. (2012). "Embryonic signaling pathways and rhabdomyosarcoma: contributions to cancer development and opportunities for therapeutic targeting." Sarcoma **2012**: 406239.

12. Belyea, B. C., S. Naini, et al. (2011). "Inhibition of the Notch-Hey1 axis blocks embryonal rhabdomyosarcoma tumorigenesis." Clin Cancer Res **17**(23): 7324-7336.
13. Bentzinger, C. F., Y. X. Wang, et al. (2012). "Building muscle: molecular regulation of myogenesis." Cold Spring Harb Perspect Biol **4**(2).
14. Bhat, R. A., B. Stauffer, et al. (2007). "Structure-function analysis of secreted frizzled-related protein-1 for its Wnt antagonist function." J Cell Biochem **102**(6): 1519-1528.
15. Bild, A. H., G. Yao, et al. (2006). "Oncogenic pathway signatures in human cancers as a guide to targeted therapies." Nature **439**(7074): 353-357.
16. Blum, J. M., L. Ano, et al. (2013). "Distinct and overlapping sarcoma subtypes initiated from muscle stem and progenitor cells." Cell Rep **5**(4): 933-940.
17. Bodine, P. V., B. Stauffer, et al. (2009). "A small molecule inhibitor of the Wnt antagonist secreted frizzled-related protein-1 stimulates bone formation." Bone **44**(6): 1063-1068.
18. Boland, G. M., G. Perkins, et al. (2004). "Wnt 3a promotes proliferation and suppresses osteogenic differentiation of adult human mesenchymal stem cells." J Cell Biochem **93**(6): 1210-1230.
19. Borello, U., B. Berarducci, et al. (2006). "The Wnt/beta-catenin pathway regulates Gli-mediated Myf5 expression during somitogenesis." Development **133**(18): 3723-3732.
20. Borello, U., M. Coletta, et al. (1999). "Transplacental delivery of the Wnt antagonist Frzb1 inhibits development of caudal paraxial mesoderm and skeletal myogenesis in mouse embryos." Development **126**(19): 4247-4255.
21. Bouche, M., R. Canipari, et al. (2000). "TGF-beta autocrine loop regulates cell growth and myogenic differentiation in human rhabdomyosarcoma cells." FASEB J **14**(9): 1147-1158.

22. Bouron-Dal Soglio, D., A. L. Rougemont, et al. (2009). "Beta-catenin mutation does not seem to have an effect on the tumorigenesis of pediatric rhabdomyosarcomas." *Pediatr Dev Pathol* **12**(5): 371-373.
23. Bovolenta, P., P. Esteve, et al. (2008). "Beyond Wnt inhibition: new functions of secreted Frizzled-related proteins in development and disease." *Journal of Cell Science* **121**(6): 737-746.
24. Brack, A. S., I. M. Conboy, et al. (2008). "A Temporal Switch from Notch to Wnt Signaling in Muscle Stem Cells Is Necessary for Normal Adult Myogenesis." *Cell Stem Cell* **2**(1): 50-59.
25. Brack, A. S., M. J. Conboy, et al. (2007). "Increased Wnt signaling during aging alters muscle stem cell fate and increases fibrosis." *Science* **317**(5839): 807-810.
26. Brunelli, S., F. Relaix, et al. (2007). "Beta catenin-independent activation of MyoD in presomitic mesoderm requires PKC and depends on Pax3 transcriptional activity." *Dev Biol* **304**(2): 604-614.
27. Bryson-Richardson, R. J. and P. D. Currie (2008). "The genetics of vertebrate myogenesis." *Nat Rev Genet* **9**(8): 632-646.
28. Burks, T. N. and R. D. Cohn (2011). "Role of TGF-beta signaling in inherited and acquired myopathies." *Skelet Muscle* **1**(1): 19.
29. Cao, L., Y. Yu, et al. (2010). "Genome-Wide Identification of PAX3-FKHR Binding Sites in Rhabdomyosarcoma Reveals Candidate Target Genes Important for Development and Cancer." *Cancer Research* **70**(16): 6497-6508.
30. Carbone, P. P., V. Bono, et al. (1963). "Clinical studies with vincristine." *Blood* **21**: 640-647.
31. Chang, J. T., M. L. Gatz, et al. (2011). "SIGNATURE: a workbench for gene expression signature analysis." *BMC Bioinformatics* **12**: 443.
32. Charytonowicz, E., C. Cordon-Cardo, et al. (2009). "Alveolar rhabdomyosarcoma: is the cell of origin a mesenchymal stem cell?" *Cancer Lett* **279**(2): 126-136.
33. Chen, E. Y., M. T. Deran, et al. (2014). "Glycogen synthase kinase 3 inhibitors induce the canonical WNT/beta-catenin pathway to suppress growth and self-

- renewal in embryonal rhabdomyosarcoma." Proc Natl Acad Sci U S A **111**(14): 5349-5354.
34. Chen, J. L., D. Merl, et al. (2010). "Lactic acidosis triggers starvation response with paradoxical induction of TXNIP through MondoA." PLoS Genet **6**(9): e1001093.
 35. Chen, X., E. Stewart, et al. (2013). "Targeting oxidative stress in embryonal rhabdomyosarcoma." Cancer Cell **24**(6): 710-724.
 36. Clement-Lacroix, P., M. Ai, et al. (2005). "Lrp5-independent activation of Wnt signaling by lithium chloride increases bone formation and bone mass in mice." Proc Natl Acad Sci U S A **102**(48): 17406-17411.
 37. Clevers, H. (2006). "Wnt/ β -Catenin Signaling in Development and Disease." Cell **127**(3): 469-480.
 38. Coghlan, M. P., A. A. Culbert, et al. (2000). "Selective small molecule inhibitors of glycogen synthase kinase-3 modulate glycogen metabolism and gene transcription." Chem Biol **7**(10): 793-803.
 39. Collu, G. M., A. Hidalgo-Sastre, et al. (2012). "Dishevelled limits Notch signalling through inhibition of CSL." Development **139**(23): 4405-4415.
 40. Collu, G. M., A. Hidalgo-Sastre, et al. (2014). "Wnt-Notch signalling crosstalk in development and disease." Cell Mol Life Sci **71**(18): 3553-3567.
 41. Crist, W., E. A. Gehan, et al. (1995). "The Third Intergroup Rhabdomyosarcoma Study." J Clin Oncol **13**(3): 610-630.
 42. Crose, L. E., K. T. Etheridge, et al. (2012). "FGFR4 blockade exerts distinct antitumorigenic effects in human embryonal versus alveolar rhabdomyosarcoma." Clin Cancer Res **18**(14): 3780-3790.
 43. Crose, L. E., K. A. Galindo, et al. (2014). "Alveolar rhabdomyosarcoma-associated PAX3-FOXO1 promotes tumorigenesis via Hippo pathway suppression." J Clin Invest **124**(1): 285-296.
 44. Cruciat, C. M. and C. Niehrs (2013). "Secreted and transmembrane wnt inhibitors and activators." Cold Spring Harb Perspect Biol **5**(3): a015081.

45. Davis, R. J., C. M. D'Cruz, et al. (1994). "Fusion of PAX7 to FKHR by the variant t(1;13)(p36;q14) translocation in alveolar rhabdomyosarcoma." Cancer Res **54**(11): 2869-2872.
46. De Salvo, M., L. Raimondi, et al. (2014). "Hyper-activation of Notch3 amplifies the proliferative potential of rhabdomyosarcoma cells." PLoS One **9**(5): e96238.
47. Descamps, S., H. Arzouk, et al. (2008). "Inhibition of myoblast differentiation by Sfrp1 and Sfrp2." Cell Tissue Res **332**(2): 299-306.
48. Fontenot, E., E. Rossi, et al. (2013). "A novel monoclonal antibody to secreted frizzled-related protein 2 inhibits tumor growth." Mol Cancer Ther **12**(5): 685-695.
49. Fredericks, W. J., K. Ayyanathan, et al. (2000). "An engineered PAX3-KRAB transcriptional repressor inhibits the malignant phenotype of alveolar rhabdomyosarcoma cells harboring the endogenous PAX3-FKHR oncogene." Mol Cell Biol **20**(14): 5019-5031.
50. Galili, N., R. J. Davis, et al. (1993). "Fusion of a fork head domain gene to PAX3 in the solid tumour alveolar rhabdomyosarcoma." Nat Genet **5**(3): 230-235.
51. Gonsalves, F. C., K. Klein, et al. (2011). "An RNAi-based chemical genetic screen identifies three small-molecule inhibitors of the Wnt/wingless signaling pathway." Proc Natl Acad Sci U S A **108**(15): 5954-5963.
52. Guo, Y., J. Xie, et al. (2008). "Frzb, a Secreted Wnt Antagonist, Decreases Growth and Invasiveness of Fibrosarcoma Cells Associated with Inhibition of Met Signaling." Cancer Research **68**(9): 3350-3360.
53. Hall, C. L., H. Zhang, et al. (2010). "p21CIP-1/WAF-1 induction is required to inhibit prostate cancer growth elicited by deficient expression of the Wnt inhibitor Dickkopf-1." Cancer Res **70**(23): 9916-9926.
54. Harper, J. W., G. R. Adami, et al. (1993). "The p21 Cdk-interacting protein Cip1 is a potent inhibitor of G1 cyclin-dependent kinases." Cell **75**(4): 805-816.
55. Hecker, R. M., R. A. Amstutz, et al. (2010). "p21 Downregulation is an important component of PAX3/FKHR oncogenicity and its reactivation by HDAC inhibitors enhances combination treatment." Oncogene **29**(27): 3942-3952.

56. Hettmer, S., J. Liu, et al. (2011). "Sarcomas induced in discrete subsets of prospectively isolated skeletal muscle cells." Proc Natl Acad Sci U S A **108**(50): 20002-20007.
57. Hettmer, S. and A. J. Wagers (2010). "Muscling in: Uncovering the origins of rhabdomyosarcoma." Nat Med **16**(2): 171-173.
58. Himes, R. H., R. N. Kersey, et al. (1976). "Action of the vinca alkaloids vincristine, vinblastine, and desacetyl vinblastine amide on microtubules in vitro." Cancer Res **36**(10): 3798-3802.
59. Hinson, A. R., R. Jones, et al. (2013). "Human rhabdomyosarcoma cell lines for rhabdomyosarcoma research: utility and pitfalls." Front Oncol **3**: 183.
60. Hirata, H., Y. Hinoda, et al. (2010). "Role of Secreted Frizzled-Related Protein 3 in Human Renal Cell Carcinoma." Cancer Research **70**(5): 1896-1905.
61. Hitchins, L., F. Fletcher, et al. (2013). "Role of Sulf1A in Wnt1- and Wnt6-induced growth regulation and myoblast hyper-elongation." FEBS Open Bio **3**: 30-34.
62. Hoang, B., M. Moos, Jr., et al. (1996). "Primary structure and tissue distribution of FRZB, a novel protein related to Drosophila frizzled, suggest a role in skeletal morphogenesis." J Biol Chem **271**(42): 26131-26137.
63. Huang, S. M., Y. M. Mishina, et al. (2009). "Tankyrase inhibition stabilizes axin and antagonizes Wnt signalling." Nature **461**(7264): 614-620.
64. Huh, W. W. and S. X. Skapek (2010). "Childhood rhabdomyosarcoma: new insight on biology and treatment." Curr Oncol Rep **12**(6): 402-410.
65. Hutcheson, D. A., J. Zhao, et al. (2009). "Embryonic and fetal limb myogenic cells are derived from developmentally distinct progenitors and have different requirements for beta-catenin." Genes Dev **23**(8): 997-1013.
66. Imbimbo, B. P. (2008). "Therapeutic potential of gamma-secretase inhibitors and modulators." Curr Top Med Chem **8**(1): 54-61.

67. Ishiguro, H., T. Shimokawa, et al. (2002). "Isolation of HELAD1, a novel human helicase gene up-regulated in colorectal carcinomas." Oncogene **21**(41): 6387-6394.
68. Jho, E. H., T. Zhang, et al. (2002). "Wnt/beta-catenin/Tcf signaling induces the transcription of Axin2, a negative regulator of the signaling pathway." Mol Cell Biol **22**(4): 1172-1183.
69. Jones, S. E. and C. Jomary (2002). "Secreted Frizzled-related proteins: searching for relationships and patterns." BioEssays **24**(9): 811-820.
70. Kanazawa, A., S. Tsukada, et al. (2005). "Wnt5b partially inhibits canonical Wnt/beta-catenin signaling pathway and promotes adipogenesis in 3T3-L1 preadipocytes." Biochem Biophys Res Commun **330**(2): 505-510.
71. Kassam-Duchossoy, L., B. Gayraud-Morel, et al. (2004). "Mrf4 determines skeletal muscle identity in Myf5:Myod double-mutant mice." Nature **431**(7007): 466-471.
72. Katoh, M. (2007). "WNT antagonist, DKK2, is a Notch signaling target in intestinal stem cells: augmentation of a negative regulation system for canonical WNT signaling pathway by the Notch-DKK2 signaling loop in primates." Int J Mol Med **19**(1): 197-201.
73. Keller, C., B. R. Arenkiel, et al. (2004). "Alveolar rhabdomyosarcomas in conditional Pax3:Fkhr mice: cooperativity of Ink4a/ARF and Trp53 loss of function." Genes Dev **18**(21): 2614-2626.
74. Kikuchi, A., H. Yamamoto, et al. (2011). "New insights into the mechanism of Wnt signaling pathway activation." Int Rev Cell Mol Biol **291**: 21-71.
75. Kim, D., O. Rath, et al. (2007). "A hidden oncogenic positive feedback loop caused by crosstalk between Wnt and ERK pathways." Oncogene **26**(31): 4571-4579.
76. Kim, H. A., B. K. Koo, et al. (2012). "Notch1 counteracts WNT/beta-catenin signaling through chromatin modification in colorectal cancer." J Clin Invest **122**(9): 3248-3259.
77. Kinzler, K. W., M. C. Nilbert, et al. (1991). "Identification of FAP locus genes from chromosome 5q21." Science **253**(5020): 661-665.

78. Klein, P. S. and D. A. Melton (1996). "A molecular mechanism for the effect of lithium on development." Proc Natl Acad Sci U S A **93**(16): 8455-8459.
79. Kwon, C., P. Cheng, et al. (2011). "Notch post-translationally regulates beta-catenin protein in stem and progenitor cells." Nat Cell Biol **13**(10): 1244-1251.
80. Labbe, E., A. Letamendia, et al. (2000). "Association of Smads with lymphoid enhancer binding factor 1/T cell-specific factor mediates cooperative signaling by the transforming growth factor-beta and wnt pathways." Proc Natl Acad Sci U S A **97**(15): 8358-8363.
81. Lagutina, I. V., V. Valentine, et al. (2015). "Modeling of the human alveolar rhabdomyosarcoma Pax3-Foxo1 chromosome translocation in mouse myoblasts using CRISPR-Cas9 nuclease." PLoS Genet **11**(2): e1004951.
82. Le Grand, F., A. E. Jones, et al. (2009). "Wnt7a activates the planar cell polarity pathway to drive the symmetric expansion of satellite stem cells." Cell Stem Cell **4**(6): 535-547.
83. Leyns, L., T. Bouwmeester, et al. (1997). "Frzb-1 is a secreted antagonist of Wnt signaling expressed in the Spemann organizer." Cell **88**(6): 747-756.
84. Linardic, C. M., S. Naini, et al. (2007). "The PAX3-FKHR Fusion Gene of Rhabdomyosarcoma Cooperates with Loss of p16INK4A to Promote Bypass of Cellular Senescence." Cancer Research **67**(14): 6691-6699.
85. Lodewyckx, L., F. Cailotto, et al. (2012). "Tight regulation of wntless-type signaling in the articular cartilage - subchondral bone biomechanical unit: transcriptomics in Frzb-knockout mice." Arthritis Res Ther **14**(1): R16.
86. Logan, C. Y. and R. Nusse (2004). "The Wnt signaling pathway in development and disease." Annu Rev Cell Dev Biol **20**: 781-810.
87. Lopez-Rios, J., P. Esteve, et al. (2008). "The Netrin-related domain of Sfrp1 interacts with Wnt ligands and antagonizes their activity in the anterior neural plate." Neural Development **3**(1): 19.
88. Lubner, S. J., M. Kunnimalaiyaan, et al. (2011). "A preclinical and clinical study of lithium in low-grade neuroendocrine tumors." Oncologist **16**(4): 452-457.

89. Lustig, B., B. Jerchow, et al. (2002). "Negative feedback loop of Wnt signaling through upregulation of conductin/axin2 in colorectal and liver tumors." Mol Cell Biol **22**(4): 1184-1193.
90. Mabeta, P. and M. S. Pepper (2009). "A comparative study on the anti-angiogenic effects of DNA-damaging and cytoskeletal-disrupting agents." Angiogenesis **12**(1): 81-90.
91. MacDonald, B. T., K. Tamai, et al. (2009). "Wnt/ β -Catenin Signaling: Components, Mechanisms, and Diseases." Developmental Cell **17**(1): 9-26.
92. Madan, B. and D. M. Virshup (2015). "Targeting Wnts at the Source-New Mechanisms, New Biomarkers, New Drugs." Mol Cancer Ther **14**(5): 1087-1094.
93. Martz, C. A., K. A. Ottina, et al. (2014). "Systematic identification of signaling pathways with potential to confer anticancer drug resistance." Sci Signal **7**(357): ra121.
94. McDonald, S. L. and A. Silver (2009). "The opposing roles of Wnt-5a in cancer." British Journal of Cancer **101**(2): 209-214.
95. Minoo, P. and C. Li (2010). "Cross-talk between transforming growth factor-beta and Wnt/Wingless/Int pathways in lung development and disease." Int J Biochem Cell Biol **42**(6): 809-812.
96. Molenaar, M., M. van de Wetering, et al. (1996). "XTcf-3 transcription factor mediates beta-catenin-induced axis formation in *Xenopus* embryos." Cell **86**(3): 391-399.
97. Murphy, M. and G. Kardon (2011). "Origin of vertebrate limb muscle: the role of progenitor and myoblast populations." Curr Top Dev Biol **96**: 1-32.
98. Naini, S., K. T. Etheridge, et al. (2008). "Defining the Cooperative Genetic Changes That Temporally Drive Alveolar Rhabdomyosarcoma." Cancer Research **68**(23): 9583-9588.
99. Nalesso, G., J. Sherwood, et al. (2011). "WNT-3A modulates articular chondrocyte phenotype by activating both canonical and noncanonical pathways." The Journal of cell biology **193**(3): 551-564.

100. Newport, D. J., A. C. Viguera, et al. (2005). "Lithium placental passage and obstetrical outcome: implications for clinical management during late pregnancy." Am J Psychiatry **162**(11): 2162-2170.
101. Ng, T. L., A. M. Gown, et al. (2005). "Nuclear beta-catenin in mesenchymal tumors." Mod Pathol **18**(1): 68-74.
102. Niehrs, C. (2012). "The complex world of WNT receptor signalling." Nat Rev Mol Cell Biol **13**(12): 767-779.
103. Nishisho, I., Y. Nakamura, et al. (1991). "Mutations of chromosome 5q21 genes in FAP and colorectal cancer patients." Science **253**(5020): 665-669.
104. Nishita, M., M. K. Hashimoto, et al. (2000). "Interaction between Wnt and TGF-beta signalling pathways during formation of Spemann's organizer." Nature **403**(6771): 781-785.
105. Nusse, R. and H. Varmus (2012). "Three decades of Wnts: a personal perspective on how a scientific field developed." EMBO J **31**(12): 2670-2684.
106. Nusse, R. and H. E. Varmus (1982). "Many tumors induced by the mouse mammary tumor virus contain a provirus integrated in the same region of the host genome." Cell **31**(1): 99-109.
107. Ognjanovic, S., A. M. Linabery, et al. (2009). "Trends in childhood rhabdomyosarcoma incidence and survival in the United States, 1975-2005." Cancer **115**(18): 4218-4226.
108. Orth, J. D., A. Loewer, et al. (2012). "Prolonged mitotic arrest triggers partial activation of apoptosis, resulting in DNA damage and p53 induction." Mol Biol Cell **23**(4): 567-576.
109. Osada, T., M. Chen, et al. (2011). "Antihelminth compound niclosamide downregulates Wnt signaling and elicits antitumor responses in tumors with activating APC mutations." Cancer Res **71**(12): 4172-4182.
110. Otto, A., C. Schmidt, et al. (2008). "Canonical Wnt signalling induces satellite-cell proliferation during adult skeletal muscle regeneration." J Cell Sci **121**(Pt 17): 2939-2950.

111. Ougolkov, A. V., M. E. Fernandez-Zapico, et al. (2005). "Glycogen synthase kinase-3beta participates in nuclear factor kappaB-mediated gene transcription and cell survival in pancreatic cancer cells." Cancer Res **65**(6): 2076-2081.
112. Pandey, P. P., S. M. Hewitt, et al. (2015). "PAX3-FOXO1 is essential for initiation but not for recurrence during rhabdomyosarcoma tumorigenesis. [abstract]." In: Proceedings of the 106th Annual Meeting of the American Association for Cancer Research Apr 18-22; (Philadelphia, PA. Philadelphia (PA): AACR; 2015. Abstract nr 3273).
113. Park, E. J., S. J. Choi, et al. (2009). "Novel small molecule activators of beta-catenin-mediated signaling pathway: structure-activity relationships of indirubins." Bioorg Med Chem Lett **19**(8): 2282-2284.
114. Parker, M. H., P. Seale, et al. (2003). "Looking back to the embryo: defining transcriptional networks in adult myogenesis." Nat Rev Genet **4**(7): 497-507.
115. Pearlstein, T. (2008). "Perinatal depression: treatment options and dilemmas." J Psychiatry Neurosci **33**(4): 302-318.
116. Perez-Ruiz, A., Y. Ono, et al. (2008). "beta-Catenin promotes self-renewal of skeletal-muscle satellite cells." J Cell Sci **121**(Pt 9): 1373-1382.
117. Pizzo, P. A. and D. G. Poppo (2011). Principles and practice of pediatric oncology. Philadelphia, PA, Wolters Kluwer/Lippincott Williams & Wilkins Health.
118. Poleskaya, A., P. Seale, et al. (2003). "Wnt Signaling Induces the Myogenic Specification of Resident CD45+ Adult Stem Cells during Muscle Regeneration." Cell **113**(7): 841-852.
119. Powell, S. M., N. Zilz, et al. (1992). "APC mutations occur early during colorectal tumorigenesis." Nature **359**(6392): 235-237.
120. Raimondi, L., R. Ciarapica, et al. (2012). "Inhibition of Notch3 signalling induces rhabdomyosarcoma cell differentiation promoting p38 phosphorylation and p21(Cip1) expression and hampers tumour cell growth in vitro and in vivo." Cell Death Differ **19**(5): 871-881.

121. Ren, Y. X., F. G. Finckenstein, et al. (2008). "Mouse mesenchymal stem cells expressing PAX-FKHR form alveolar rhabdomyosarcomas by cooperating with secondary mutations." Cancer Res **68**(16): 6587-6597.
122. Roma, J., A. Masia, et al. (2011). "Notch pathway inhibition significantly reduces rhabdomyosarcoma invasiveness and mobility in vitro." Clin Cancer Res **17**(3): 505-513.
123. Rottinger, E., L. Besnardeau, et al. (2004). "A Raf/MEK/ERK signaling pathway is required for development of the sea urchin embryo micromere lineage through phosphorylation of the transcription factor Ets." Development **131**(5): 1075-1087.
124. Rubin, B. P., K. Nishijo, et al. (2011). "Evidence for an unanticipated relationship between undifferentiated pleomorphic sarcoma and embryonal rhabdomyosarcoma." Cancer Cell **19**(2): 177-191.
125. Saab, R., S. L. Spunt, et al. (2011). "Myogenesis and rhabdomyosarcoma the Jekyll and Hyde of skeletal muscle." Curr Top Dev Biol **94**: 197-234.
126. Satoh, W., M. Matsuyama, et al. (2008). "Sfrp1, Sfrp2, and Sfrp5 regulate the Wnt/beta-catenin and the planar cell polarity pathways during early trunk formation in mouse." Genesis **46**(2): 92-103.
127. Scardigli, R., C. Gargioli, et al. (2008). "Binding of sFRP-3 to EGF in the extracellular space affects proliferation, differentiation and morphogenetic events regulated by the two molecules." PLoS One **3**(6): e2471.
128. Schmitt-Ney, M. and G. Camussi (2015). "The PAX3-FOXO1 fusion protein present in rhabdomyosarcoma interferes with normal FOXO activity and the TGF-beta pathway." PLoS One **10**(3): e0121474.
129. Shern, J. F., L. Chen, et al. (2014). "Comprehensive genomic analysis of rhabdomyosarcoma reveals a landscape of alterations affecting a common genetic axis in fusion-positive and fusion-negative tumors." Cancer Discov **4**(2): 216-231.
130. Shukla, N., N. Ameer, et al. (2012). "Oncogene mutation profiling of pediatric solid tumors reveals significant subsets of embryonal rhabdomyosarcoma and neuroblastoma with mutated genes in growth signaling pathways." Clin Cancer Res **18**(3): 748-757.

131. Singh, S., C. Vinson, et al. (2010). "Impaired Wnt Signaling in Embryonal Rhabdomyosarcoma Cells from p53/c-fos Double Mutant Mice." American Journal Of Pathology **177**(4): 2055-2066.
132. Surana, R., S. Sikka, et al. (2013). "Secreted frizzled related proteins: Implications in cancers." Biochim Biophys Acta **1845**(1): 53-65.
133. Swain, R. K., M. Katoh, et al. (2005). "Xenopus frizzled-4S, a splicing variant of Xfz4 is a context-dependent activator and inhibitor of Wnt/beta-catenin signaling." Cell Commun Signal **3**: 12.
134. Tajbakhsh, S., U. Borello, et al. (1998). "Differential activation of Myf5 and MyoD by different Wnts in explants of mouse paraxial mesoderm and the later activation of myogenesis in the absence of Myf5." Development **125**(21): 4155-4162.
135. Tang, X., J. E. Lucas, et al. (2012). "Functional interaction between responses to lactic acidosis and hypoxia regulates genomic transcriptional outputs." Cancer Res **72**(2): 491-502.
136. Thalhammer, V., L. A. Lopez-Garcia, et al. (2015). "PLK1 phosphorylates PAX3-FOXO1, the inhibition of which triggers regression of alveolar Rhabdomyosarcoma." Cancer Res **75**(1): 98-110.
137. Thomas, T., L. Stansifer, et al. (2011). "Psychopharmacology of pediatric bipolar disorders in children and adolescents." Pediatr Clin North Am **58**(1): 173-187, xii.
138. Tighe, A., A. Ray-Sinha, et al. (2007). "GSK-3 inhibitors induce chromosome instability." BMC Cell Biol **8**: 34.
139. Tostar, U., R. Toftgard, et al. (2010). "Reduction of human embryonal rhabdomyosarcoma tumor growth by inhibition of the hedgehog signaling pathway." Genes & cancer **1**(9): 941-951.
140. Valenta, T., J. Lukas, et al. (2003). "HMG box transcription factor TCF-4's interaction with CtBP1 controls the expression of the Wnt target Axin2/Conductin in human embryonic kidney cells." Nucleic Acids Res **31**(9): 2369-2380.

141. Veeman, M. T., D. C. Slusarski, et al. (2003). "Zebrafish prickle, a modulator of noncanonical Wnt/Fz signaling, regulates gastrulation movements." Curr Biol **13**(8): 680-685.
142. Vijayakumar, S., G. Liu, et al. (2011). "High-Frequency Canonical Wnt Activation in Multiple Sarcoma Subtypes Drives Proliferation through a TCF/ β -Catenin Target Gene, CDC25A." Cancer Cell **19**(5): 601-612.
143. Wang, S., M. Krinks, et al. (1997). "Frzb-1, an antagonist of Wnt-1 and Wnt-8, does not block signaling by Wnts -3A, -5A, or -11." Biochem Biophys Res Commun **236**(2): 502-504.
144. Wang, Z., K. S. Smith, et al. (2008). "Glycogen synthase kinase 3 in MLL leukaemia maintenance and targeted therapy." Nature **455**(7217): 1205-1209.
145. Watanabe, K. and X. Dai (2011). "Winning WNT: race to Wnt signaling inhibitors." Proc Natl Acad Sci U S A **108**(15): 5929-5930.
146. Weeraratna, A. T., Y. Jiang, et al. (2002). "Wnt5a signaling directly affects cell motility and invasion of metastatic melanoma." Cancer Cell **1**(3): 279-288.
147. Westfall, T. A., R. Brimeyer, et al. (2003). "Wnt-5/pipetail functions in vertebrate axis formation as a negative regulator of Wnt/beta-catenin activity." J Cell Biol **162**(5): 889-898.
148. Wu, Z. Q., X. Y. Li, et al. (2012). "Canonical Wnt signaling regulates Slug activity and links epithelial-mesenchymal transition with epigenetic Breast Cancer 1, Early Onset (BRCA1) repression." Proc Natl Acad Sci U S A **109**(41): 16654-16659.
149. Xavier, C. P., M. Melikova, et al. (2014). "Secreted Frizzled-related protein potentiation versus inhibition of Wnt3a/beta-catenin signaling." Cell Signal **26**(1): 94-101.
150. Yamada, A., T. Iwata, et al. (2013). "Diverse functions of secreted frizzled-related proteins in the osteoblastogenesis of human multipotent mesenchymal stromal cells." Biomaterials **34**(13): 3270-3278.
151. Yan, D., M. Wiesmann, et al. (2001). "Elevated expression of axin2 and hnkcd mRNA provides evidence that Wnt/beta -catenin signaling is activated in human colon tumors." Proc Natl Acad Sci U S A **98**(26): 14973-14978.

152. Yost, C., M. Torres, et al. (1996). "The axis-inducing activity, stability, and subcellular distribution of beta-catenin is regulated in *Xenopus* embryos by glycogen synthase kinase 3." Genes Dev **10**(12): 1443-1454.
153. Yun, M. S., S. E. Kim, et al. (2005). "Both ERK and Wnt/beta-catenin pathways are involved in Wnt3a-induced proliferation." J Cell Sci **118**(Pt 2): 313-322.
154. Zeng, F.-Y., H. Dong, et al. (2010). "Glycogen synthase kinase 3 regulates PAX3-FKHR-mediated cell proliferation in human alveolar rhabdomyosarcoma cells." Biochemical and Biophysical Research Communications **391**(1): 1049-1055.
155. Zhao, P. and E. P. Hoffman (2004). "Embryonic myogenesis pathways in muscle regeneration." Dev Dyn **229**(2): 380-392.
156. Zi, X., Y. Guo, et al. (2005). "Expression of Frzb/secreted Frizzled-related protein 3, a secreted Wnt antagonist, in human androgen-independent prostate cancer PC-3 cells suppresses tumor growth and cellular invasiveness." Cancer Res **65**(21): 9762-9770.

Biography

Julie Jeanne Grondin Kephart

Born March 11, 1984 in Kingston, Ontario, Canada

EDUCATION

PhD in Pharmacology

Certificate in Cell and Molecular Biology

Certificate in College Teaching

Duke University, Durham, North Carolina, July 2015

BS in Biology

Second major in Linguistics

The University of North Carolina at Chapel Hill, May 2006

PUBLICATIONS

Kephart J, Tiller R, Crose L, Slemmons KK, Chen PH, Hinson A, Bentley R, Chi JT, and Linardic C. Secreted frizzled related protein 3 (SFRP3) is required for tumorigenesis of PAX3-FOXO1-positive alveolar rhabdomyosarcoma. *Clin Cancer Res.* 2015 Jun 12. pii: clincanres.1797.2014

Crose L, Galindo K, **Kephart J**, Chen C, Fitamant J, Bardeesy N, Bentley R, Galindo R, Chi JT, Linardic C, Alveolar rhabdomyosarcoma-associated PAX3-FOXO1 promotes tumorigenesis via Hippo pathway suppression. *J Clin Invest.* 2014 Jan 2;124(1):285-96

Belyea B, **Kephart J**, Blum J, Kirsch D, Linardic C, Embryonic Signaling Pathways and Rhabdomyosarcoma: Contributions to Cancer Development and Opportunities for Therapeutic Targeting. *Sarcoma.* 2012;2012:406239.

Besheer J, Fisher KR, **Grondin JJ**, Cannady R, Hodge CW, The effects of repeated corticosterone exposure on the interoceptive effects of alcohol in rats. *Psychopharmacology (Berl).* 2012 Apr;220(4):809-22.

Besheer J, Fisher KR, Cannady R, **Grondin JJ**, Hodge CW, Intra-amygdala inhibition of ERK(1/2) potentiates the discriminative stimulus effects of alcohol. *Behav Brain Res.* 2012 Mar 17;228(2):398-405.

Cannady R, **Grondin JJ**, Fisher KR, Hodge CW, Besheer J, Activation of Group II metabotropic glutamate receptors inhibits the discriminative stimulus effects of alcohol via selective activity within the amygdala. *Neuropsychopharmacology.* 2011 Oct;36(11):2328-38.

Besheer J, **Grondin JJ**, Cannady RD, Sharko AC, Faccidomo S, Hodge CW, mGlu5 receptor activity in the nucleus accumbens is required for the maintenance of ethanol self-administration in a rat genetic model of high alcohol intake. *Biological Psychiatry.* 2010 May 1;67(9):812-22

Besheer J, **Grondin JJ**, Salling MC, Spanos M, Stevenson RA, Hodge CW. Introceptive effects of alcohol require mGlu5 receptor activity in the nucleus accumbens. *J Neurosci*. 2009 Jul 29;29(30):9582-91.

Besheer J, Faccidomo S, **Grondin JJ**, Hodge CW. Effects of mGlu1-receptor blockade on ethanol self-administration in inbred alcohol-preferring rats. *Alcohol*. 2008 Feb;42(1):13-20.

Besheer J, Faccidomo S, **Grondin JJ**, Hodge CW Regulation of motivation to self-administer ethanol by mGluR5 in alcohol-preferring (P) rats. *Alcohol Clin Exp Res*. 2008 Feb;32(2):209-21.

AWARD

Pediatric Oncology Student Training (POST) Program

Alex's Lemonade Stand Foundation, 2011